BARISHAL UNIVERSITY JOURNAL
ISSN: 2411-247X

BARISHAL UNIVERSITY JOURNAL OF SCIENCE AND ENGINEERING

Volume - 8, December - 2023

FACULTY OF SCIENCE AND ENGINEERING
UNIVERSITY OF BARISHAL

BARISHAL UNIVERSITY JOURNAL OF SCIENCE AND ENGINEERING

Volume -8, December - 2023

Published by
Faculty of Science and Engineering, University of Barishal

Editor-in-Chief
Dr. Md. Shafiul Alam
Dean
Faculty of Science and Engineering,
University of Barishal, Barishal-8254, Bangladesh

Price
500.00 Taka
10.00 $ (USD)

Printed by
Asbi Traders
Morium Saleha Market, Nilkhet, Dhaka-1205
Cell : 01301816868

CONTENTS

Editorial

We are delighted to present the Volume 8, December 2023 of Barishal University Journal of Science and Engineering (BUJSE). We want to express our deepest gratitude to the editorial board, reviewers, and authors for their significant contributions to the journal. The BUJSE is inter-disciplinary and proceeded to issuing quality articles through rigorous and quick review processing schemes. The unbiased peer review system of the BUJSE is very effective in filtering the authentic and significant research manuscripts in various relevant fields. One of the objectives of BUJSE is to encourage publications from different streams of research in the field of Mathematics, Computer Science & Engineering, Physics, Chemistry, Geology and Mining, and Statistics.

There is a pressing necessity for exemplifying research findings in the form of articles, which could be beneficial in enriching the learning process in grasping fundamental principles to apply scientific and engineering applications. The journal aims to open a space of creativity and research of international standard by incorporating innovative modalities of perceptions and ideas. As far as ensuring the quality of the journal is concerned, the editorial panel of the journal has raised the bar. Articles submitted are reviewed with utmost rigor by eminent scholars corresponding to the field of the articles. The research papers in this journal reflect the breadth of the research being conducted by our academicians in the fields of Science and Engineering. It is our firm believe that this journal will flourish over time and be established as one of the finest journals of Science and Engineering in the country. We hope that the readers will find the present volume of BUJSE much informative, interesting, and useful.

We want to express our deepest gratitude to the honourable Vice-Chancellor Professor Dr. Mohammad Badruzzaman Bhuiyan for his continuous support and encouragement to publish the journal. We would like to thank everyone who has contributed to the journal in various capacities, and urge researchers in various fields of Science and Engineering to continue submitting their research findings to publish in the journal. Your cooperation will be highly appreciated. If you have any suggestions or questions, please directly contact the journal coordinator (bujournalscience@gmail.com). We look forward to hearing from you.

Dr. Md. Shafiul Alam
Editor-in-Chief
Barishal University Journal of Science and Engineering
University of Barishal, Barishal-8254, Bangladesh.

SYNTHESIS AND CHARACTERIZATION OF THIOMORPHOLINOMETHYL DERIVATIVES OF ISATIN AND IT'S HYDRAZINECARBOXAMIDES

Md. Ahad Khan[1], Md. Emdad Hossain[2] and Halima Bagum[1,*]

[1] *Department of Chemistry, University of Barishal, Barishal-8254, Bangladesh*

[2] *Wazed Miah Science Research Centre, Jahangirnagar University, Savar, Dhaka-1342, Bangladesh*

Abstract

A general route, which provides thiomorpholinomethyl indolin-3-ylidene derivative of hydrazinecarboxamide, is examined. Herein, we report the development of methodology for easy access to thiomorpholinomethyl derivatives of isatin and it's hydrazinecarboxamides. The products are obtained with high yield. We have characterized the products synthesized by using IR and NMR spectroscopic techniques. A good agreement is observed for the spectral data with the structure of the compounds synthesized.

Keywords: *Isatin, Heterocycles, Mannich Bases, Schiff Bases.*

Introduction

Heterocycles are remarkable class of compounds for their wide application as pharmacological active products, neurotransmitters, analgesic agents etc(Katritzky & Fan, 1990). Moreover, they serve as useful tool for the synthesis of biologically active compounds(Jampilek, 2019).

*Corresponding author.
E-mail address: halimaju35@gmail.com

Isatin (1H-indole-2,3-dione) is the 2,3-diketo derivative of indole. It has extraordinary uses by chemists as an starting material of various synthetic protocol, especially isatin and it's derivatives represent a group of heterocyclic compounds that can be used as a precursor of drug synthesis(Pakravan et al., 2013; Silva et al., 2001; Varun et al., 2019). Mannich bases and Schiff bases of Isatin have found synthetic utilities(Afsah et al., 2015; Bekircan & Bektas, 2008) and biological activities(Abdulghani & Abbas, 2011; Ferraz de Paiva et al., 2021). Previously, morpholinomethyl and piperidin-1-ylmethyl derivatives of isatin was synthesized and tested for cytotoxicity(Bagum et al., 2013; Bagum & Islam, 2015). In this research paper, we report the synthesis and characterization of thiomorpholinomethyl derivatives of isatin and it's hydrazinecarboxamides. Earlier, researcher worked on the various complexes of Mannich bases(Raman et al., 2004). We take the opportunity to prepare both Mannich bases and Schiff bases to introduce heterocycle as well as functionality. The significance of this research is that the functionalized heterocyclic compounds can be accessed easily which would be useful as precursor for further studies.

Materials and Methods

Starting materials were obtained from Sigma Aldrich, Apollo Scientific, or Acros Organics. Reactions were carried out in oven-dried glassware. Minutes (min), hours (h) and days (d) were used to record reaction times. Light petroleum ether of boiling point 40-60°C was used, without further purification, as purchased from the commercial suppliers. Solvents were evaporated under reduced pressure at 40 °C. Büchi R-100 rotary evaporator, attached to a vacuum pump V-100 and recirculating chiller F-100 system were used to evaporate solvents.

Merck aluminium foil backed sheets precoated with 0.2 mm Kielselgel 60 F_{254} was used to perform Analytical thin-layer chromatography (TLC). Kielselgel 60 silica gel (60-120 mesh particle size) was used to accomplish column chromatography. The eluents are identified clearly for each column.

IRPrestige-21 was used to record IR spectra and Bruker Ascend^{TM} 400 (400 MHz) was used to record NMR spectra by the assistance at the Wazed Miah Science Research Centre, Jahangirnagar University, Dhaka.

Synthesis of 1-(thiomorpholinomethyl)indoline-2,3-dione **2**

A mixture of isatin **1** (0.5g, 3.397 mmol), formaldehyde (0.75 mL) and thiomorpholine (0.665 mL, 3.397 mmol) in 10 mL methanol was refluxed for 4h at 100°C. The reaction mixture was kept at refrigerator overnight. The crystal thus deposited was filtered and re-crystallized with methanol to embellish yellowish orange crystalline solid **2** having the percent of yield 86% and R_f 0.81 (Ethyl acetate:$CHCl_3$, 1:2).

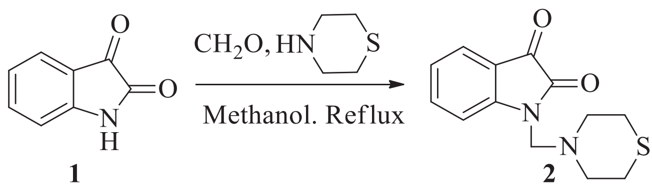

1 Isatin **2**

Scheme 1: Synthesis of 1-(thiomorpholinomethyl)indoline-2,3-dione **2**

IR (cm^{-1}): 3050 (aromatic C-H str.), 2928, 2866, 2824 (aliphatic C-H str.), 1732 (C=O str.), 1609 (C=O str., amide), 1472 (aromatic C=C str.); ^{1}H NMR (ppm): 7.6-7.1 (4H, m, aromatic-H), 4.5 (2H, s, N-C$\underline{H}_2$-N), 2.9 (4H, s, C$\underline{H}_2$-N-C$\underline{H}_2$), 2.7 (4H, s, C$\underline{H}_2$-S-C$\underline{H}_2$); ^{13}C NMR (ppm): 183.0 ($\underline{C}$=O), 159 ($\underline{C}$=O, amide), 151.0, 138.0, 125.0, 124.0, 117.6, 111.7 (aromatic C), 63.2 (N-$\underline{\mathrm{C}}$H$_2$-N), 52.6 ($\underline{\mathrm{C}}$H$_2$-N-$\underline{\mathrm{C}}$H$_2$), 27.6 ($\underline{\mathrm{C}}$H$_2$-S-$\underline{\mathrm{C}}$H$_2$).

*Synthesis of (Z)-2-(2-oxo-1-(thiomorpholinomethyl)indolin-3 ylidene) hydrazine-ecarboxamide **3***

A mixture of 0.25g of 1-(thiomorpholinomethyl)indoline-2,3-dione **2**, 0.106g of semicarbazide and 7.5 mL of methanol was refluxed for 11-12 hours at 100℃. The reaction mixture was kept in room temperature for several hours. Solvent was then removed by rotary evaporator. The crude product was then recrystallized in methanol to furnish dark yellow crystalline product **3** having a yield of 90%. TLC ran in ethyl acetate:n-hexane (1:1) gave single spot with R$_f$ value 0.20.

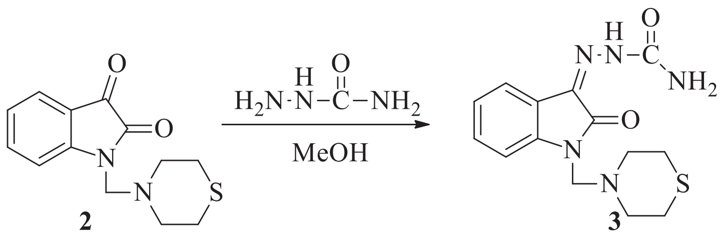

Scheme 2: Synthesis of (Z)-2-(2-oxo-1-(thiomorpholinomethyl)indolin-3-ylidene)-hydrazinecarboxamide

IR(cm^{-1}): 3470, 3302 (NH$_2$ str.), 3238 (NH str.), 3134, 3003 (aromatic C-H str.), 2822 (aliphatic C-H str.), 1705, 1624 (C=O str.), 1578, 1466 (aromatic C=C str.); ^{1}H NMR (ppm): 7.6-6.9 (4H, m, aromatic-H), 5.1 (1H, s, N$\underline{\mathrm{H}}$), 3.5 (2H, s, N-C$\underline{\mathrm{H}}_2$-N), 3.3 (4H, s, C$\underline{\mathrm{H}}_2$-N-C$\underline{\mathrm{H}}_2$) 2.7 (4H, s, C$\underline{\mathrm{H}}_2$-S-C$\underline{\mathrm{H}}_2$), 1.6 (2H, s, N$\underline{\mathrm{H}}_2$).

*Synthesis of (Z)-2-(2-oxo-1-(thiomorpholinomethyl)indolin-3-ylidene)-N-(thiomorpholinomethyl)hydrazinecarboxamide **4***

In 20 mL distilled methanol, 0.1g of (Z)-2-(2-oxo-1-(thiomorpholinomethyl)indolin-3-ylidene)hydrazinecarboxamide **3**, 0.09 mL of formaldehyde and 0.0613 mL of thiomorpholine in molar ratio 1:1 (**3**:thiomorpholine) were added orderly with vigorous stirring. The reaction mixture was then refluxed for 4 hours at 100℃ and kept overnight at room temperature. Solvent was removed by rotary evaporator. The crude product was re-crystallized in methanol to furnish yellow crystal **4**. The product was then weighed and the calculated percent of yield was 77% and R_f value 0.28 (Ethyl acetate: n-hexane, 1:2).

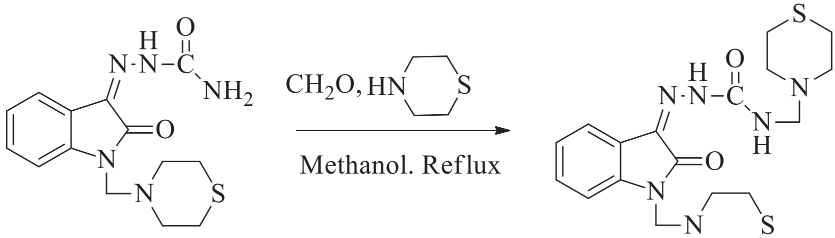

3

4

Scheme 3: Synthesis of (Z)-2-(2-oxo-1-(thiomorpholinomethyl)indolin-3-ylidene)-N-(thiomorpholinomethyl)hydrazinecarboxamide **4**

IR(cm^{-1}): 3356, 3265 (NH str.), 3050 (aromatic C-H str.), 2909, 2805 (aliphatic C-H str.), 1678, 1612 (C=O str.), 1526, 1468 (aromatic C=C str.); ^{1}H NMR (ppm): 7.6-7.0 (4H, m, aromatic-H), 6.8 (1H, s, N<u>H</u>), 4.8 (1H, s, N<u>H</u>), 4.70 (2H, s, N-C<u>H</u>$_2$-N), 4.5-4.1 (8H, m, C<u>H</u>$_2$-N-C<u>H</u>$_2$) 2.8 (8H, s, C<u>H</u>$_2$-S-C<u>H</u>$_2$); ^{13}C NMR (ppm): 162.2 154.6 (<u>C</u>=O, amide and semicarbazide), 143.0, 130.6, 123.2, 120.2, 119.7, 110.5 (aromatic C), 82.2 (N-<u>C</u>H$_2$-N), 53.4 (<u>C</u>H$_2$-N-<u>C</u>H$_2$), 27.9 (<u>C</u>H$_2$-S-<u>C</u>H$_2$).

Results and Discussion

The compound 1-(thiomorpholinomethyl)indoline-2,3-dione **2** was prepared according to the protocol described in materials and method section. The hydrazinecarboxamide **3** was prepared by the reaction of **2** with semicarbazide in glacial acetic acid. The compound (Z)-2-(2-oxo-1-(thiomorpholinomethyl)indolin-3-ylidene)-N-(thiomorpholinomethyl) hydrazinecarboxamide **4** was synthesized by the reaction of **3** with thiomorpholine and formaldehyde in methanol.

The spectroscopic analysis revealed the formation of **2**, **3** and **4**.

The IR data showed the characteristic stretching frequencies for compound **2**. In ^{1}H NMR, signals at chemical shift value 4.5, 2.9 and 2.7 ppm confirms the presence of thiomorpholinomethyl group. The ^{13}C NMR supported the structure of **2**.

Similarly, the formation of **3** was confirmed by spectroscopic analysis. In IR, the presence of stretching frequencies at 3470 and 3302 cm^{-1} is due to the asymmetric and symmetric stretching of NH_2 group respectively; band at 3238 cm^{-1} is for NH stretching, besides other characteristic frequencies. The disappearance of band at 1732 cm^{-1} confirms the formation of Schiff base **3**. The ^{1}H NMR supported the structure of **3** as predicted in scheme 2, δ 7.6-6.9 ppm correspond to aromatic hydrogen, δ 5.1 ppm corresponds to NH, δ 3.5, 3.3 and 2.7 ppm correspond to thiomorpholinomethyl group and δ 1.6 corresponds to NH_2.

Finally, the structure of the product **4** was elucidated by IR, ^{1}H NMR and ^{13}C NMR techniques. The disappearance of two band pattern in IR with stretching frequencies at 3470 and 3302 cm^{-1} for NH_2 group indicates the formation of Mannich base **4** from **3**. The predicted structure showed in scheme 3 was confirmed by ^{1}H NMR. The ^{13}C NMR supported the structure of **4**.

Conclusion

A simple route was developed to synthesize thiomorpholinomethyl derivatives of isatin and it's hydrazinecarboxamides, functionalized heterocyclic compounds.

The structure of the synthesized compounds was elucidated by IR, ^{1}H NMR and ^{13}C NMR techniques. It was found that the spectral data are in accordance with the structures of the novel compounds.

Supplementary Information

The supplementary information to this article is available and can be found following the references of this article as the following order.

IR (cm^{-1})

^{1}H NMR (ppm)

^{13}C NMR (ppm)

Acknowledgement

We greatly acknowledge the University Grants Commission Bangladesh for funding the research.

References

Abdulghani, A. J., and Abbas, N. M., 2011. Synthesis Characterization and Biological Activity Study of New Schiff and Mannich Bases and Some Metal Complexes Derived from Isatin and Dithiooxamide. *Bioinorganic Chemistry and Applications*, *2011*, pp. 1-5.

Afsah, E. M., Elmorsy, S. S., Abdelmageed, S. M., and Zaki, Z. E., 2015. Synthesis of some new mixed azines, Schiff and Mannich bases of pharmaceutical interest related to isatin. *Zeitschrift Für Naturforschung B*, *70*(6), pp. 393–402.

Bagum, H., Hossain, M. A., Al-Amin, M., and Islam, M. R., 2013. Synthesis of a

Serties of Mannich Bases as Cytotoxic Agents. *Journal of Bangladesh Chemical Society*, *26(1)*, pp. 93–99.

Bagum, H., and Islam, M. R., 2015. Synthesis of Some Mannich and Schiff Bases from Isatin and Theis Cyclization Products. *Journal of Bangladesh Chemical Society*, *27(1&2)*, pp. 69–77.

Bekircan, O., and Bektas, H., 2008. Synthesis of Schiff and Mannich Bases of Isatin Derivatives with 4-Amino-4,5-Dihydro-1H-1,2,4-Triazole-5-Ones. *Molecules*, *13*(9), pp. 2126–2135.

Ferraz de Paiva, R. E., Vieira, E. G., Rodrigues da Silva, D., Wegermann, C. A., and Costa Ferreira, A. M., 2021. Anticancer Compounds Based on Isatin-Derivatives: Strategies to Ameliorate Selectivity and Efficiency. *Frontiers in Molecular Biosciences*, *7,* pp. 627272.

Jampilek, J., 2019. Heterocycles in Medicinal Chemistry. *Molecules*, *24*(21), pp. 3839.

Katritzky, A. R., and Fan, W., 1990. The chemistry of benzotriazole. A novel and versatile synthesis of 1-alkyl-, 1-aryl-, 1-(alkylamino)-, or 1-amido-substituted and of 1,2,6-trisubstituted piperidines from glutaraldehyde and primary amines or monosubstituted hydrazines. *The Journal of Organic Chemistry*, *55*(10), pp. 3205–3209.

Pakravan, P., Kashanian, S., Khodaei, M. M., and Harding, F. J., 2013. Biochemical and pharmacological characterization of isatin and its derivatives: from structure to activity. *Pharmacological Reports*, *65*(2), pp. 313–335.

Raman, N., Esthar, S., and Thangaraja, C., 2004. A new Mannich base and its transition metal (II) complexes — Synthesis, structural characterization and electrochemical study. *Journal of Chemical Sciences Volume*, *116*, pp. 209–213.

Silva, J. F. M. da, Garden, S. J., and Pinto, A. C., 2001. The chemistry of isatins: a review from 1975 to 1999. *Journal of the Brazilian Chemical Society*, *12*(3), pp. 273–324.

Varun, V., Sonam, S., and Kakkar, R., 2019. Isatin and its derivatives: a survey of recent syntheses, reactions, and applications. *MedChemComm*, *10*(3), pp. 351–368.

Supplementary Information

SYNTHESIS AND CHARACTERIZATION OF THIOMORPHOLINOMETHYL DERIVATIVES OF ISATIN AND IT'S HYDRAZINECARBOXAMIDES

Md. Ahad Khan[1], Md. Emdad Hossain[2] and Halima Bagum[1]*

[1] Department of Chemistry, University of Barishal, Barishal-8254, Bangladesh

[2] Senior Scientific Officer, Wazed Miah Science Research Centre, Jahangirnagar University, Savar, Dhaka-1342, Bangladesh.

Contents

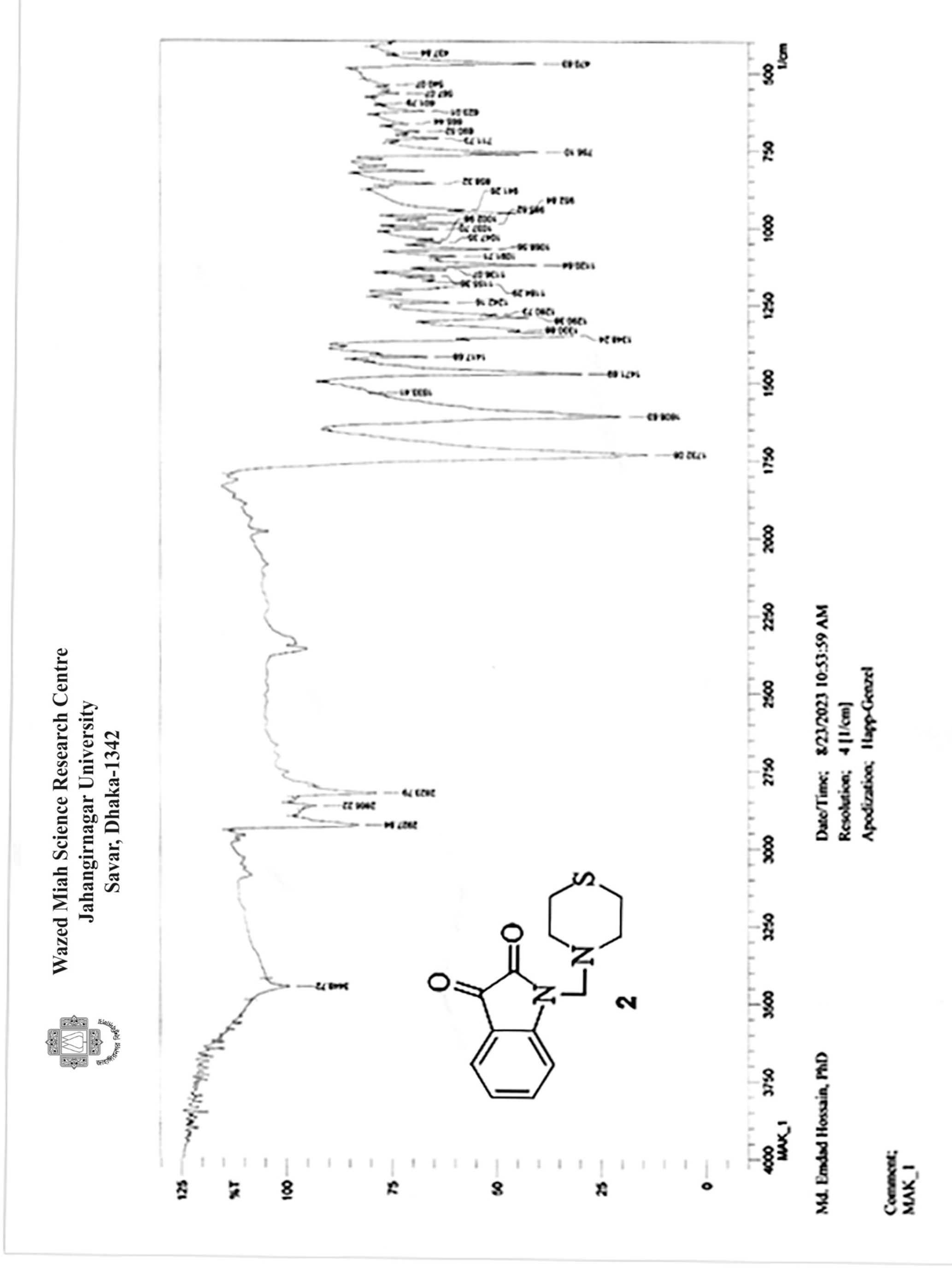
Wazed Miah Science Research Centre
Jahangirnagar University
Savar, Dhaka-1342
2
Date/Time; 8/23/2023 10:53:59 AM
Resolution; 4 [1/cm]
Apodization; Happ-Genzel
Md. Emdad Hossain, PhD
Comment;
MAK_1

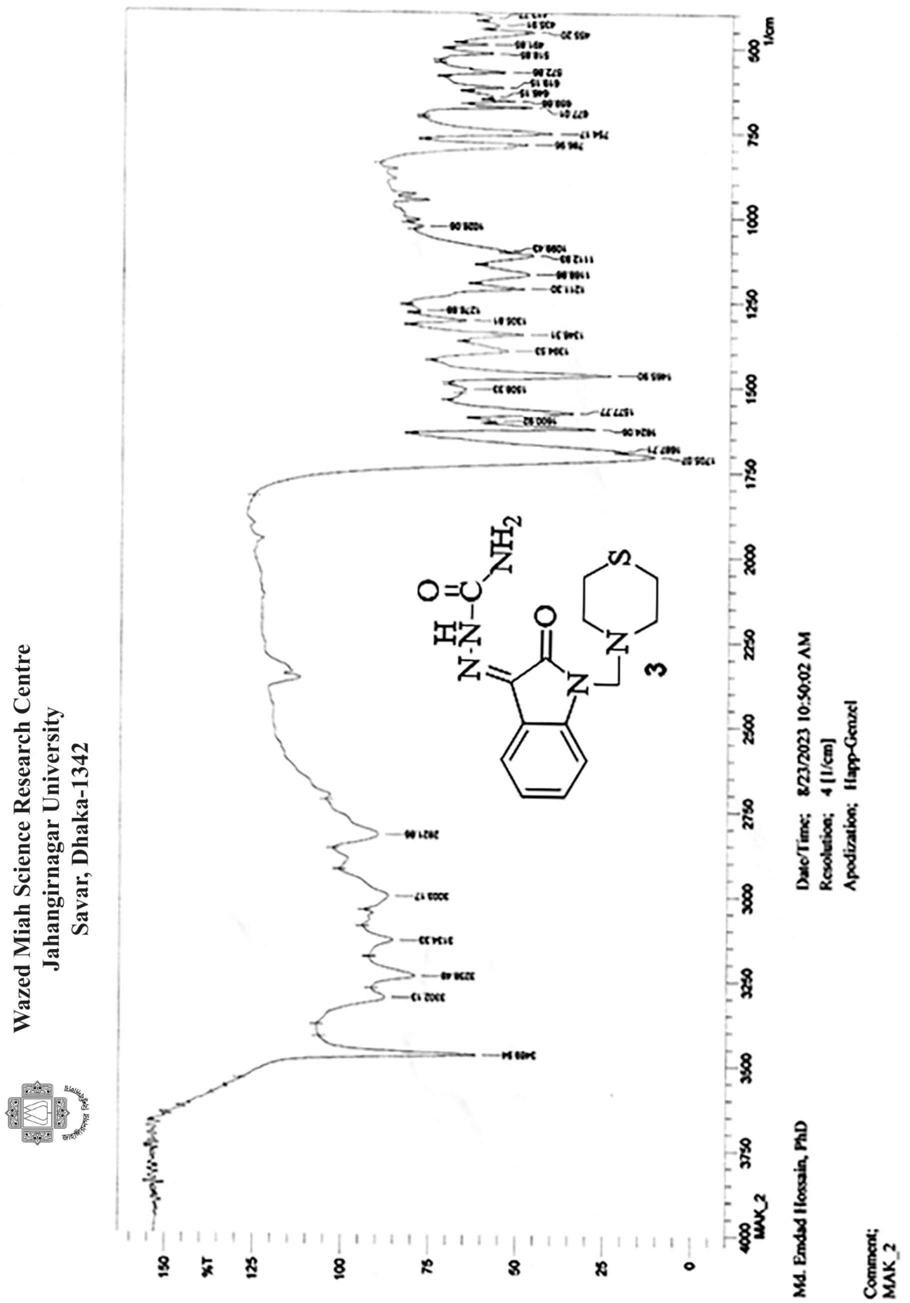
Wazed Miah Science Research Centre
Jahangirnagar University
Savar, Dhaka-1342
3
Date/Time; 8/23/2023 10:50:02 AM
Resolution; 4 [1/cm]
Apodization; Happ-Genzel
Md. Emdad Hossain, PhD
Comment;
MAK_2

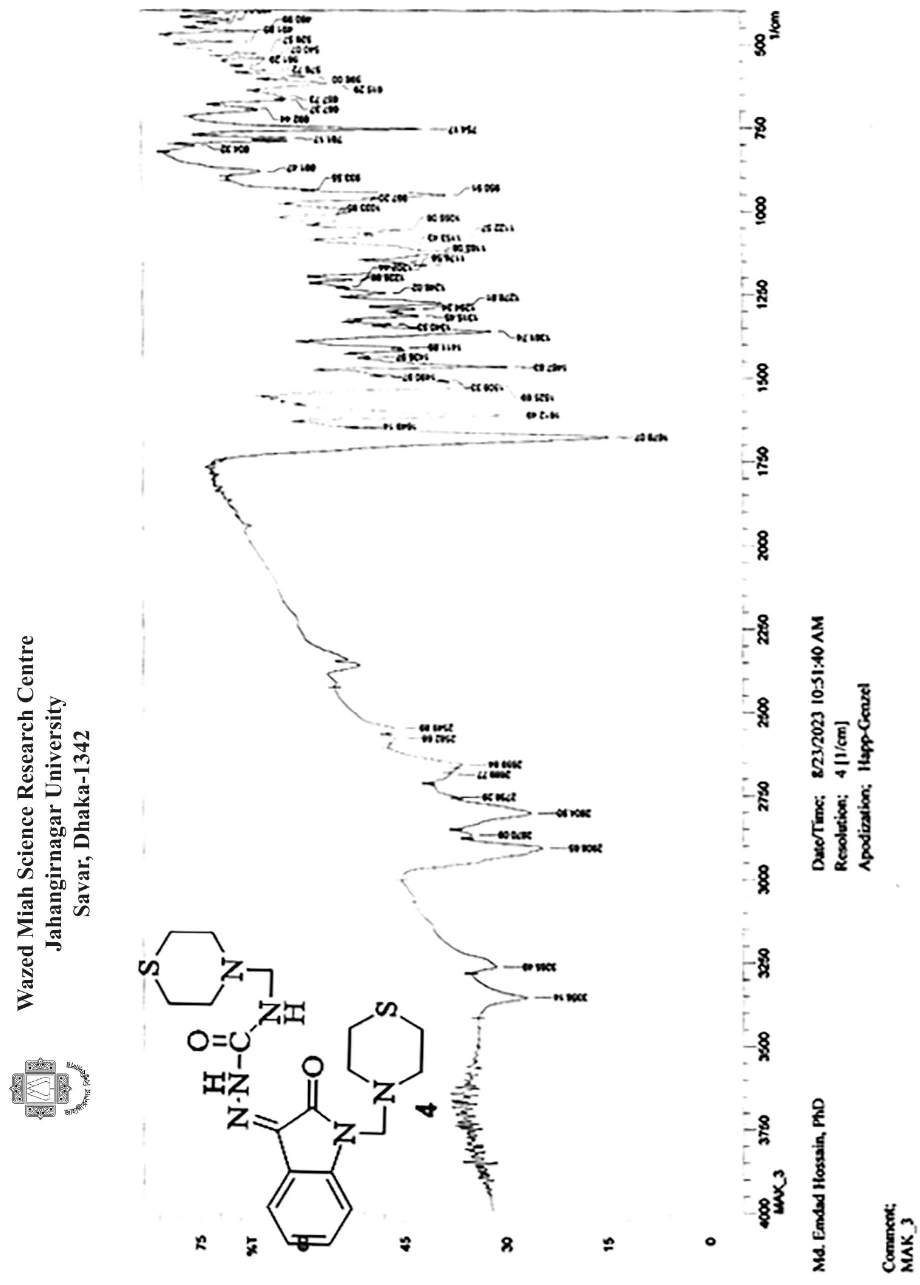
Wazed Miah Science Research Centre
Jahangirnagar University
Savar, Dhaka-1342
4
Date/Time; 8/23/2023 10:51:40 AM
Resolution; 4 [1/cm]
Apodization; Happ-Genzel
Md. Emdad Hossain, PhD
Comment;
MAK_3

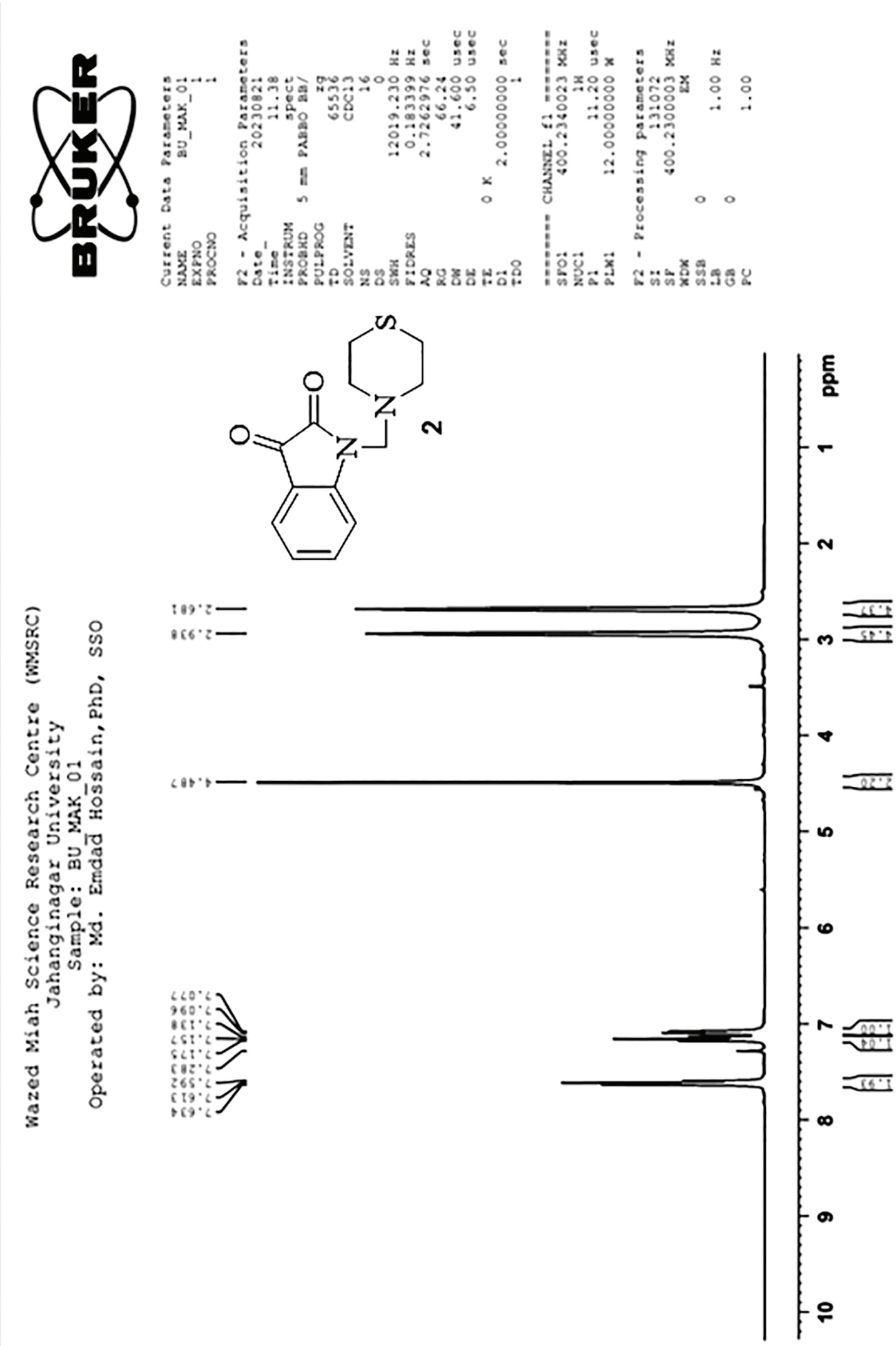
Wazed Miah Science Research Centre (WMSRC)
Jahanginagar University
Sample: BU_MAK_01
Operated by: Md. Emdad Hossain,PhD, SSO
BRUKER
2
ppm

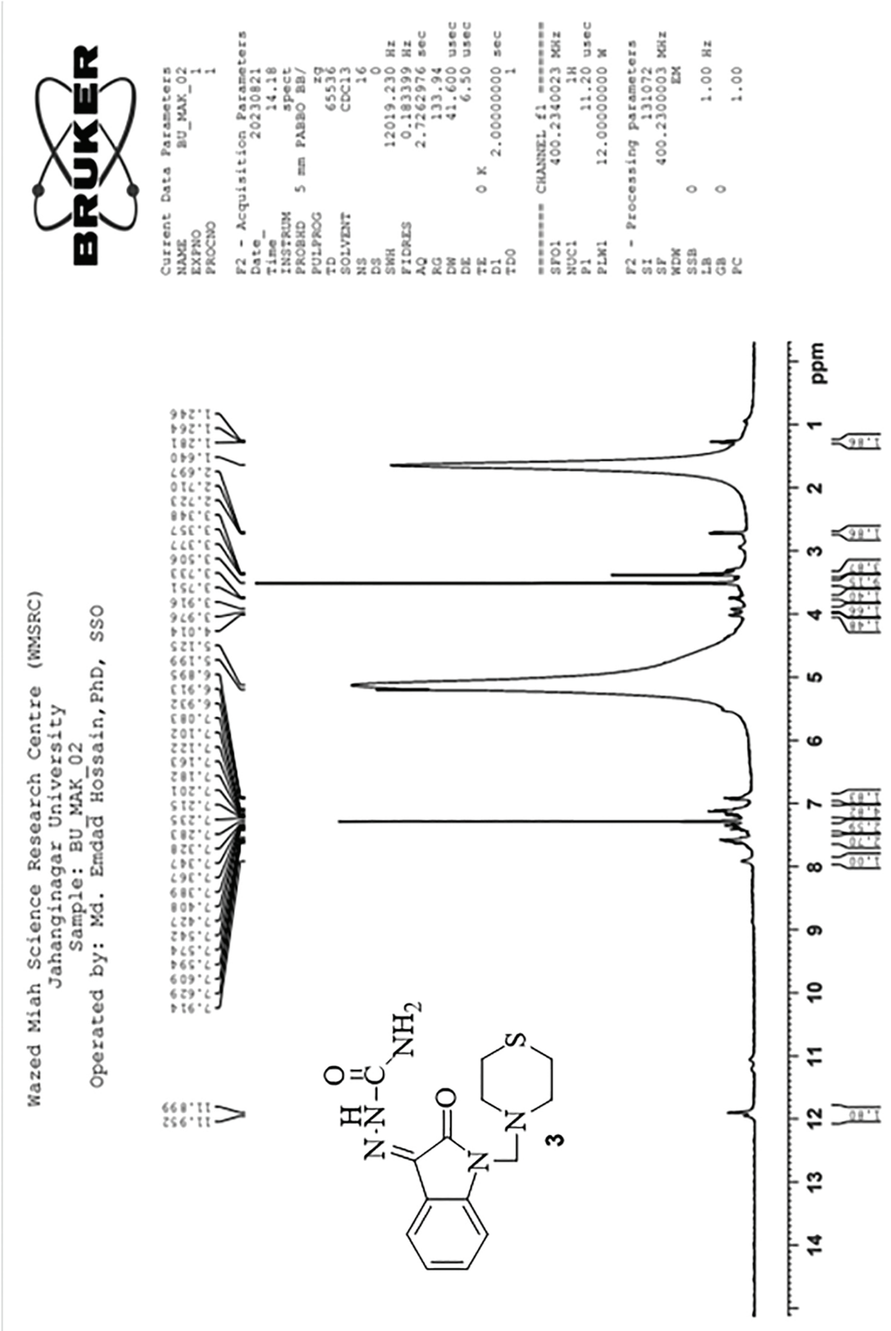
Wazed Miah Science Research Centre (WMSRC)
Jahanginagar University
Sample: BU_MAK_02
Operated by: Md. Emdad Hossain, PhD, SSO
BRUKER
ppm

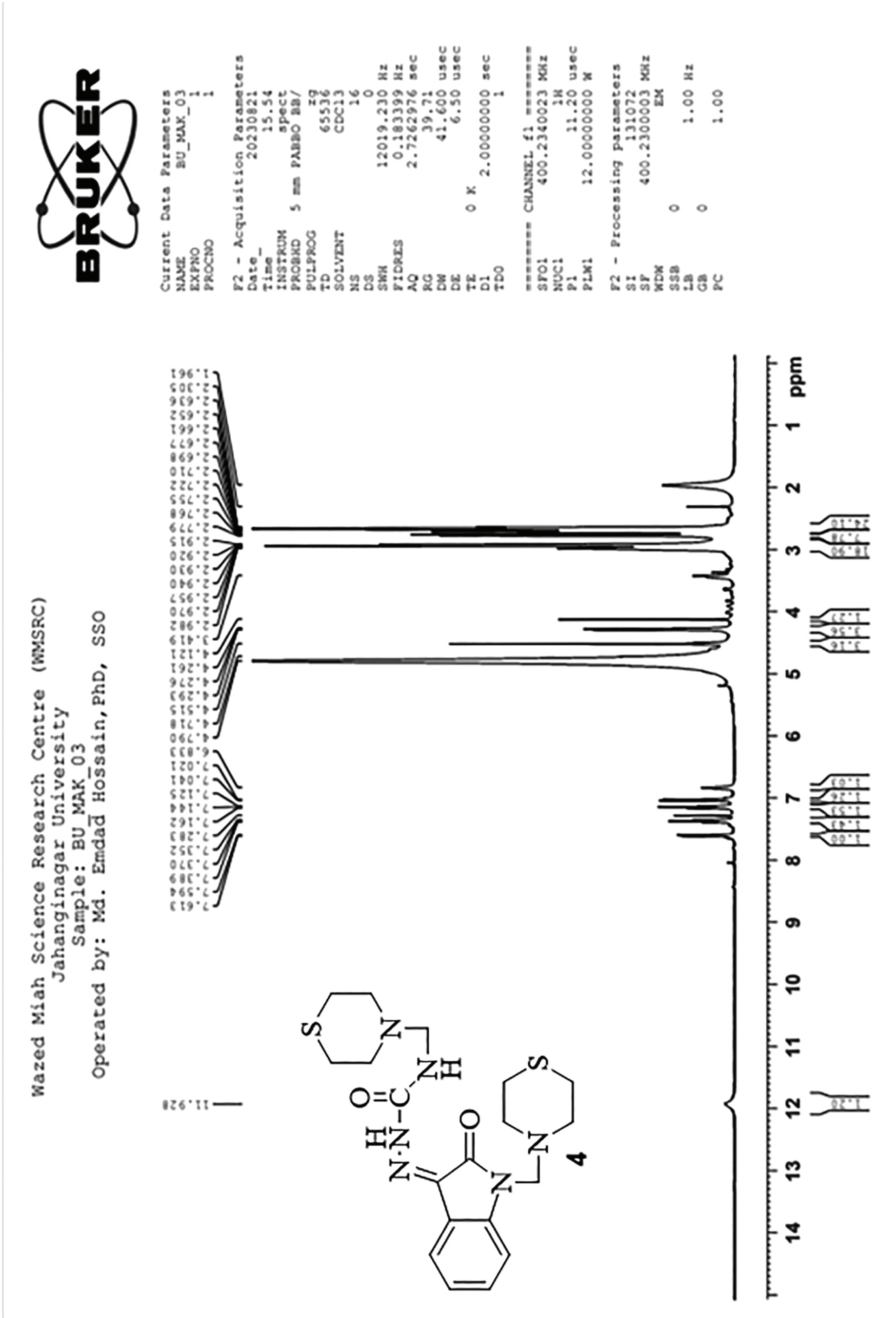

Wazed Miah Science Research Centre (WMSRC)
Jahanginagar University
Sample: BU_MAK_03
Operated by: Md. Emdad Hossain, PhD, SSO
BRUKER
4
ppm

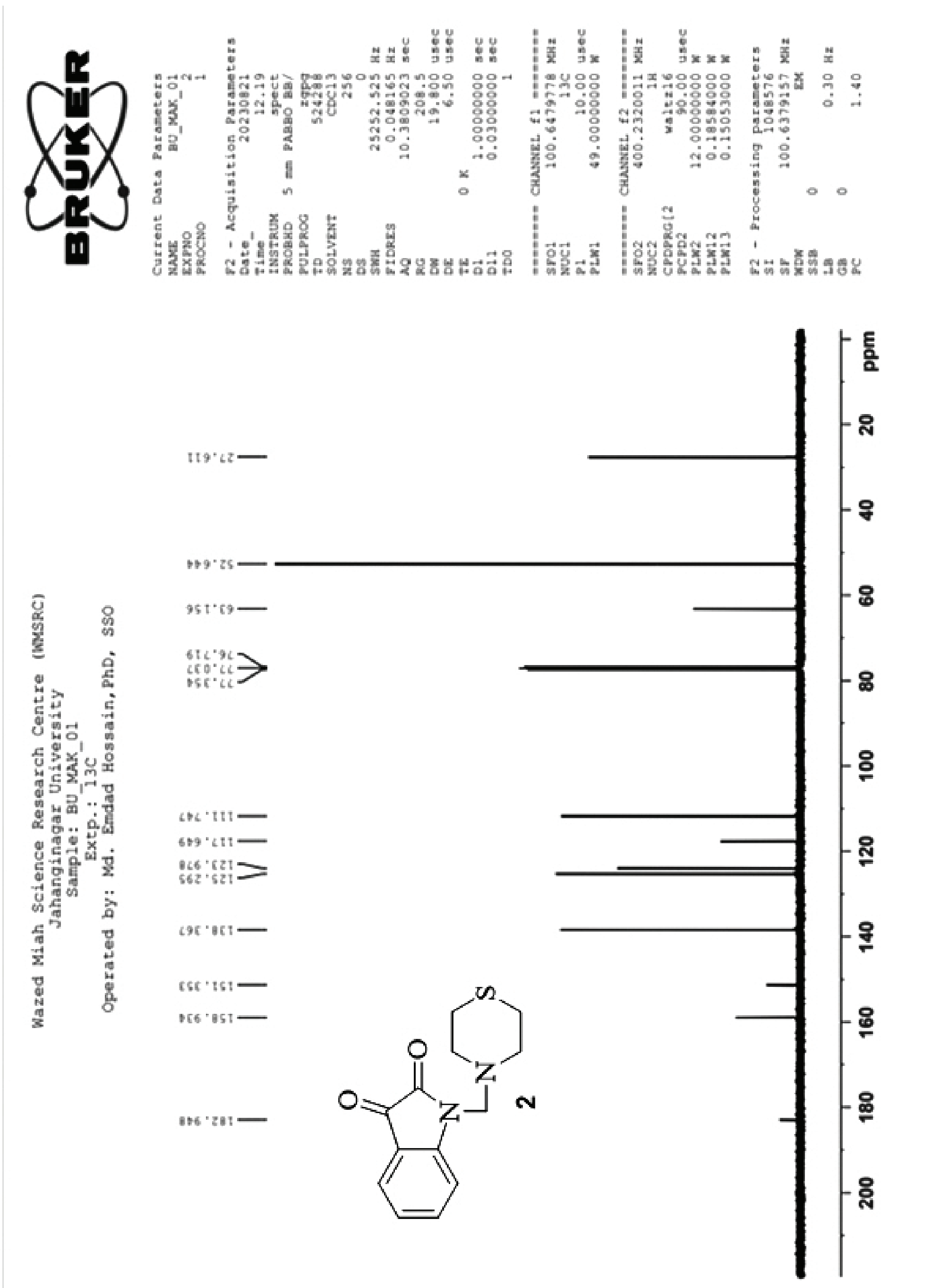
Wazed Miah Science Research Centre (WMSRC)
Jahanginagar University
Sample: BU_MAK_01
Extp.: 13C
Operated by: Md. Emdad Hossain,PhD, SSO
BRUKER
27.611
52.644
63.156
76.719
77.037
77.354
111.747
117.649
123.978
125.295
138.367
151.353
158.934
182.948
2
ppm

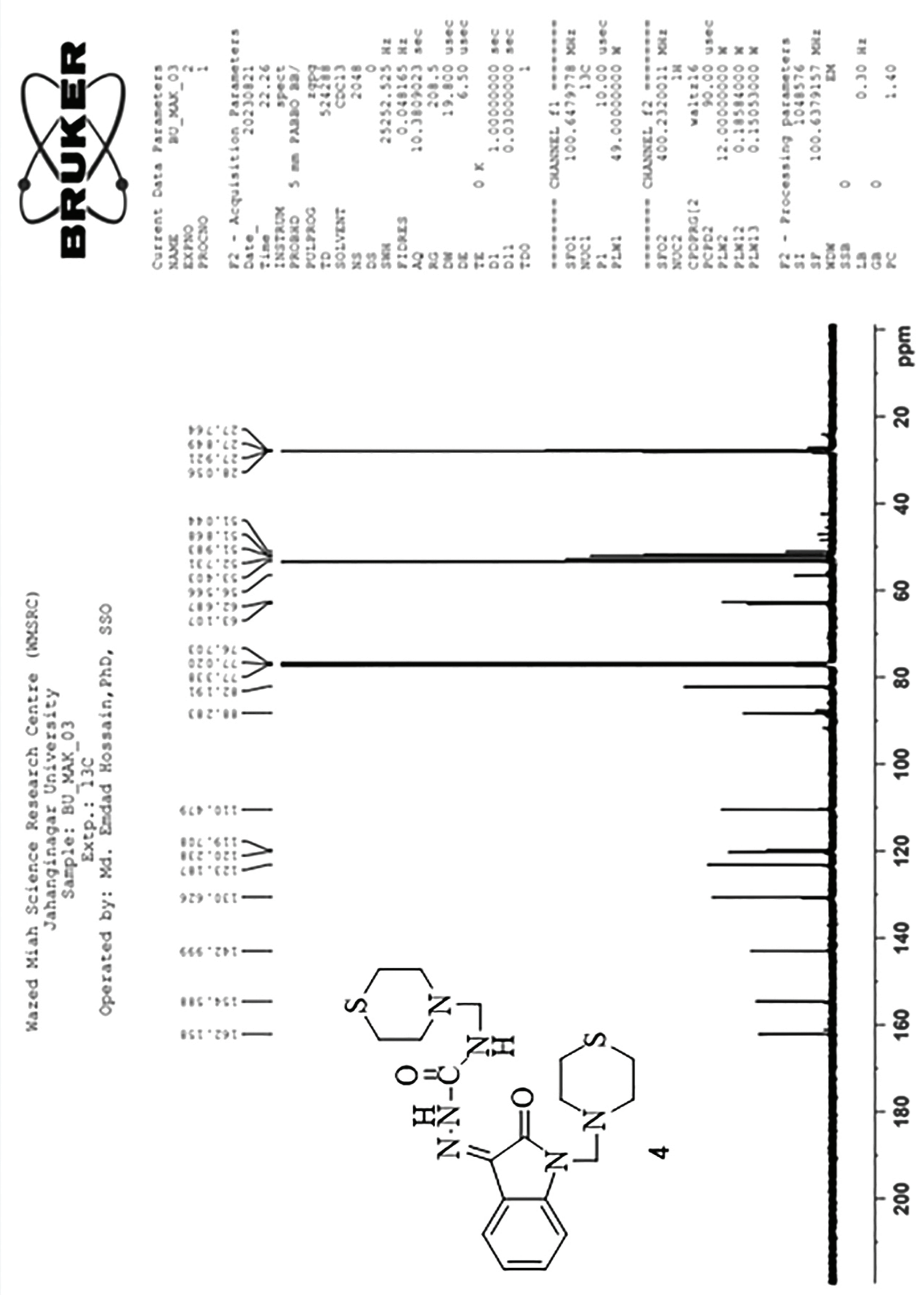
Wazed Miah Science Research Centre (WMSRC)
Jahanginagar University
Sample: BU_MAX_03
Extp.: 13C
Operated by: Md. Emdad Hossain, PhD, SSO
4
ppm

Barishal University Journal of Science and Engineering, Vol. 8: 19-45 (2023) ISSN: 2411-247X

Geochemical Characterization of Dupi Tila Formation, Sitapahar Anticline, Kaptai, Rangamati, Bangladesh: Implication for Tectonic Setting, Weathering, Climate and Provenance

Shinikdha Akter Simu[1], Mrinal Kanti Roy[1], Ayon Saha[2], Tahsin Islam Ornee[2], Raman Kumar Biswas[3], Sukhen Goswami[2] and Dhiman Kumer Roy[2,*]

[1] *Department of Geology and Mining, University of Rajshahi, Rajshahi-6205, Bangladesh.*

[2] *Department of Geology and Mining, University of Barishal, Barishal-8254, Bangladesh.*

[3] *Department of Disaster Resilience and Engineering, Patuakhali Science and Technology University, Patuakhali, Bangladesh.*

Abstract

The geochemistry of Dupi Tila sandstones from Sitapahar anticline, Kaptai, Rangamati, Bangladesh reveals several factors that have operated in the geological past. The study of major and trace elemental compositions are examined by XRF analysis to determine the integrated information that was imprinted in the sediments due to variations of several geological factors such as provenance, weathering, sorting, tectonic setting and climate in the Plio-Pleistocene period. Geochemical characteristics of the sediments show quite large variations in their elemental composition. (e.g. SiO2 ranges from 58.02 to 75.59 wt. %, Al_2O_3 11.01 to 21.17 wt. %) indicating the diacritic provenance. Geochemically sandstones are classified as litharenites to arkosic in nature with an increasing percentage of quartz. Chemical Index of Alteration (CIA*) and Weathering (CIW*) values of investigated sediments vary from 65.04 to 79.52 and 79 to 94 indicating, respectively, a low level of maturity and a significant non-steady state chemical weathering in the rising Himalayan source. The geochemical characteristics indicate a passive margin to an active continental margin setting for the Dupi Tila sandstone. Discrimination function diagrams for provenance signatures of the studied sediments using major element exhibits felsic to quartzose sedimentary provenance, which is comparable to sedimentary rocks in Bangladesh and Siwalik, India. The bulk geochemical characteristics and discrimination diagrams show that the sediment of the

study area might have been derived from both passive margin setting experiencing semi-arid to semi-humid paleoclimatic conditions during the time of deposition.

*Corresponding author.
E-mail address: dhimans14@yahoo.com

Keywords: Sitapahar anticline, Dupi Tila sandstone, Geochemistry, Provenance, Tectonic settings

1. Introduction

Geochemistry is described as the science that deals with the chemistry of the earth's composition and processes that controls the distribution of chemical elements (Schufle, 1967). Considering the Himalayan orogenic belt's history and structure, particularly the Bengal Basin, the world's deepest sedimentary basin, makes it easier to understand the tectonic development of the Indian subcontinent (Curray & Moore, 1971). The Bengal Basin has contributed much to our understanding of the history of tectonic uplift and erosion of the Himalayas and also paleo-weathering (Hossain et al., 2014). The Plio-Pliestocene Dupi Tila Sandstone Formation of Sitapahar anticline exhibits a large variation in their major element as well as trace element geochemistry. The chemical composition of detrital sediments is largely controlled by provenance (Roser & Korsch, 1986, 1988; Hayashi et al., 1997; Paikaray et al., 2008; Keskin, 2011; Roy & Roser, 2012; Roy & Roser, 2013; Hossain, 2020; and Kettanah et al., 2021) source area weathering (Nesbitt & Young, 1982; Amajor, 1987; Cox et al., 1995; Asiedu et al., 2000; Potter et al., 2005; LaMaskin et al., 2008; Parthasarathy et al., 2020; and Boruah & Laskar, 2022), maturity of sediment with climatic condition (Cox et al., 1995; Fedo et al., 1995; Armstrong-Altrin et al., 2021; and El-Sayed et al., 2022), climate (Suttner & Dutta, 1986), sorting (Dokuz & Tanyolu, 2006; and Roy & Roser, 2012), and tectonic setting of the source area and depositional basin (Bhatia, 1983; and Roser & Korsch, 1986). Various geochemical investigations on Himalayan detrital sediments have been developed and revealed some significant details about this region's history of depositional processes (Dalai et al., 2004; Sinha et al., 2007; Najman et al., 2008; Hossain et al., 2010; and Roy & Roser, 2012). Although these clastic sediments carried on a great significance, a comprehensive study of the Plio-Pliestocene Dupi Tila sediments from the Sitapahar anticline, Kaptai, Bangladesh is still inadequate. The geochemistry of sedimentary rock exhibits mainly the nature of source rock, tectonic setting and the redistribution of elements throughout deposition and since their provenance (Bhatia, 1983; and Roser & Korsch, 1986). Several detailed studies about different formation of Sitapahar anticline have been conducted but, few has been conducted to study the provenance of the Dupi Tila sediments of Sitapahar anticline based on detailed geochemical analysis. For these reasons present study deals with both major and trace elements geochemistry of the Dupi Tila sandstone of Sitapahar anticline to delineate sediment types, weathering, climate and provenance of sediments as well as tectonic settings.

2. Geological setting

Bangladesh is wholly covered by sedimentary rocks with varying thickness according to the depth of the depositional basin, which is also known as the Bengal Basin. The Bengal Basin is an example of a basin that is distinguished by being asymmetrical and having a significant rise in sediment thickness toward the southeast (Curray & Moore, 1971). Tectonically the study area belongs to eastern gentle sub-zone of the folded flank of the Bengal Basin (Khan, 1991) and the structure is also located in the western region of the Bengal Basin's folded flank of Chittagong and the Chittagong Hill Tracts. The Chittagong Hill Tracts are considered to be the westernmost extension of the folded Arakan-Yoma belt, and the regional strike extends from NNW to SSE. The axis of the anticline is trending about N15°W-S15°E with a plunge of 8°. The amount of dip of the strata in both flanks varies from 4°-62° towards northeast and southwest respectively, occasionally, which rises to about 84°. In the study area, no fault has been found. Dips and strikes of the Sitapahar anticline indicate the asymmetric nature of the fold that extends along NNW-SSE direction and it can be subdivided into two parts as eastern flank and western flank. The western flank has steep slope and faulting, whereas the eastern flank is characterized by gentle slope. In the eastern flank the average amount of dip is about 30° to NE direction. The study area is characterized by an unconformity, which is found between Girujan Clay Formation and Dupi Tila Formation. Geographically, the investigated area of the Sitapahar anticline is situated in the Rangamati district of Bangladesh. It is about 70 km (N-S) long and 12 km (E-W) wide and covers about 550 sq. km of Rangamati district.

The study area is limited by 22°29' N to 22°31' N latitude and 92°10' E to 92°14' E longitude respectively (Fig 1). The study area is well communicated to Chittagong and Rangamati by road and by waterways.

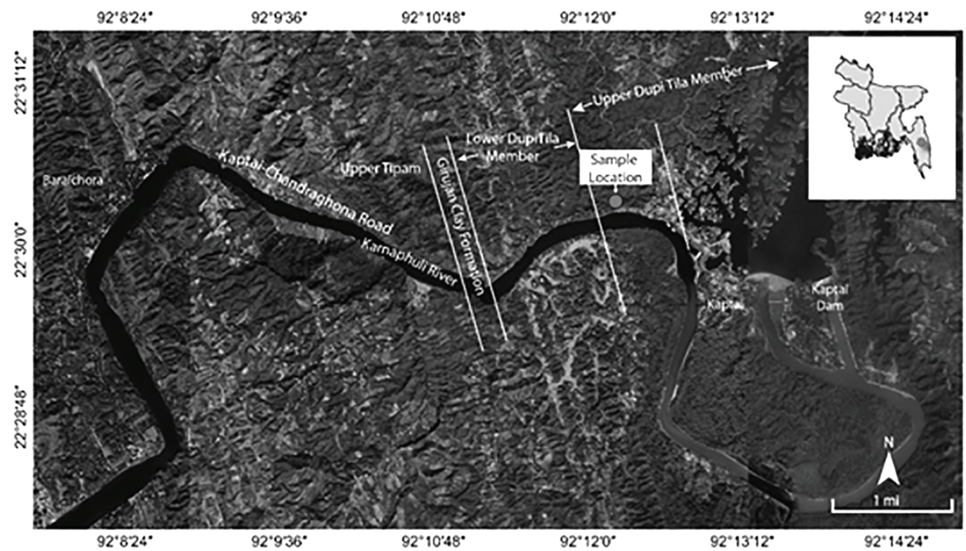

Fig 1. Study area map of Kaptai and Kaptai-Chandraghona road cut section.

3. Sampling and method

Eighteen samples has been collected from different stations of the Chondraghona-Kaptai road cut section in the Dupi Tila Sandstones Formation, Sitapahar anticline. The collected

samples were kept in polyethene bags, and the wet samples were dried over the period of two to three days mostly using sunshine.18 samples were collected in total, however only 10 of them were examined using an X-Ray Fluorescence spectrometer (XRF) (Fig 2).

Each sample was crushed into a fine powder in a planetary ball mill for 20 minutes under well-mixing conditions (PM-200, Retsch, Germany). The finely powdered sediments were dried in an oven. The dry powder samples were homogenized for two minutes with a binder (stearic acid: sample at a ratio of 1:10). The mixture was then poured into an aluminum cap (30 mm). Using a manual hydraulic press with a pressure of 10-15 ton/sq. inch for two minutes, the cap was compressed between two tungsten carbide pellets, and then the pressure was gradually released.

The X-ray analysis of the pellet may then begin. The elements were identified using the X-ray fluorescence spectrometer (XRF) method at the Institute of Mining, Mineralogy and Metallurgy, Joypurhat, by using the Rigaku ZSX Primus XRF machine equipped with an end window of 4 kW Rh-anode X-ray tube, in accordance with the procedures of (Goto and Tatsumi, 1994).

From geochemical data (Table 2), different plots and diagrams are constructed by using major oxides.

Table 1. Generalized stratigraphic succession of the Bangal Foredeep (the Basinal area and the Chittagong Tripura Folded Belt), (Modified after Muminullah, 1978)

Age	**Group**	**Formation with thickness (m)**		**Lithology**	**Depositional Environment**
		Basinal Area	**Chittagong FB**		
Plio-Pleistocene		Dihing (400-800)	Dihing	Boulder beds, sandstone & clay	Peidmont deposit
Pliocene	Dupi Tila	Upper Dupi Tila (1000-2800)	Dupi Tila (758-900)	Claystone, siltstone, sandstone	Alluvial fan
		Lower Dupi Tila (500-930)		Sandstone and conglomerate	
Middle to Upper Miocene	Tipam	Girujan Clay	Girujan clay	Clay, shale, mudstone with vegetal matter	Flood plain
		Tipam sandstone	Tipam sandstone (total thickness 1200m)	Reddish, Yellowish and brownish Cross-bedded sandstone with subordinate shale	Channel deposit

Such as SiO_2 vs Log (K_2O/Na_2O), $Al_2O_3/(CaO+Na_2O)$ vs Fe_2O_3+MgO, wt% of K_2O vs wt% Na_2O, Al_2O_3 vs TiO_2, log (SiO_2/Al_2O_3) vs log (Na_2O+K_2O), Fe_2O_3+MgO vs TiO_2, Fe_2O_3+MgO vs Al_2O_3/SiO_2, Fe_2O_3+MgO vs K_2O/Na_2O, log (SiO_2/Al_2O_3 vs log ($Fe_2O_3+K_2O$), Al_2O_3 vs TiO_2 plots are drawn. Plots are also done by using discrimination factors F_1, F_2 and

$$CIA^* = 100 \times [Al_2O_3/ (Al_2O_3+CaO^*+Na2O+K2O],$$

$$CIW^* = 100\times [Al_2O_3/ (Al_2O_3+CaO^*+Na2O)] \text{ and}$$

$$ICV = [(Fe_2O_3^*+K_2O+Na_2O+CaO+MgO+MnO+TiO_2)/Al_2O_3].$$

Total iron is $Fe_2O_3^*$, while CaO^* solely indicates the quantity found in silicates. In this study, the CaO is adjusted using a new approach developed McLennan et al., 1993. According to this methodology, CaO values are only accepted if $CaO<Na_2O$, and when $CaO>Na_2O$, it is assumed that the concentration of CaO is the same as that of Na_2O. P_2O_5 was used to adjust the CaO concentration for apatite (CaO^*=-CaO-($10/3^*P_2O_5$)).These plots may be used to determine the paleoclimate of the source re gion and recreate the relationship between provenance and tectonic setting of the depositional basin.

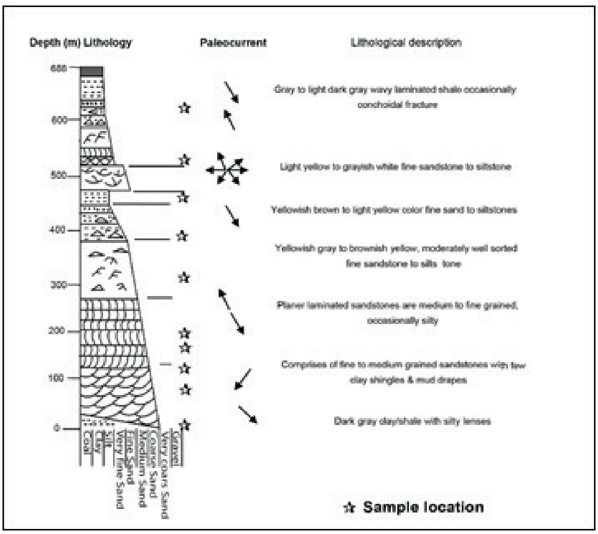

Fig 2. Concise lithosuccession with paleocurrent, lithological description and sample location.

4. Results

The major and trace element composition of 10 representative sandstone samples were selected for analysis and all the compositional values of sediment from Dupi Tila Formation, Sitapahar Anticline (Eastern Flank), Kaptai, Rangamati Hill District, Bangladesh are reported in Table 2.

Major Oxides and Trace Element Geochemistry

The bulk geochemical compositions of the sediment relatively exhibit large variations, especially SiO_2 from 58.02 wt.% (LDMS1) to 75.59 wt.% (LDMS5) (average ~66.38 wt.%) and Al_2O_3 from 11.01 wt.% (LDMS8) to 21.17 wt.% (LDMS1) (average ~15.51 wt.%) (Table 2).

Table 2. Major element (wt.%) and trace element (ppm) abundances and CIA*, CIW*, ICV, F_1, F_2 value of the investigated Dupi Tila sediment samples, Kaptai, Rangmati.

Oxide (wt%)	LDMS 1	LDMS 2	LDMS 3	LDMS 4	LDMS 5	LDMS 8	LDMS 9	LDMS 10	LDMS 12	UDMS 17	Mean	UCC	PAAS
SiO_2	58.02	74.97	69.00	59.00	75.59	73.40	70.86	61.23	61.56	60.17	66.38	66.00	62.80
Al_2O_3	21.17	11.70	14.39	20.32	11.08	11.02	12.96	17.56	17.17	17.78	15.51	15.20	18.90
CaO	1.07	1.70	1.51	0.93	1.41	1.68	1.72	1.26	2.78	3.20	1.73	4.20	1.30
Fe_2O_3	9.36	4.61	7.26	10.43	5.48	5.65	6.47	11.10	8.23	8.18	7.68	4.50	6.50
K_2O	4.41	2.91	3.13	4.16	2.76	3.15	3.12	3.85	4.42	4.68	3.66	3.40	3.70
MgO	3.13	1.07	1.60	2.36	1.07	1.74	1.60	2.04	2.70	3.00	2.03	2.20	2.20
Na_2O	0.98	1.70	1.18	0.93	1.37	1.50	1.43	0.91	1.36	1.25	1.26	3.90	1.20
TiO_2	1.03	0.54	0.79	1.00	0.48	0.62	0.73	0.96	0.88	0.88	0.79	0.50	1.00
P_2O_5	0.19	0.10	0.13	0.24	0.14	0.13	0.16	0.32	0.18	0.18	0.18	0.17	0.16
MnO	0.15	0.07	0.11	0.21	0.09	0.08	0.09	0.16	0.13	0.15	0.12	-	-
Element (ppm)													
F	1287.00	0.00	0.00	788.00	0.00	1149.00	0.00	0.00	0.00	734.00	989.50	-	-
S	401.20	52.50	84.97	80.96	73.35	127.05	64.93	97.39	160.32	232.06	137.49	-	-
Cl	152.00	235.00	1157.00	190.00	170.00	956.00	1606.00	350.00	534.00	247.00	560.00	-	-
Cr	498.78	3090.53	3872.57	781.36	2681.38	4287.19	3547.57	2378.27	1889.07	991.41	2401.80	35.00	110.00
Co	0.00	0.00	0.00	0.00	0.00	0.00	0.00	36.95	0.00	30.56	33.75	10.00	23.00
Ni	124.94	115.51	156.37	126.51	69.15	93.51	103.73	165.80	118.66	96.65	117.08	20.00	55.00
Cu	74.29	0.00	40.74	67.10	0.00	0.00	0.00	0.00	80.68	72.69	67.08	-	-
Zn	129.33	42.57	70.69	133.35	43.38	48.20	65.87	110.05	117.28	106.84	86.75	-	-

Ga	40.92	0.00	0.00	0.00	0.00	0.00	0.00	0.00	0.00	0.00	40.92	-	-
As	31.81	0.00	0.00	0.00	0.00	0.00	0.00	0.00	37.87	0.00	34.84	-	-
Rb	219.46	99.67	135.33	199.34	91.44	119.79	128.02	182.88	214.89	240.49	163.13	112.00	160.00
Sr	158.02	194.35	177.45	163.09	157.17	153.79	175.76	172.38	198.58	217.17	176.80	350.00	200.00
Y	121.27	0.00	96.07	94.49	0.00	75.59	77.17	126.78	114.18	156.70	107.78	22.00	27.00
Zr	158.42	142.88	277.61	196.92	123.63	285.02	276.13	231.71	198.40	207.28	209.80	190.00	210.00
Ba	608.01	533.69	630.40	638.46	430.71	481.75	565.93	669.80	640.25	703.83	590.28	550.00	650.00
*CIA**	78.45	66.11	77.68	79.52	68.59	65.04	69.26	78.03	70.61	71.21	72.45	57.00	75.00
*CIW**	94.00	79.00	86.00	86.00	83.00	80.00	83.00	94.00	86.31	87.65	85.89	-	-
ICV	0.95	1.07	1.08	0.98	1.14	1.31	1.17	1.15	1.19	1.20	1.12	1.30	0.80
F_1	0.11	-2.70	-0.94	1.81	-2.47	-3.87	-2.03	1.77	-1.03	-1.26	-	-	-
F_2	-2.65	-0.78	-2.28	-2.59	-1.89	-1.78	-1.76	-2.93	-0.89	-0.78	-	-	-

Abbreviations: CIA*- Chemical Index of Alteration (wt %); CIW*- Chemical Index of Weathering (wt.%); ICV- Index of Compositional Variability (wt.%); UCC- Upper Continental Crust; PAAS- Post-Archean Australian Shale(Taylor & McLennan, 1985); (Condie, 1993).

The variation of SiO2 exhibits a continuous increasing trend with increasing depth. The Amount of SiO2 in the studied sample shows the same or nearly higher than the mean value of Upper Continental Crust (UCC) (Taylor & McLennan, 1985; McLennan, 2001; and Rudnick et al., 2003).

Al2O3 is the second most abundant element in the analyzed samples. Harker variation diagrams show clear separate trends in major oxides in Dupi Tila Formation. The characteristics of themajor oxide (e.g. MgO, Al2O3, K2O, TiO2, Fe2O3, TiO2 and MnO) shows a strong linear negative trend with SiO2 and only CaO, Na2O show positive linear trend with SiO2 (Fig 4a).

MgO, K2O, TiO2, MnO, Fe2O3, and P2O5 reveal positive/increasing correlations with Al2O3 (Fig 4b), whereas CaO exhibits a negative correlation with Al2O3 (Fig 4b) suggesting major influences of hydraulic fractionation (Roy & Roser, 2012). In the compositional variation of major oxides, it is remarkable that the value of K2O is higher than CaO/ K2O that of which is comparatively high with a greater value (2.76 wt. % to 4.68 wt. %), indicating the presence of alkali feldspar with some carbonate minerals. The average K2O (3.66 wt. %) contents are similar to the UCC and to that of the Post Archaean Australian Shales (PAAS) (Taylor & McLennan, 1985) (Table 2). The lower content of Na2O sediments is depleted to the UCC and is mostly similar to PAAS. In that time the average content of K2O is about 3.66% and the highest and the lowest values of K2O are 4.68% (UDMS17) and 2.76% (LDMS5) respectively, those values are relatively higher than UCC and slightly depleted to PAAS (Taylor and McLennan, 1985; and Condie, 1993). The low degree of maturation of the sediments is indicated by the ratio Na2O/K2O (0.22 to 0.58) of sediments which is comparatively low (Pettijohn et al., 1972; Roser and Korsch, 1986; Fedo et al., 1995; Paikaray et al., 2008; and Hossain et al., 2014). The studied sediments also have a higher amount of TiO2 (avg. 0.79 wt. %) values compared to UCC (Taylor and McLennan, 1985; and Condie, 1993), which shows that the source rocks had more felsic to intermediate igneous material. The average P2O5 level in the samples is 0.17 wt. %, which explains why there are less accessory phases such apatite and monazite than in UCC (Condie, 1993).The SiO2/Al2O3 ratios display a higher value (2.74 to 6.82 wt. %), which is indicative of the excess quartz and feldspar content (Potter, 1978; and I. Hossain et al., 2014).

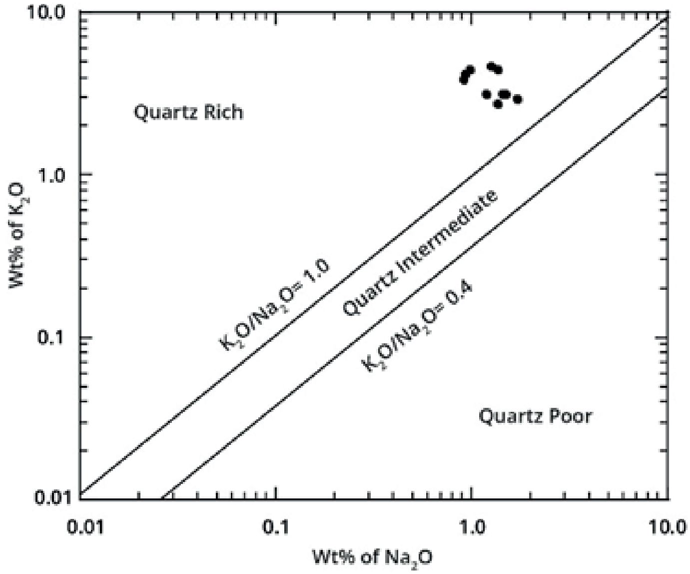

Fig 3. Geochemical classification of Dupi Tila Formation, Sitapahar anticline, Kaptai, according to the richness of quartz (After Crook, 1974).

Fifteen trace elements have been found in ten studied samples which are F, S, Cl, Cr, Co, Ni, Cu, Zn, Ga As, Rb, Sr, Y, Zr, and Ba. Among all the trace element, especially the transition element (Cr and Ni) shows higher concentration, varies from (499 to 4287) ppm and (69 to 166) ppm respectively than the mean values of UCC (Condie, 1993) and PAAS (Taylor and McLennan, 1985) the examined sediments had a lower level of Co (0 to 37) ppm. ppm (Table 2).The trace element contains an average amount of the large ion lithophile elements (LILE) and high field strength elements (HFSE) viz. Rb (avg. 163.13), Sr (avg. 176.8), Zr (avg. 209.80), and Ba (avg.590.28) ppm, reflect higher concentrations than average upper crustal composition and lower than PAAS (Taylor and McLennan, 1985). With Al2O3 a few trace elements (e.g. Ba, Rb, Ni) indicate both linear and scattered positive trends (Fig 4c), especially Rb (r = + 0.94) verifying clear hydrodynamic fractionation (Roy and Roser, 2012).

The studied Dupi Tila sediments reveal similar and higher concentrations in most of the major and trace elements in comparison to the UCC (Taylor and McLennan, 1985) (Table 2). The abundance of SiO2 and Cr suggests that chemical weathering resulted in the hydrodynamic removal of more soluble elements from the clastic fractions than insoluble elements (Nagarajan et al., 2015). These relative depletions or enrichments of various compositional elements are widely acceptable for weathering conditions and provenance characteristics (Etemad-Saeed et al., 2011; and Hossain et al., 2014).s

5. Discussions

The geochemistry of Dupi Tila sediments from Sitapahar anticline, Kaptai, Rangamati, Bangladesh reveals several factors that have operated in the geological past.

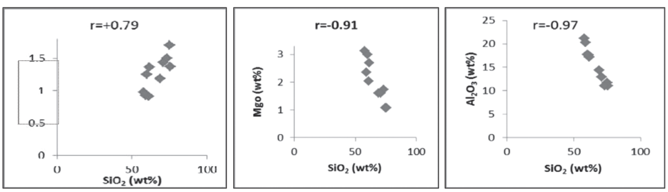

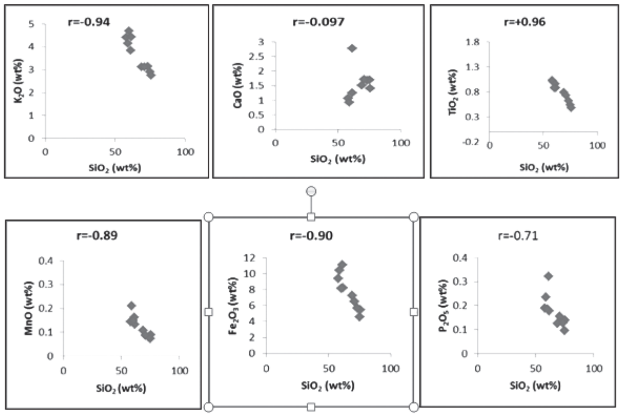

Fig 4a. Harker variation diagram of major oxides with SiO_2 for investigated sandstones from the Bengal Basin.

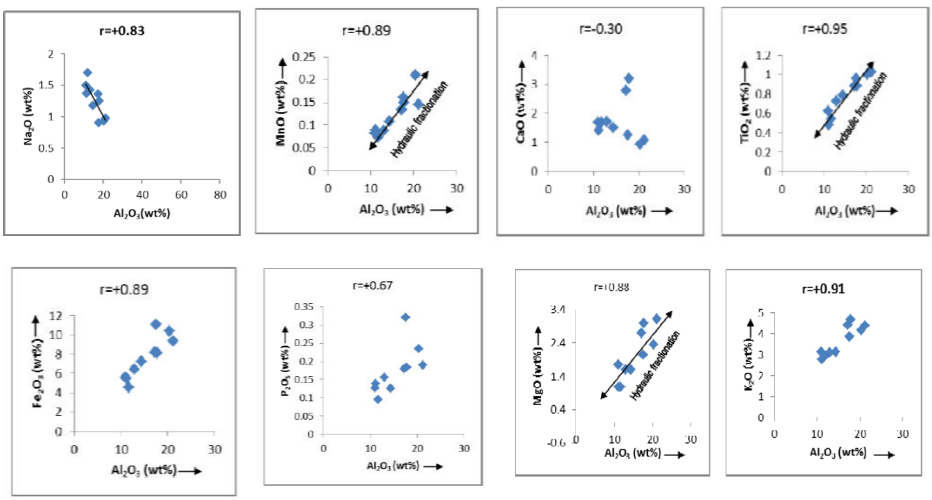

Fig 4b. Harker variation diagram of major oxides with Al_2O_3 for investigated sandstones from the Bengal Basin.

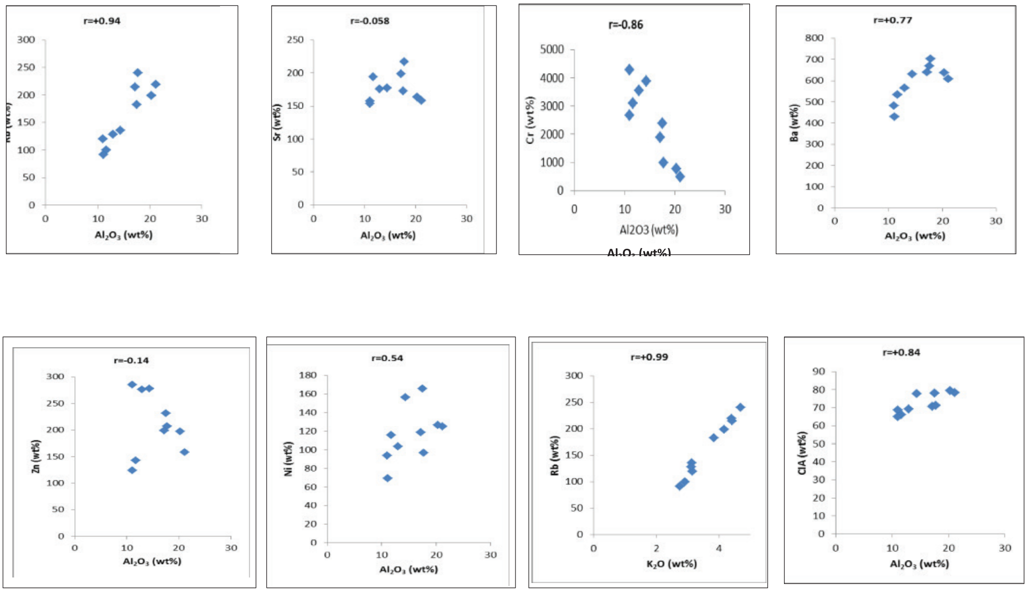

Fig 4c. Harker variation diagram of Trace element with Al_2O_3 and K_2O and Al_2O_3 with CIV value for investigated sandstones from the Bengal Basin.

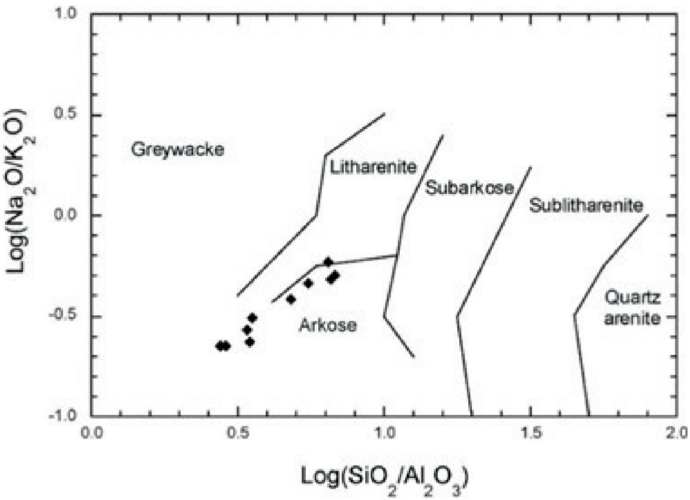

Fig 5. Geochemical classification diagram of investigated Dupi Tila Sediments, log (Na2O/K2O) vs. log (SiO2/Al2O3) (after Pettijohn et al., 1972).

(Nesbitt and Young, 1982) and also calculating by the chemical index of weathering (CIW*).

In this equation CaO* represents the amount of CaO, that incorporates in the silicate phases. Nesbitt and Young (1982) proposed a CIA value ranges from 50 to 60 indicates an incipient weathering, 60 to 80 an intermediate weathering and CIA>80 extreme weathering whereas low values (i.e. 50 or less) indicate unweather source areas. The calculated CIA* values vary from 65.04 to 79.52 with an average of 71.46. This high value of CIA* indicates moderate to intensive weathering conditions in the source area of the Dupi Tila sediments and this value is higher than that of the CIA value (57) of UCC. The CIW* values of the studied samples vary from 79 to 94 with an average value of 85.89, which indicates moderate to strong weathering (recycling) for these samples. These results are also supported by the index of compositional variability (ICV). The maturity of the sediments can be evaluated by the index of compositional variability (ICV) (Cox et al., 1995). Higher values indicate plagioclase, K-feldspar, amphiboles, and pyroxenes, whereas values of ICV <0.84 indicate minerals like kaolinite, illite, and muscovite. The average value of the index of compositional variability (ICV), which ranges from 0.95 to 1.31, is 1.11 (Nesbitt and Young, 1982; Fedo et al., 1995; and Cox et al., 1995).

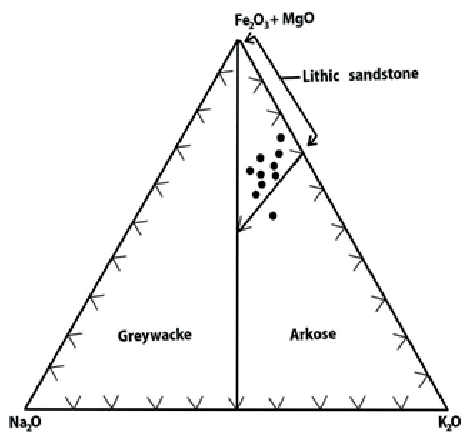

Fig 6. (Fe2O3+MgO) −Na2O−K2O classification diagram for the sediments from Sitapahar anticline, Kaptai, Bangladesh (Blatt et al., 1980).*

The high concentration of iron oxide (Fe2O3) is indicative of oxidation of the Dupi Tila Formation, Kaptai. The low content of Na2O (av. 1.26 wt.%) of studied samples also indicates intensive to moderate weathering of the source rock.

A plot of CIA vs ICV (Cox et al., 1995; Potter et al., 2005; and LaMaskin et al., 2008) can be used to determine how the nature of the source rock and the degree of weathering relate to one another. From that plot (Fig 7) it can be seen that most of the studied samples indicate moderate chemical weathering in the source area and minor sedimentary recycling for the studied samples. Their intermediate type source as granite (Jacobson et al., 2002) emphasized the rise in chemical weathering, which may indicate a decline in tectonic activity or a change in the climate toward warmer, more humid conditions. The climatic conditions that occurred in the source area were established using the relation between SiO_2 and (Al_2O_3+K_2O+Na_2O) (Suttner and Dutta, 1986). In this plot, it is revealed that all the samples lie inside of semi-arid to semi-humid condition with SiO_2 (Fig 8).

The TiO_2 vs Al_2O_3 plot shows that most of the samples of Dupi Tila Formation directly evolved or came as a by-product of granitic and basaltic source rock weathering (Amajor, 1987) (Fig 9).

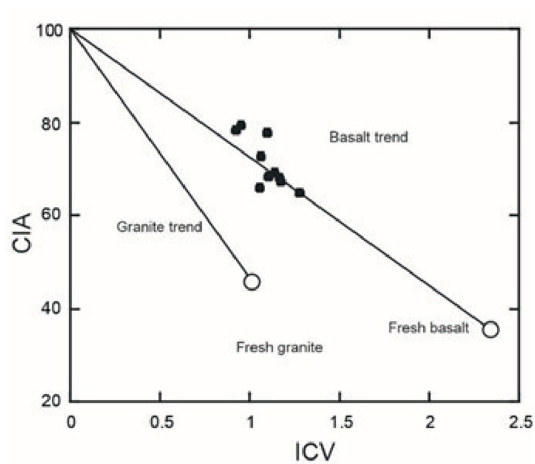

Fig 7. CIA vs ICV plot for Dupi Tila sandstone of Sitapahar anticline (after Cox et. al., 1995; Potter et. al., 2005; and LaMaskin et. al, 2008).

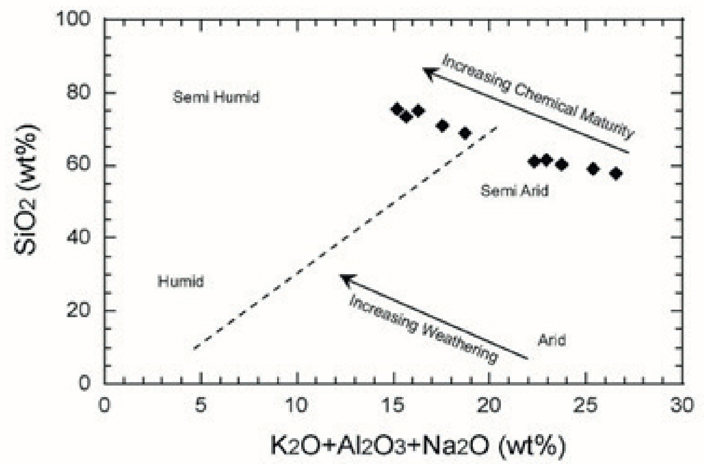

Fig 8. Bivariate plot of SiO2 vs (Al2O3+K2O+Na2O) to determine the chemical maturity and paleoclimatic conditions of the Dupi Tila Formation (after Suttner and Dutta, 1986).

Following Nesbitt and Young (1982) in the Al_2O_3-(CaO^*+Na_2O)-K_2O (A-CN-K) molecular proportion diagram (Fig 10), the analyzed samples spell away from the plagioclase-alkali feldspar tie line and very close to clay mineral and mica group line, indicating extensive weathering conditions also. The moderate concentration of SiO2 (58.02 to 75.59 wt. %) in terms of showing quartz dominance in sediments, and the ratios of K_2O/Na_2O are > 1, showing quartz abundance in the sediments. The variation in medium Al_2O_3 content (11.69 wt. % to 21.16 wt. %) indicates clay minerals input rather than feldspar that are less frequently present in the samples. In such cases, most of the weathering indicates intensive weathering. Additionally, the degree of source-rock weathering is also determined by the Rb/Sr ratio of sediments (McLennan et al., 1993). The average Rb/Sr ratio of the investigated sediments is 0.92, which is much higher than the average for the upper continental crust (0.32) and PASS (0.80; McLennan et al., 1993). These important results show that source area weathering was likely more severe than poor weathering (Asiedu et al., 2000).

Interbedded shales from the Dupi Tila Formation show a higher CIA value (~65-78) that is comparable with the interbedded shale's CIA values of Surma Group (~70-78) (Rahman & Faupl, 2003).

All the results, CIW, CIA*, ICV values, the concentration of iron that preserved in the ferric state, and SiO2 vs (Al2O3+K2O+Na2O) suggest that the sediments in the source area were derived by an extensive weathering process and there prevailed semi-arid to semi-humid climatic condition.

5.3 Sorting of the studied sediment

The degree of sorting is determined by the source to sink distance, the energy of the transport system, a number of other factors, and the geochemical variation produced by sorting among sand, silt, and clay connected to the separation of these grains by hydraulic fractionation (DoKuz and Tanyolu, 2006; and Roy and Roser, 2012). Harker variation diagrams are so useful to evaluate sorting effects and their degrees of such sediments. The major oxides versus Al2O3 plots (Fig 4b) suggesting poor linear trend except K2O (r =+.91), TiO2 (r = +.95), MnO (r = +.89) exhibiting positive trends that explain how mineral sorting increased fractionation. The ICV value of studied Dupi Tila varies from 0.95 to 1.19 with an average of 1.12, indicating that they are not compositionally mature (Cullers, 2000); with decreasing ratio of SiO2/Al2O3 in the range of (25.74 to 6.82) and as the grain size increases, the sediment's maturity and recycling rate both decline. The strong relationships between the CIA and other

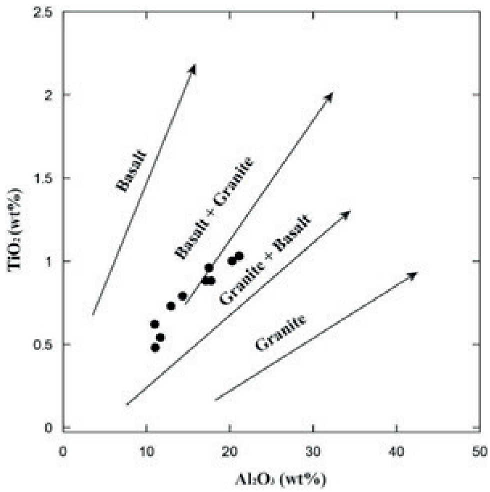

Fig 9. TiO2 vs Al2O3 diagram adopted from (Amajor, 1987) showing the source rock of Dupi Tila sandstone of Sitapahar anticline, Kaptai.

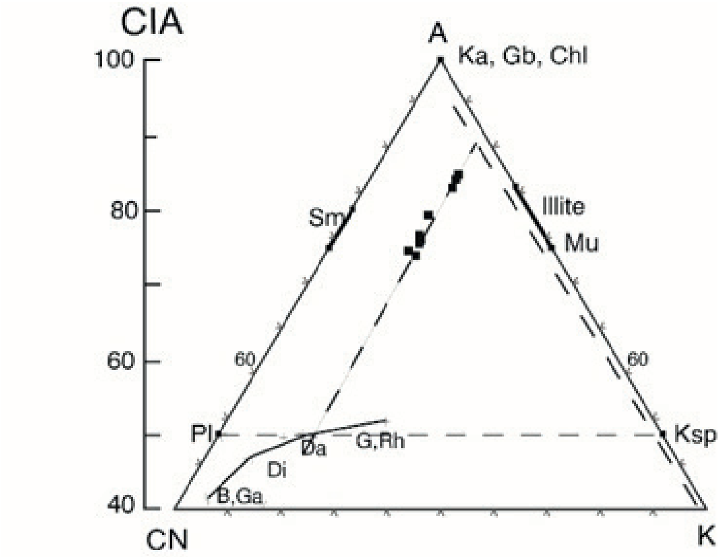

Fig 10: Al_2O_3-(CaO^*+Na_2O)-K_2O (A-CN-K) diagram for the investigated sediments of the Dupi Tila Formation (after Nesbitt and Young, 1982).

components, such as CIA–Al_2O_3 (r=+0.84) (Fig 4c) show that the CIA values were significantly influenced by grain size and sorting. Because of the increase in weathering, the CIA values and strong correlations between CIA and Al_2O_3 indicate low to moderate recycling.

5.4 Provenance

Sedimentary provenance and sandstone compositions are very intimately related. Geochemical data and its various accesses are particularly helpful for defining the origin of the source rock (Keskin, 2011; Armstrong-Altrin et al., 2004; Taylor and McLennan, 1985; Cox et al., 1995; and Condie et al., 1992). Major elements interpret the behaviors of the source rock and finally serve definite characteristics of the sedimentary history (Dickinson, 1985; 1988). To analyze the provenance of Dupi Tila sandstone based on major element analysis, several plots are established. SiO_2 versus log K_2O/Na_2O plot is drawn after (Roser & Korsch, 1988). Typically quartz-rich and low in feldspar, sediments from stable continental regions are plotted on the Passive Margin (PM) field (Roser & Korsch, 1986).

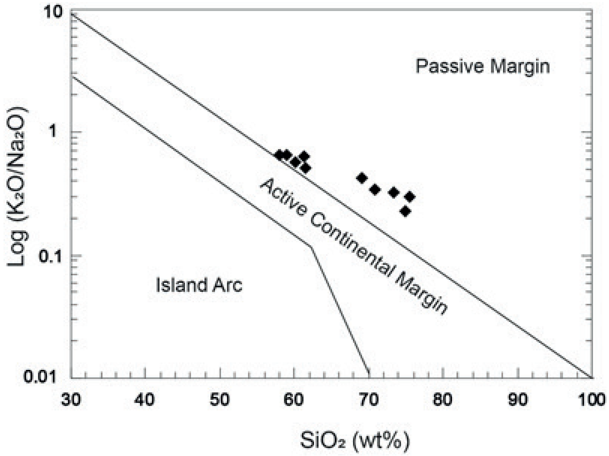

Fig 11. Tectonic discrimination diagram of SiO2 vs. log (K2O/Na2O) proposed by Roser and Korsch (1986) for the investigated Dupi Tila sandstones sediment.

Consequently, increased sedimentary sorting by hydrodynamic transportation leads clay-rich sediments to be dispersed back into the Active Continental Margin (ACM) region. The samples are likely considered to be the Passive Margin settings. In this diagram, samples are plotted in the passive continental margin zone (Fig 11). It indicates that the sediment of the study area might have been derived from both passive continental marginal zone through unidirectional riverine flow from uplands in the Shillong plateau and Himalayas in the north. The provenance was also established by using various major oxide ratios, such as SiO_2/Al_2O_3 (2.74-6.82) and K_2O/Na_2O (1.17-4.51) ratios indicating a large concentration than those ratios of UCC (Taylor and McLennan, 1985; and Condie, 1993) suggesting that studied Dupi Tila sediments have come greatly from crustal granitic sources. But the concentrations of MgO (avg. 1.73 wt. %) and CaO (avg. 2.03 wt. %) are not negligible. It may have little contribution to indicate the basaltic source of the sediments. The Al_2O_3/TiO_2 ratio (avg. 19.73 wt.%) is indicated to be come from felsic to intermediate source rocks(Keskin, 2011 and Hayashi et al., 1997).

Discrimination Diagram

Different categories have been proposed to distinguish between different tectonic settings (Bhatia, 1983; Bhatia and Crook, 1986; Roser and Korsch, 1986).

The Dupi Tila sediments' provenance signatures show quartzose sedimentary provenance using major elements discrimination function diagrams, which are related to Tertiary sedimentary rock formations in Bangladesh (Hossain et al., 2010; and Roy and Roser, 2012) and Siwalik, India (Ranjan & Banerjee, 2009) (Fig 12). The studied Dupi Tila sediments exhibit a close relation with Tertiary sedimentary rocks and are very closely related to the Siwalik deposits. It can be concluded that sediments were derived from Siwalik type sediments, which are mafic in origin and quartzose type rocks which are basically recycled quartz rich sedimentary rocks. Discrimination function diagrams are basically obtained by given Equation 1. This equation is illustrated by using major elements' values. In discrimination function fields for dominantly mafic, intermediate and felsic igneous provenance are shown with the field for a quartzose sedimentary provenance.

The discrimination functions for provenance signature for sandstone suits is given by

F1 = = $(-1.773\times TiO_2) + (0.607\times Al_2O_3) + (0.760\times Fe_2O_3t) + (-1.500\times MgO) + (0.616 \times CaO) + (0.509 \times Na_2O) + (-1.224 \times K_2O) - 9.090$ and

F2 = = $(0.4455 \times TiO_2) + (0.070 \times Al_2O_3) + (-0.2501 \times Fe_2O_3t + (- 1.142 \times MgO) + (0.438 \times CaO) + (1.4753 \times Na_2O) + (1.426 \times K_2O) - 6.861$………………Equation 1

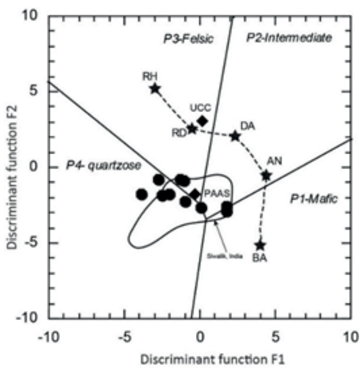

Fig 12. Discriminant plot F1 and F2 (Roser and Korsch, 1988), contain fields for Siwalik, India (Ranjan and Banerjee, 2009), Tertiary sedimentary rocks Dupi Tila (Hossain et al., 2010), Hatia trough (Roy and Roser, 2012), UCC and PAAS (Taylor and McLennan, 1985). Average basalt, andesite, dacite, rhyodacite, and rhyolite are represented by BA, AN, DA, RD, and RH, asplotted by Roser and Korsch (1988)

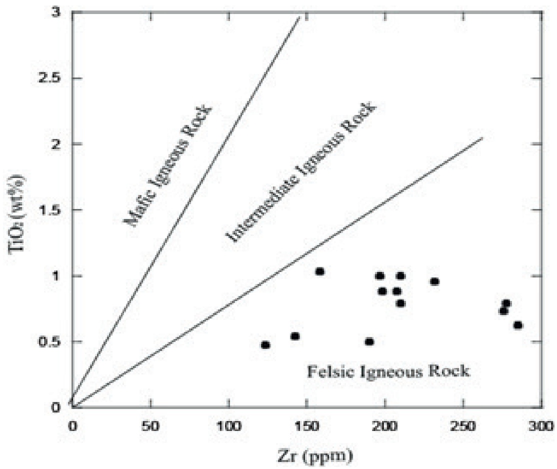

Fig 13. TiO2 vs Zr plot for the samples in the diagram of Hayashiet al. (1997)

Zircon concentration is used to determine the type and composition of the source rock (Hayashi et al., 1997; and Paikaray et al., 2008). Felsic source rocks are indicated by the sediments' low TiO_2/Zr ratios (13 to 38) (Keskin, 2011) (Fig 13). The TiO_2/Zr ratios are a very helpful indicator for distinguishing between the felsic, intermediate, and mafic source rock types (Hayashi et al., 1997). Some trace element ratios are also important to explain the provenance of sediments. So the ratio of Cr/Ni (3.99 to 45.85) is very significant to illustrate the provenance from mafic to felsic sources which is supported by the ratio of Y/Ni (0 to 1.62) that is identical to the value of sediment from felsic sources.

5.5. Tectonics of the Depositional Basin

A lot of limitations prevail to identify tectonic settings, when the actual sources have been totally removed or eroded, derived sediments only contain records of sources (Bhatia and Crook, 1986).

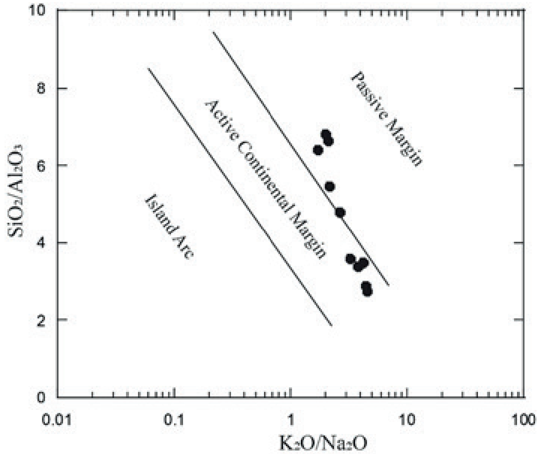

Fig 14. Discrimination diagrams of SiO2/Al2O3 versus K2O/Na2O (after Maynard et al., 1982) for determination of tectonic settings of the investigated Dupi Tila sediments.

The tectonic setting of the depositional basin of the Dupi Tila Formation is formulated on the basis of major and trace-elements and their various bivariate and multivariate plots with discrimination functions. The plot of (K2O/Na2O) vs. SiO2 (Fig 11) generates an analysis of the examined sediments' tectonic settings (Roser and Korsch, 1986) reveals a passive margin (PM) tectonic setting with an active continental margin (ACM). Tectonic discrimination diagram highly supports that the deposition of Dupi Tila Formation occurred in a basin along passive continental margin to active continental margin setting (Roser and Korsch, 1986) (Fig 11). The plots proposed by Maynard et al., (1982) are employed for the determination of tectonic settings.

It represents that all the samples of the investigated Dupi Tila sediments plotted within the passive margin field to active continental margin setting (Fig 14).

Conclusions

Clastic sediments provide important details on the composition, tectonic setting, and evolution of the depositional basin. The major element geochemistry of sediments from the Dupi Tila Formation, Sitapahar anticline, and Kaptai region exhibits mostly broad variability. Geochemically the Dupi Tila Formation represents a significant correlation with UCC, having all major oxides only Na2O and CaO are diminished to UCC. Trace elements of this Formation, are also in conflict with the average upper continental crust (UCC), where Cr, Co, Ni, Rb, Y, Zr, Ba are increased and Sr is depleted. Geochemically the sediments are classified mainly litharenite to arkosic. The ratio of SiO2/Al2O3 (2.7 to 6.82 wt.%), CIA* values (65.04 to 79.52 wt.%), CIW* values (83 to 94 wt.%) and ICV values (0.95 to 1.31 wt.%) show low degree of maturity and exhibiting extensive chemical weathering in source areas, which is supported by textural immaturity. Geochemistry of the whole rock body indicates to a mostly felsic to intermediate igneous provenance. i.e. granitic origin, whereas TiO2 vs Al2O3 diagram suggests basaltic and granitic source. These types of source rocks may be found over a large region of the Himalayan belt, the Shillong massif, and Ganges catchment basins. From discrimination diagram, Dupi Tila sediments provide a close relation with Tertiary sedimentary rocks and very closely related to the Siwalik deposits. From the major and trace element analysis, it is denoted that these sandstones were deposited in passive to active continental margin setting experiencing semi-arid to humid paleoclimatic conditions during the time of deposition. The value of K2O/Na2O ratio for sandstone being greater than unity also supports the similar tectonic setting. The moderate value of SiO2/Al2O3, K2O/Na2O, low value of Na2O and high concentration of iron that preserved in the ferric state suggest relatively intensive to moderate weathering (recycling) history of Dupi Tila Formation, Sitapahar anticline (eastern flank) Kaptai, Rangamati district, Bengal Basin.

References

A. Goto, Y. T. (1994). Quantitative analysis of rock samples by an X-ray fluorescence spectrometer (I). Rigaku Journal, 11, 40–59.

Amajor, L. C. (1987). Major and trace element geochemistry of Albian and Turonian shales from the Southern Benue trough, Nigeria. Journal of African Earth Sciences (1983), 6(5), 633–641.

Armstrong-Altrin, J. S., Madhavaraju, J., Vega-Bautista, F., Ramos-Vázquez, M. A., Pérez-Alvarado, B. Y., Kasper-Zubillaga, J. J., & Bessa, A. Z. E. (2021). Mineralogy and geochemistry of Tecolutla and Coatzacoalcos beach sediments, SW Gulf of Mexico. Applied Geochemistry, 134, 105103.

Asiedu, D. K., Suzuki, S., Nogami, K., & Shibata, T. (2000). Geochemistry of Lower Cretaceous sediments, Inner Zone of Southwest Japan: Constraints on provenance and tectonic environment. Geochemical Journal, 34(2), 155–173.

Bhatia, M. R. (1983). Plate tectonics and geochemical composition of sandstones. The Journal of Geology, 91(6), 611–627.

Blatt, H., Middleton, G. V, & Murray, R. C. (1972). Origin of sedimentary rocks.

Boruah, R., & Laskar, J. J. (2022). Geochemical characteristics of Neogene sandstones of the East and West Siang Districts of Arunachal Pradesh, NE India: implications for source-area weathering, provenance, and tectonic setting. Acta Geochimica, 41(1), 100–120.

Condie, K. C. (1993). Chemical composition and evolution of the upper continental crust: contrasting results from surface samples and shales. Chemical Geology, 104(1–4), 1–37.

Cox, R., Lowe, D. R., & Cullers, R. L. (1995). The influence of sediment recycling and basement composition on evolution of mudrock chemistry in the southwestern United States. Geochimica et Cosmochimica Acta, 59(14), 2919–2940.

Crook, K. A. W. (1974). Lithogenesis and geotectonics: the significance of compositional variation in flysch arenites (graywackes).

Curray, J. R., & Moore, D. G. (1971). Growth of the Bengal deep-sea fan and denudation in the Himalayas. Geological Society of America Bulletin, 82(3), 563–572.

Dalai, T. K., Rengarajan, R., & PP, P. (2004). Sediment geochemistry of the Yamuna River System in the Himalaya: Implications to weathering and transport. Geochemical Journal, 38(5), 441–453.

Dickinson, W. R. (1985). Interpreting provenance relations from detrital modes of sandstones. In Provenance of arenites (pp. 333–361). Springer.

Dickinson, W. R. (1988). Provenance and sediment dispersal in relation to paleotectonics and paleogeography of sedimentary basins. In New perspectives in basin analysis (pp. 3–25). Springer.

Dokuz, A., & Tanyolu, E. (2006). Geochemical constraints on the provenance, mineral sorting and subaerial weathering of Lower Jurassic and Upper Cretaceous clastic rocks of the eastern Pontides, Yusufeli (Artvin), NE Turkey. Turkish Journal of Earth Sciences, 15(2), 181–209.

El-Sayed, S. A., Hassan, H. B., & El-Sabagh, M. E. I. (2022). Geochemistry and mineralogy of Qaroun Lake and relevant drain sediments, El-Fayoum, Egypt. Journal of African Earth Sciences, 185, 104388.

Etemad-Saeed, N., Hosseini-Barzi, M., & Armstrong-Altrin, J. S. (2011). Petrography and geochemistry of clastic sedimentary rocks as evidences for provenance of the Lower Cambrian Lalun Formation, Posht-e-badam block, Central Iran. Journal of African Earth Sciences, 61(2), 142–159. https://doi.org/https://doi.org/10.1016/j.jafrearsci.2011.06.003

Fedo, C. M., Wayne Nesbitt, H., & Young, G. M. (1995). Unraveling the effects of potassium metasomatism in sedimentary rocks and paleosols, with implications for paleoweathering conditions and provenance. Geology, 23(10), 921–924.

Hayashi, K.-I., Fujisawa, H., Holland, H. D., & Ohmoto, H. (1997). Geochemistry of 1.9 Ga sedimentary rocks from northeastern Labrador, Canada. Geochimica et Cosmochimica Acta, 61(19), 4115–4137.

Herron, M. M. (1988). Geochemical classification of terrigenous sands and shales from core or log data. Journal of Sedimentary Research, 58(5), 820–829.

Hossain, H M Z, Roser, B. P., & Kimura, J.-I. (2010). Petrography and whole-rock geochemistry of the Tertiary Sylhet succession, northeastern Bengal Basin, Bangladesh: Provenance and source area weathering. Sedimentary Geology, 228(3–4), 171–183.

Hossain, H M Zakir. (2020). Major, trace, and REE geochemistry of the Meghna River sediments, Bangladesh: Constraints on weathering and provenance. Geological Journal, 55(5), 3321–3343.

Hossain, I., Roy, K. K., Biswas, P. K., Alam, M., Moniruzzaman, M., & Deeba, F. (2014). Geochemical characteristics of Holocene sediments from Chuadanga district, Bangladesh: Implications for weathering, climate, redox conditions, provenance and tectonic setting. Chinese Journal of Geochemistry, 33(4), 336–350. https://doi.org/10.1007/s11631-014-0696-9

Jacobson, A. D., Blum, J. D., & Walter, L. M. (2002). Reconciling the elemental and Sr isotope composition of Himalayan weathering fluxes: insights from the carbonate geochemistry of stream waters. Geochimica et Cosmochimica Acta, 66(19), 3417–3429.

Keskin, Ş. (2011). Geochemistry of Çamardı Formation sediments, central Anatolia (Turkey): implication of source area weathering, provenance, and tectonic setting. Geosciences Journal, 15(2), 185–195.

Kettanah, Y. A., Armstrong-Altrin, J. S., & Mohammad, F. A. (2021). Petrography and geochemistry of siliciclastic rocks of the Middle Eocene Gercus Formation, northern Iraq: Implications for provenance and tectonic setting. Geological Journal, 56(5), 2528–2549.

Khan, F. H. (1991). Geology of Bangladesh. Wiley Eastern.

LaMaskin, T. A., Dorsey, R. J., & Vervoort, J. D. (2008). Tectonic controls on mudrock geochemisry, Mesozoic rocks of eastern Oregon and western Idaho, USA: Implications for cordilleran tectonics. Journal of Sedimentary Research, 78(12), 765–783.

Maynard, J. B., Valloni, R., & Yu, H.-S. (1982). Composition of modern deep-sea sands from arc-related basins. Geological Society, London, Special Publications, 10(1), 551–561.

McLennan, S. M. (2001). Relationships between the trace element composition of sedimentary rocks and upper continental crust. Geochemistry, Geophysics, Geosystems, 2(4).

McLennan, S. M., Hemming, S. R., McDaniel, D. K., & Hanson, G. N. (1993). Geochemical approaches to sedimentation, provenance, and tectonics.

Muminullah, M. (1978). Geology of the northern part of Chittagong district, Bangladesh. Geological Survey of Bangladesh, Government of the People's Republic of ….

Nagarajan, R., Armstrong-Altrin, J. S., Kessler, F. L., Hidalgo-Moral, E. L., Dodge-Wan, D., & Taib, N. I. (2015). Provenance and tectonic setting of Miocene siliciclastic sediments, Sibuti Formation, northwestern Borneo. Arabian Journal of Geosciences, 8(10), 8549–8565.

Najman, Y., Bickle, M., BouDagher-Fadel, M., Carter, A., Garzanti, E., Paul, M., Wijbrans, J., Willett, E., Oliver, G., & Parrish, R. (2008). The Paleogene record of Himalayan erosion: Bengal Basin, Bangladesh. Earth and Planetary Science Letters, 273(1–2), 1–14.

Nesbitt, Hw., & Young, G. M. (1982). Early Proterozoic climates and plate motions inferred from major element chemistry of lutites. Nature, 299(5885), 715–717.

Paikaray, S., Banerjee, S., & Mukherji, S. (2008). Geochemistry of shales from the Paleoproterozoic to Neoproterozoic Vindhyan Supergroup: Implications on provenance, tectonics and paleoweathering. Journal of Asian Earth Sciences, 32(1), 34–48.

Parthasarathy, P., Madhavaraju, J., Ramirez Montoya, E., & Ramasamy, S. (2020). Geochemistry of estuarine sediments from Marakkanam area, Tamil Nadu, India: source area weathering and provenance implications. Arabian Journal of Geosciences, 13(4), 1–13.

Pettijohn, F. J., Potter, P. E., & Siever, R. (1972). Sand and Sandstone. Plate motions inferred from major element chemistry of lutites. Precambrian Research, 147, 124–147.

Potter, Paul E, Maynard, J. B., & Depetris, P. J. (2005). Mud and mudstones: Introduction and overview. Springer Science & Business Media.

Potter, Paul Edwin. (1978). Petrology and chemistry of modern big river sands. The Journal of Geology, 86(4), 423–449.

Rahman, M. J. J., & Faupl, P. (2003). 40Ar/39Ar multigrain dating of detrital white mica of sandstones of the Surma Group in the Sylhet Trough, Bengal Basin, Bangladesh. Sedimentary Geology, 155(3–4), 383–392.

Ranjan, N., & Banerjee, D. M. (2009). Central Himalayan crystallines as the primary source for the sandstone–mudstone suites of the Siwalik Group: New geochemical evidence. Gondwana Research, 16(3–4), 687–696.

Roser, B P, & Korsch, R. J. (1986). Determination of tectonic setting of sandstone-mudstone suites using SiO2 content and K2O/Na2O ratio. The Journal of Geology, 94(5), 635–650.

Roser, Barry P, & Korsch, R. J. (1988). Provenance signatures of sandstone-mudstone suites determined using discriminant function analysis of major-element data. Chemical Geology, 67(1–2), 119–139.

Roy, D. K., & Roser, B. P. (2012). Geochemistry of Tertiary sequence in Shahbajpur-1 well, Hatia trough, Bengal basin, Bangladesh: provenance, source weathering and province affinity. Journal of Life and Earth Science, 7, 1–13.

Roy, D. K., & Roser, B. P. (2013). Geochemical evolution of the Tertiary succession of the NW shelf, Bengal basin, Bangladesh: Implications for provenance, paleoweathering and Himalayan erosion. Journal of Asian Earth Sciences, 78, 248–262.

Rudnick, R. L., Gao, S., Holland, H. D., & Turekian, K. K. (2003). Composition of the continental crust. The Crust, 3, 1–64.

Schufle, J. A. (1967). Principles of geochemistry (Mason, Brian). Journal of Chemical Education, 44(7), A610. https://doi.org/10.1021/ed044pA610

Sinha, S., Islam, R., Ghosh, S. K., Kumar, R., & Sangode, S. J. (2007). Geochemistry of Neogene Siwalik mudstones along Punjab re-entrant, India: Implications for source-area weathering, provenance and tectonic setting. Current Science, 1103–1113.

Suttner, L. J., & Dutta, P. K. (1986). Alluvial sandstone composition and paleoclimate; I, Framework mineralogy. Journal of Sedimentary Research, 56(3), 329–345.

Taylor, S. R., & McLennan, S. M. (1985). The continental crust: its composition and evolution.

Big Data Analysis Using Re-sampling Techniques in a Finite Population Inference

Md. Ayub Ali[1],*,Faija Farjana[2], Md. Maeen Molla[2], Dulal Chandra Roy[3] and Papia Sultana[3]

[1] *Department of Statistics, University of Barishal, Barishal-8254*

[2, 3] *Department of Statistics, University of Rajshahi, Rajshahi-6205*

Abstract

In the analysis of big data for making inferences about a finite population, it is crucial to address the mean selection bias inherent in the big data sample (BDS). This paper introduces a re-sampling technique, commonly known as repetitive sampling technique, to mitigate the selection bias associated with the BDS. The approach involves utilizing two independent samples from separate sources and incorporating supporting information from external sources. Our results demonstrate that this method achieves a coverage rate of nearly 95% for population parameters, while also reducing the standard error (SE) in both linear and non-linear scenarios across four different cases. These outcomes surpass the performance of the existing methods, namely Naive and Bootstrap. Additionally, the research includes limited simulation studies, which reveal that the Jackknife re-sampling technique exhibits less bias and provides a higher coverage rate (94%, 93%, 94% and 95% for n=600 and 95%, 96%, 95% and 96% for n=1200 respectively) for the four scenarios compared to other established methods (In Naive 20%, 19%, 16% and 27% for n=600 and 26%, 32%, 24% and 39% for n=1200; in Bootstrapping 44%, 49%, 59% and 57% for n=600 and 46%, 57%, 65% and 66% for n=1200 respectively). It is also noted that a direct relationship exists between the increase in sample size and the subsequent increase in coverage rate. Furthermore, the practical application of this re-sampling method is straightforward.

Keywords: resampling technique, non-probability sample, selection bias, Bootstrap and Jackknife.

*Corresponding author.
E-mail address: maali@bu.ac.bd

Introduction

Re-sampling means combining similar data from different independent birthplaces and providing operators with a combined simple view of them. It can be compared as a story of "The Blind Men and the Elephant", by American poet John Godfrey Saxe (1816-1887), init, six blind men meet an elephant for the first time and each man independentlyguesseswhatkind of animalit is. After the assessment of these blind men, if the information had to be combined then it would mean something giant and informative. Our target of using re-sampling technique is alike and making inference about population parameter based on combining information extracted as several sample means. For this reason, we consider two known source but unknown size of big data, and mix them in four schemes as stated in the simulation study section below. This process is very useful in a variety of circumstances, which includes commercial as well as scientific domains (for example merging two similar companies or combining two research outcome). The more data we collect (big data) and the more we need to share existing data increase, re-sampling becomes increasingly important. Formerly, it has become the focus of wide theoretical work scope, and numerous open problems are existing unsolved. Under these circumstances, combining disparate data sources, often referred to as information silos, in a single query interface has been a problem for some time. In the early 1970s, computer scientists and researchers began designing systems for interoperability of heterogeneous databases. The first re-sampling method driven by organized metadata was developed in 1991 at the University of Minnesota for the Integrated Public Use Microdata Series (IPUMS).

In this regard, IPUMS uses a data warehousing approach that extracts data from heterogeneous sources, transforms it, and loads it into its own view schema to make data from different sources compatible and understandable. We made it simple and easy to analyze. By making millions of population databases interoperable, IPUMS established the feasibility of large-scale re-sampling technology. In general, data warehousing methods suggest a tightly coupled plan. This is because the data is already physically stored in one understandable repository, so it usually takes very little time to analyze and draw conclusions.

Data warehousing techniques are not very practical for frequently updated datasets. This is because the Extract, Transform, Load (ETL) process has to be constantly rerun to stay in sync. As a result, building a data warehouse is also difficult when you have only a query interface to aggregate independent data sources and no access to the full data. This problem typically occurs when integrating multiple commercial query functions, such as travel or advertising web applications.

The comprehensive definition of big data includes the three Vs: volume, variety, and velocity, which dispels the misconception that big data solely revolves around data volume which is stated in the paper of Russom, P. (2011). In the paper of Watson, H. J. (2014) the author argued that a multitude of organizations are now acquiring, retaining, and examining data that possesses significant volume, speed, and diversity. This data originates from various novel sources such as social media, machines, log files, video, text, image, RFID, and GPS. The utilization of these sources has placed immense pressure on conventional relational database management systems, resulting in the emergence of numerous innovative technologies, methodologies, and platforms. The potential benefits of big data analytics are substantial and have been substantiated by an increasing number of research studies like Manyika, J., Chui, M., Brown, B., Bughin, J., Dobbs, R., Roxburgh, C., & Hung Byers, A. (2011), Chen, Y., Chen, H., Gorkhali, A., Lu, Y., Ma, Y., & Li, L. (2016),Vassakis, K., Petrakis, E., & Kopanakis, I. (2018) and Hariri, R. H., Fredericks, E. M., & Bowers, K. M. (2019).

Materials and Methods

We use two independent data sources using linear and non-linear model to create the dataset. However, we need heterogeneous data to use the Bootstrap and Jackknife technique otherwise we just use Naive method which is nothing but the simple random sampling with replacement.

Naive method: Naive estimator is one kind of Non-parametric Density Estimation (Kernel analysis) which is formerly used in every field of research. Since the standard histogram is not the best way to estimate a probability density function. This method works after cataloging a set of records in ascending order and centering the bin for each selected sample of the sorted distribution. In such situations, the estimated probability densities between adjacent bins differ dramatically due to variations in the number of events.

The counting process may be represented mathematically by a weighted sum as follows: State a weight function w(x) by $$w(x) = \begin{cases} \frac{1}{2} & if\ |x| < 1 \\ 0 & otherwise \end{cases}$$

Then the approximation at a fixed point x is given by

$$\hat{p}(x) = \frac{1}{N_{tot}} \sum_{i=1}^{N_{tot}} \frac{1}{h} w(\frac{x - X_i}{h})$$

This method is applied by choosing a point $x = X_i$ and then counting all observations that lie in the interval h of this location, then divide by the total number of observation N_{tot} to achieve the likelihood, and finally divide by the bin size $2h$ to get the probability density.

Bootstrap method: In statistics, bootstrapping is any metric or test that uses a simple random sampling clause with surrogates and falls into the upper class of resampling methods. Accuracy measures (bias, variance, standard error, confidence interval, prediction error, etc.) are given by the bootstrap method. Bootstrapping provides a measure of the accuracy (bias, variance, confidence interval, prediction error, etc.) of sample estimates for a big data sample. This technique allows the sampling distribution of almost any statistic to be estimated using probabilistic sampling techniques. In bootstrap sampling, B new samples, each with the same sample size as the observed data, are drawn with replacement from the observed data. Statistics are first estimated using the observed data and then re-estimated using each new sample to produce a bootstrap distribution. The resulting iterations are used to compute bootstrap estimates of the biases and standard errors of the statistics. Suppose a probability sample S is drawn from a population U by an arbitrary sampling design without replacement. The population parameter μ is estimated by $\hat{\mu}$and we seek and an estimate of $V(\hat{\mu})$. How bootstrap can perform following is a brief description of the technique:

i) Construct an artificial population U^* using sample data, and assumed to imitate the real, but anonymous, population U.

ii) Draw a sequence of bootstrap sample from U^* using same design as S was drawn from U. Here independency means each bootstrap sample must be replaced into U^* before the next draw and compute $\hat{\mu}_a^*(a = 1,2,3,\ldots, B)$ in the same way as $\hat{\mu}$ was computed.

iii) The observed distribution of $\hat{\mu}_1^*, \hat{\mu}_2^*,\ldots,\hat{\mu}_B^*$ are considered an approximation of the sampling distribution of the estimator $\hat{\mu}$, $V(\hat{\mu})$ is estimated by

$$V(\hat{\mu})_B = \frac{1}{B-1}\sum_{a=1}^{B}(\hat{\mu}_a^* - \hat{\mu}_{(.)}^*)^2 \quad \text{where } \hat{\mu}_{(.)}^* = \frac{1}{B}\sum_{a=1}^{B}\hat{\mu}_a^*$$

iv) The bias of μ is given by, bias $= \hat{\mu}_{(.)}^* - \hat{\mu}$ and the corresponding bootstrap estimator is given by $\hat{\mu}_a = \hat{\mu} + \text{bias}$

Jackknife method: Like bootstrap technique, the Jackknife technique also originated outside the field of survey sampling. The Jackknife procedure begins by removing one item at a time and the desired statistic is then computed from remaining observations and its standard error.

Suppose we have a sample $y = y_1, y_2, \ldots, y_n$ and an estimator $\hat{\mu} = f(y)$.We desire to approximate bias and SE of $\hat{\mu}$. The i^{th} Jackknife sample consists by deleting i^{th} observation i.e. $y_{(i)} = (y_1, y_2, y_{(i-1)}, y_{(i+1)},\ldots, y_n)$ for $i = 1,2,3\ldots,n$

Let $\hat{\mu}_{(i)} = f(y_{(i)})$ be i^{th} Jackknife replication of $\hat{\mu}$. The Jackknife estimate of bias is defined by $bias_{jack} = (n-1)(\hat{\mu}_{(.)} - \hat{\mu})$ where

$\hat{\mu}_{(.)} = \frac{1}{n}\sum_{i=1}^{n}\hat{\mu}_{(i)}$

hence, the Jackknife estimator of μ

$$\hat{\mu}_{jack} = -\hat{\mu} - \text{bias}_{\text{jack}}$$

And the Jackknife estimate of standard error is given by

$$\widehat{SE}_{jack} = \left[\frac{n-1}{n}\sum_i\left(\hat{\mu}_{(i)} - \hat{\mu}_{(.)}\right)^2\right]^{\frac{1}{2}}$$

Basic Setup

Let us suppose that a finite population $\{x_i: i \in U\}$, where x_i is the i^{th} observation of the study variable X, and $U = \{1,2,3, \dots, N\}$is the corresponding index set with known size N. Also $\{x_i: i \epsilon B\}$ which is a BDS is available with $B \subset U$. Specifically, $\delta_i = 1$ if $i \in B$ and $\delta_i = 0$ otherwise, and imagine also that x_i is observed only when $\delta_i = 1$. We are interested in approximating the population mean $\bar{X}_{\text{N}} = \frac{1}{N}\sum_{i=1}^{N} x_i$.

From the BDS B, we can estimate $\bar{X}_{\text{N}}$ by $\bar{X}_{\text{B}} = N_B^{-1}\sum_{i=1}^{N} \delta_i x_i$, where $N_B = \sum_{i=1}^{N} \delta_i$ is the known size of B. Given $\{\delta_i : i \in U\}$, the error of $\bar{X}_{\text{B}}$ can be written as

$\bar{X}_B - \bar{X}_N = \frac{1}{f_B}Cov(\delta, X)$ where $f_B = \frac{N_B}{N}$ and $Cov(\delta, X) = \frac{1}{N}\sum_i(\delta_i - \bar{\delta}_N)(x_i - \bar{X}_N)$

with $\bar{\delta}_N = \frac{1}{N}\sum_i \delta_i$ and thus we have $E_\delta\{(\bar{X}_B - \bar{X}_N)^2\} = \frac{1}{f_B^2}E_\delta\{Cov(\delta, X)^2\}$ … (2.1.1)

where $E_\delta(.)$represents the expectation of a random mechanism for indicator δ_{i} .

If the stochastic mechanism of indicator δ_i is based on Bernoulli sampling, which contains indicators independently obeying the Bernoulli distribution with probability of success f_B, we can obtain

$$\begin{aligned} E_\delta\{Cov(\delta,X)^2\} &= [E_\delta\{Cov(\delta,X)\}]^2 + Var_\delta\{Cov(\delta,X)\} \\ &= 0+\frac{1}{N^2}\sum_i^N (x_i-\bar{X}_N)^2 f_B(1-f_B) \\ &= \frac{1}{N} f_B(1-f_B)\sigma^2 \end{aligned}$$

with $\sigma^2 = \frac{1}{N}\sum_i (x_i - \bar{X}_N)^2$. Hence, under Bernoulli sampling, (2.1.1) condenses to

$$E_\delta\{(\bar{X}_B - \bar{X}_N)^2\} = \frac{1}{N_B}(1-f_B)\sigma^2$$

that is regular with the classical theory for Bernoulli sampling with sample size $n = N_B$. From this point of view, (2.1.1) can be articulated as

$$\begin{aligned} E_\delta\{(\bar{X}_B - \bar{X}_N)^2\} &= \frac{1}{f_B^2} E_\delta(Corr(\delta,X)^2 \times Var(\delta) \times Var(X)) \\ &= E_\delta\{Corr(\delta,X)^2\} \times (\frac{1}{f_B} - 1) \times \sigma^2 \qquad \ldots \qquad (2.1.2) \end{aligned}$$

where the additional equality trails from $Var(\delta) = \frac{1}{N}\sum_{i=1}^N (\delta_i - \bar{\delta}_N)^2 = f_B(1-f_B)$

The above mentioned equality (2.1.2) is also articulated in the renowned paper of Meng (2018). Although there are three terms in (2.1.2) determining the selection bias of $\bar{X}_B$, the first term, $E_\delta\{Corr(\delta,X)^2\}$, is the most critical one. The author Meng (2018) specifies the term as *Data Defect Index* (DDI), which adjusts the level of departure from SRS. Under simple random sampling or in any equal probability sampling designs such that $E_{\delta}(\delta_i) = f_B$, we have $E_{\delta}(Corr(\delta,\ X)) = 0$ and DDI is of order O(1/N), which suggests $E_{\delta}\{((\bar{X}_B - \bar{X}_N)^2)\} = O(\frac{N}{N_B})$. On the contrary, $E_{\delta}(Corr(\delta,\ X)) \neq 0$ will be applicable for other sampling designs, and subsequently the DDI becomes substantial with order O(1), which indicates $E_{\delta}\{((\bar{X}_B - \bar{X}_N)^2)\} = O(\frac{N}{N_B} - 1)$. Consequently, the analysis outcomes substance to selection bias has been accumulated by using non-probability sampling strategy.

Re-sampling Technique

Survey re-sampling is an important research topic, which seeks to merge data from two surveys targeting the same population. Kim et al. (2016) proposed a fractional imputation approach for survey data integration, utilising the instrumental variable assumption from Kim (2011). Park et al. (2017) also explored combining information from two surveys by using a measurement error model for big data problems. Survey re-sampling is a technique used to combine large datasets with survey data. We focus on two types of independent data sources: survey A and big data B which is substance to selection bias.

Suppose that item$y$is available from survey data while $(x,\ y)$is available from the big data, and $\frac{n}{N_B} = o(1)$, where n is the sample size of A. We are interested in estimating the population mean$\bar{X}_N$by combining two data sources. In this stage, the sample mean $\bar{X}_B$ from the big data is prejudiced because of that selection bias. In this circumstance, an artificial data allegation could be recycled to make attributed values of x_i in the sample, if both samples were probability samples.

Simulation Study

In this section, we apply a simulation study to compare the naïve estimator with Jackknife estimator and Bootstrap estimator. We consider the following two outcome regression models for generating the finite population.

I. Linear model. That is,

$$x_i = 3 + y_{1,i} + y_{2,i} + \epsilon_i \ ; \quad i = 1,2,\dots,N \qquad \dots (2.3.1)$$

where $y_{1,i} \sim N(1,1), y_{2,i} \sim Exp(1),\ \epsilon_i \sim N(0,1),\ N = 10{,}00{,}000$ and $y_{1,i},\ y_{2,i},\ \epsilon_i$ all are pair-wise independent.

II. Non-linear model. That is,

$$x_i = 0.4\left(y_{1,i} - 1.6\right)y_{2,i} + \epsilon_i \quad ; i = 1,2,3,\dots,N \qquad \dots (2.3.2)$$

Where $(y_{1,i},\ y_{2,i},\ \epsilon_i)$ are the same characteristics as mentioned above in the linear model.

$\delta_i \sim Ber(p_i)$ is the sampling indicator for the given BDS and independently distributed for $i = 1,2,3,\dots,N$, then we state the resulting two big data propensity models as:

I. For linear logit model. We get,

$$logit(p_i) = y_{2,i} \ ; \ i = 1,2,3,\dots,N \qquad \dots (2.3.3)$$

II. For non-linear logit model. We get,

$$logit(p_i) = -0.5 + 0.5\left(y_{2,i} - 2\right)^2 \ ; \quad i = 1,2,\dots,N \qquad \dots (2.3.4)$$

This is empirically can be stated that the average sampling rates are nearly 60% in equation (2.3.1) and (2.3.2) for the BDS. Finally, to generate the finite population and subsequent BDS, we consider the four scenarios below:

I. Knowledge extracted from (2.3.1), and sampling indicator of BDS produced in (2.3.3), we generate the finite population. In this first scenario, both the outcome regression (OR) model and big data propensity (BDP) model are linear logit model.

II. Knowledge extracted from (2.3.1), and sampling indicator of BDS produced in (2.3.4), we generate the finite population. In this second scenario, the OR model is linear and BDP model is non-linear logit model.

III. Knowledge extracted from (2.3.2), and sampling indicator of BDS produced in (2.3.3), we generate the finite population. In this third scenario, the OR model is non-linear and BDP model is linear logit model.

IV. Knowledge extracted from (2.3.2), and sampling indicator of BDS produced in (2.3.4), we generate the finite population. In this fourth scenario, both the OR model and BDP model are non-linear.

In this circumstances, we are interested to estimate $\bar{X}_N$ which is the population mean. In this regard, we considered two sample size of $n = 600$ and $n = 1200$, and to get these representative samples we used simple random sampling (SRS) in A. After then, we compared the methods for estimating population mean along with its 95% CI.

The graphical representation of the datasets

Figure 1. BDS generated by linear model

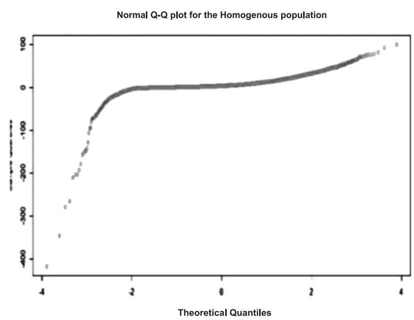

Figure 2. BDS generated by non-linear model

The aforementioned graphical representation of BDS surely indicates the simulated datasets. For checking the linearity normal q-q (quantile-quantile) plots have been shown for both cases. From Fig. 1, it is obvious that the dataset follows linearity assumption as we mentioned above and from Fig. 2, the dataset follows non-linear trend in nature. However, Kolmogorov Smirnov (K-S) one sample test has also been performed and found similar results.

Results and Discussion

Based on a sample extracted by using SRS, we've calculated the population mean $\bar{X}_N$, bias (B), standard error (SE), and coverage rate (CR) based on one thousand Monte Carlo simulation studies for the both given sample size of $n = 600$ and $n = 1200$.

The results for four scenarios are given below:

Table 1. B, SE and CR of different methods

$\bar{X}_N$	Method	Bias	SE	CR	Bias	SE	CR
			n=600			**n=1200**	
I	Naive	0.21	1.68	0.20	0.23	1.76	0.26
	Bootstrap	0.23	1.61	0.44	0.29	1.72	0.46
	Jackknife	0.13	1.44	0.94	0.1	1.34	0.95
	Naive	-0.20	1.69	0.	-0.22	1.73	0.3

				19			2
II	Bootstrap	-0.20	1.77	0.49	-0.22	1.89	0.57
	Jackknife	-0.15	1.49	0.93	-0.11	1.22	0.96
	Naive	0.29	1.58	0.16	0.29	1.73	0.24
III	Bootstrap	0.19	1.54	0.59	0.16	1.59	0.65
	Jackknife	0.21	1.49	0.94	0.19	1.43	0.95
	Naive	0.11	1.63	0.27	0.13	1.71	0.39
IV	Bootstrap	0.17	1.66	0.57	0.13	1.69	0.66
	Jackknife	0.13	1.53	0.95	0.13	1.41	0.96

Based on the Monte Carlo simulation analysis presented in Table 1, it can be inferred that each of the estimators exhibit bias across all methods. The Naive method, in particular, displays a greater degree of bias compared to the Bootstrap and Jackknife methods. This suggests that the Naive method tends to consistently underestimate or overestimate the true value of the parameter being estimated.

Furthermore, the Naive method demonstrates lower confidence interval (CI) coverage rates (CR) than the Bootstrap and Jackknife methods across all scenarios. This means that the Naive method is less likely to capture the true value of the parameter within its calculated confidence interval. On the other hand, the Bootstrap and Jackknife methods exhibit higher CR values, indicating that they provide more accurate and reliable confidence intervals.

However, when considering CR alone, the Jackknife method emerges as the superior method. This implies that the Jackknife method consistently produces confidence intervals that have a higher likelihood of containing the true value of the parameter. Therefore, if the primary concern is obtaining accurate and reliable confidence intervals, the Jackknife method would be the preferred choice.

Conversely, the Naive method is deemed the least effective in terms of CR. This means that the confidence intervals generated by the Naive method are less likely to include the true value of the parameter. Therefore, if obtaining precise and accurate confidence intervals is a priority, the Naive method should be avoided.

In summary, the Monte Carlo simulation analysis reveals that all estimators exhibit bias, with the Naive method displaying a greater degree of bias compared to the Bootstrap and Jackknife methods. Additionally, the Naive method demonstrates lower CR values than the Bootstrap and Jackknife methods across all scenarios. However, when considering CR alone, the Jackknife method emerges as the superior method while the Naive method is deemed the least effective.

For more clarification results from all scenarios for all three methods are presented in graphs in the following section:

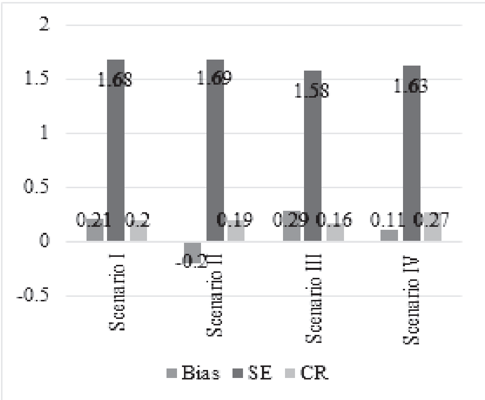

Figure 3: Bias, SE and CR for Naive Estimator for n=600

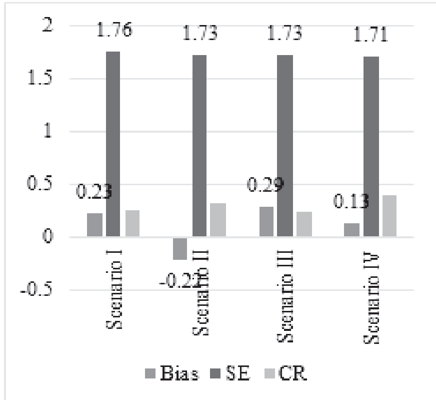

Figure 4: Bias, SE and CR for Naive Estimator for n=1200

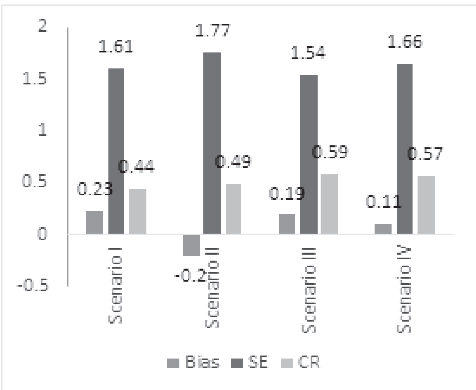

Figure 5: Bias, SE and CR for Bootstrap Estimator for n=600

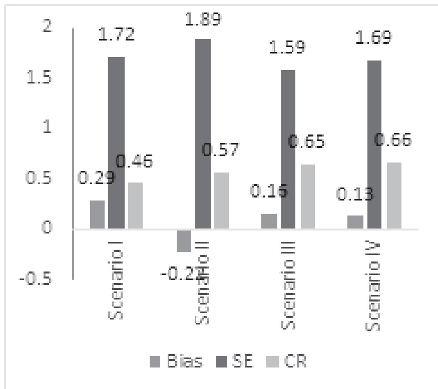

Figure 6: Bias, SE and CR for Bootstrap Estimator for n=1200

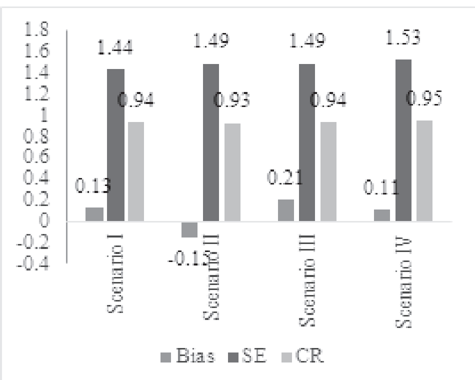

Figure 7: Bias, SE and CR for Jackknife Estimator for n=600

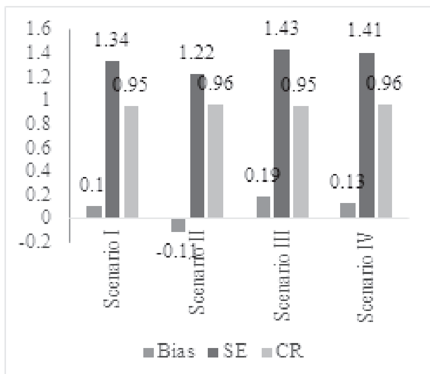

Figure 8: Bias, SE and CR for Jackknife Estimator for n=1200

Conclusion

From the Monte Carlo simulation study and aforementioned table along with its figures we can conclude that all the estimators are biased in every methods and the amount of bias in case of Naive method is comparatively more than the Bootstrap and Jackknife methods. We use contaminated data which has outlier or noise and its combinations in four scenario and found that the CR of Naive method is also less than the Bootstrap and Jackknife methods in all scenarios. But in terms of the CR Jackknife is the best method and Naive is the worst method.

Limitations and strength

The biggest limitation of this research was to use simulated dataset. There was no way to collect such big dataset freely from any sources. Another limitation is that, a very few research work has been done in this regards which leads to review few works of it. The strength of this work can be stated as a novel concept of using resampling methods again and also additional research can be done to extend this work which will be helpful for the researcher to reduce selection bias in analyzing BDS in a finite population inference.

Acknowledgments

We thank the anonymous supervisor and teachers who volunteering and contribute to discuss idea in this study. We also thank the editor of the journal, and the reviewers for their consecutive criticism and comments on our manuscript.

Author Contribution

Professor Dr. Dulal Chandra Roy and Professor Dr. Papia Sultana conceived of the presented idea and supervised the findings of this work till end. Mr. Ayub Ali discussed the theory and performed the computations section.Dr. Dulal Chandra Roy verified the analytical methods and encouraged Fiaja Farjana to investigate linearity of simulated dataset. Mrs. Faija Farjana and Md. Maeen Molla together tabulated and handled the figures of this research work. All authors discussed the results and contributed to the final manuscript.

References

Chen, Y., Chen, H., Gorkhali, A., Lu, Y., Ma, Y., & Li, L. (2016). Big data analytics and big data science: a survey. *Journal of Management Analytics*, *3*(1), 1-42.

Efron, B. *(1979). Bootstrap methods: Another look at the Jackknife. The Annals of Statistics*. 7 (1):1–26. doi:10.1214/aos/1176344552.

Efron, B.; Tibshirani, R. *(1993). An Introduction to the Bootstrap. Boca Raton, FL: Chapman & Hall/CRC. ISBN 0-412-04231-2.*SoftwareArchived 2012-07-12 at Archive. TodaySecond Thoughts on the Bootstrap – Bradley Efron, 2003.

Efron, Bradley (1982). The Jackknife, the bootstrap, and other resampling plans. Philadelphia, PA: Society for Industrial and Applied Mathematics. ISBN 9781611970319.

Efron, Bradley; Stein, Charles *(May 1981). The Jackknife Estimate of Variance. The Annals of Statistics. 9 (3):* 586–596. doi:10.1214/aos/1176345462. JSTOR 2240822.

Franke, B., Plante, J.-F., Roscher, R., Lee, E.-S.A., Smyth, C., Hatefi, A., Chen, F., Gil, E., Schwing, A., Selvitella, A., Hoffman, M.M., Grosse, R., Hendricks, D. & Reid, N. (2016). *Statistical inference, learning and models in big data*, Int. Stat. Rev., 84, 371–389.

Hariri, R. H., Fredericks, E. M., & Bowers, K. M. (2019). Uncertainty in big data analytics: survey, opportunities, and challenges. *Journal of Big Data*, *6*(1), 1-16.

Kim, J.K. & Rao, J.N.K. (2011). *Combining data from two independent surveys: a model assisted approach*, Biometrika, 99, 85–100.

Kim, J.K., Berg, E. & Park, T. (2016). *Statistical matching using fractional imputation*, Surv. Methodol., 42, 19–40.

Manyika, J., Chui, M., Brown, B., Bughin, J., Dobbs, R., Roxburgh, C., & Hung Byers, A. (2011). Big data: The next frontier for innovation, competition, and productivity.

Park, S., Kim, J.K. & Stukel, D. (2017). *A measurement error model for survey data integration: combining information from two surveys*, Metron, 75, 345–357.

Quenouille, Maurice H. (1956). Notes on Bias in Estimation. Biometrika. 43 (3–4): 353–360. doi:10.1093/biomet/43.3-4.353. JSTOR 2332914.

Russom, P. (2011). Big data analytics. *TDWI best practices report, fourth quarter*, *19*(4), 1-34.

Tam, S.-M. & Clarke, F. (2015). *Big data, official statistics and some initiatives by the Australian bureau of statistics*, Int. Stat. Rev., 83, 436–448.

Tam, S.-M. & Kim, J.K. (2018). *Big data, selection bias and ethics – an official statistician's perspective*, Stat. J. IAOS. Accepted for publication.

Tukey, John W. *(1958). Bias and confidence in not quite large samples (abstract). The Annals of Mathematical Statistics.* 29 (2): 614. doi:10.1214/aoms/1177706647.

Varian, H.(2005). *Bootstrap Tutorial*. Mathematica Journal, 9, 768–775.

Vassakis, K., Petrakis, E., & Kopanakis, I. (2018). Big data analytics: Applications, prospects and challenges. *Mobile big data: A roadmap from models to technologies*, 3-20.

Watson, H. J. (2014). Tutorial: Big data analytics: Concepts, technologies, and applications. *Communications of the Association for Information Systems*, *34*(1), 65.

Analyzing Level of Psychological Stress among Young Adults in Bangladesh Due to COVID-19 Pandemic

Md. Ayub Ali[1*], Samiul Islam[2], Md. Maeen Molla[2], Dulal Chandra Roy[3] and Papia Sultana[3]

[1] *Department of Statistics, University of Barishal, Barishal-8254, Bangladesh*

[2,3] *Department of Statistics, University of Rajshahi, Rajshahi-6205, Bangladesh*

Abstract

Due to pandemic related restrictions and global economic recession young generation were passing through a challenging time with extreme psychological stress. Suicide attempts and psychological disorders were the consequences of COVID-19 pandemic. In this write up, we focused to analyse the level of psychological stress among young adults in Bangladesh due to COVID-19 pandemic. The analysis was done using primary data using purposive sampling through online survey from 15 October to 25 October, 2022. An online cross-sectional study has been conducted among young adult of Bangladesh aged 18-30 using "Google form." The participants completed the questionnaire examining socio-demographic factors along with psychological stress component through online platforms. A total of 1035 respondents have been examined in the study using multiple linear regression model (MLRM). The fitted MLRM reveals that if all other independent variables remain zero then a young adult had at least 16.93 (p-value<0.001) score stress (out of 20.88). Urban young adults are 0.27 (p-value=0.42) score more stressed than rural young adults. Southern Bengal, central Bengal and eastern Bengal young adults are respectively 0.16 (p-value=0.69) score, 0.17 (p-value=0.69) score and 0.85 (p-value=0.85) score less stressed than northern Bengal. Female are 1.31 (p-value<0.001) score less stressed than male. Young adults those are below higher secondary are 0.94 (p-value=0.02) score more stressed than higher secondary and above. Apart from these, the effect of income and family members are found to be insignificant in the model in our investigation. This study revealed that the

*Corresponding author.
E-mail address: maali@bu.ac.bd

young adults belong to urban area, nuclear family, unmarried, lower income family has more score to be stressed compared to the young adults belong to rural area, joint family status, married and higher family income status.

Keywords: Psychological stress, Pandemic, COVID-19 and Young adults.

1. Introduction

An epidemic, originating from Wuhan, China, prompted by the novel coronavirus strain SARS-CoV-2, has enforced threats on both mental and physical health since December 2019 on young adults. This novel virus has spread worldwide which had previously not been detected in humans or animals. Due to the rapid worldwide exposure of COVID-19 and the challenges it brought with, World Health Organization (WHO) had to declare it as a pandemic in early March 2020. The most common COVID-19 symptoms are fever, fatigue, dry cough, dyspnoea, myalgia etc. which may progress within 2-14 days of infection through close contact and respiratory droplets (Naser et al., 2020; Wang et al., 2020).

Bangladesh confirmed its first three case of COVID-19 on 8 March, 2020 (The Daily Star 2020a). For preventing the spread of COVID-19, the Bangladesh govt. had to introduce many measures, including lockdown, social distancing, home quarantine etc. The govt. also declared a nationwide lockdown from 26 March to 30 May 2020 extending it seven times (The Daily Star 2020a, 2020b). In addition, various types of pandemic related restrictions have been placed on public activities and movement across the country until 31 August, 2020. Nontherapeutic interventions as well as vaccines has been provided to control the spread of the virus which are the most active measures to control the disease, billions of people stopped their working at the working place and are staying at home to minimize the transmission of the disease. In these circumstances, the general population is gradually experiencing various types of psychological distress such as anxiety, tension, fear, panic, depression and frustration just because of continuing spread of this virus and pandemic related restrictions.

There is ample evidence worldwide that during this COVID-19 pandemic many people developed psychiatric symptoms such as anxiety, tension, anxiety, panic attacks, sleep disturbances, depression, frustration and even self-harm. (Xiong et al., 2020; Shammi et al. al., 2020; Islam et al., 2020a). A study conducted on the general population in China reported that 16.5% of participants suffered from depression, 28.8% from anxiety, and 8.1% from stress during the early stages of the COVID-19 outbreak. (Wang et al., 2020). A similar study conducted among people in Bangladesh during the early stages of the pandemic showed that 37.3% of participants suffered from generalized anxiety disorder (Islam et al., 2020a). Additionally, a survey conducted among home-isolated Bangladeshi students showed that 46.92% suffered from depression, 33.28% from anxiety, and 28.5% from stress (Khan et al. 2020).

Evidence suggests that the psychological problems that can arise after a catastrophe like the COVID-19 pandemic can change over time. Some scientific studies suggest an increase in mental health problems in the first months or years after a disaster (Goldmann and Galea, 2014; McFarlane and Williams, 2012). It suggests that mental health problems decrease after such events (Morganstein and Ursano, 2020; Gerstner et al., 2020).

The study used an online survey to gather data from 1035 young adults in Bangladesh using purposive sampling aged from 18 to 30, ensuring a diverse representation. Socio-demographic factors were included in the questionnaire to understand the variables influencing psychological stress during the pandemic. A multiple linear regression model was used for data analysis, including both quantitative and categorical variables. These methodological choices enhance the study's credibility and robustness.

In this write-up, we briefly articulate the psychological stress score among young adults due to COVID-19 Pandemic in Bangladesh and we will provide some recommendations on how the country can combat this situation.

2. Materials and Methods

2.1 Participants and procedure

An online cross-sectional survey was carried out among young adults of Bangladesh who use Facebook, WhatsApp and Emails and age group 18-30 are the target population for this research work. Data has been collected from 15 October to 25 October, 2022 using “Google Form.” Proper data frame for this study is not available that’s why non-probability Purposive sampling was used to collect the data, with informed contacts from all members. The participants were shortly briefed in the first step and accordingly. They were also told that their given information would be confidential. No incentives were given to the participants in this research, and could withdraw their opinion any time without strict evidence. The survey took place between October 15 and October 25, 2022, to research group member’s personal contacts through online platforms. Ethical approval was renounced by Institution of Biological Science, University of Rajshahi, Rajshahi-6205, Bangladesh following its equivalent ethical principles. Finally, a size of 1035 young adults were considered as a sample of this study.

2.2 Measures

In this present study, a semi-structured questionnaire having informed consent, query regarding post COVID-19 pandemic and its associated factors were used to collect data. Socio-demographics were also included in the questionnaire. Psychological stress is measured with total scoring method which is explained in section 2.3.

2.3 Socio-demographics and Scoring Method

Socio-demographic factors included residence, geographical location, sex, qualification of education, profession, marital status and family type. This study also includes three important quantitative variables respondents' age, monthly family income and number of family member.

In this section the psychological stress has been measured using a dependent variable named total stress score (SS). Respective SS which we're focusing on, psychological stress scores for each respondent were calculated from their responses based on 10 related questions. We have used ten Likert scale questions to get the value of total stress score. Firstly, we take summation of each response of the young adults using the score in ascending order for 4-point Likert-type scale as strongly agreed=1, agreed=2, disagreed=3 and strongly disagreed=4. This SS generally indicates that the less the value of SS, the more the young adults are stressed.

2.4 Statistical Analysis

After calculating the respective psychological stress scores (SS) for each respondent, a normality test of SS using Kolmogorov-Smirnov statistic has been found to be normally distributed. Since the response variable has been measured in quantity a multiple linear regression model has been used to explore the stress among young adults using explanatory variables, (like residence, location, sex, profession etc.) instead of finding correlation and association directly. Lastly, the interpretation of regression analysis has been shown in regards of taking reference categories.

3. Results and Discussion

3.1 Socio-demographic characteristics of the participants

The characteristics of the respondents are summarized in Table 1. It concludes that 58% young adults are from rural area and 42% young adult are from urban area. It has also observed that 61% young adults are from northern Bengal, 18.1% respondent are from southern Bengal, 17.60% young adult are from central Bengal and 2.9% respondent are from eastern Bengal. In addition, the male-female percentage of sex indicates that 72.9% young adults are male and 27.1% young adult are female. If we look at the qualification of education of the respondents then we can see that 76% young adult are from higher secondary and above group and 24% young adults are from below higher secondary group. As expected, most of the participants (92%) are student and 8% young adult are Non-student category.

Similarly, marital status of the respondents conclude that 92% young adults are unmarried where 8% young adult are from others i.e. married, widow and divorced. It has been also found that 73.9% young adult are from nuclear family and 26.1% young adults are from joint family.

Table 1. Characteristics of the study subjects (N=1035)

Characteristics	Frequency (N)	Percentage (%)
Residence		
Urban	433	41.8
Rural	602	58.2
Location		
Southern Bengal	187	18.1
Central Bengal	182	17.6
Eastern Bengal	30	2.9
Northern Bengal	636	61.4
Sex		
Male	755	72.9
Female	280	27.1
Qualification of Education		
Below Higher Secondary	246	23.8
Higher Secondary and Adobe	789	76.2
Profession		
Non-student	85	8.2
Student	950	91.8
Marital Status		
Others	79	7.6
Unmarried	956	92.4
Family Type		
Joint Family	270	26.1
Nuclear Family	765	73.9

3.2 Frequency Distribution of the responses according to psychological stress

The distribution of respondent's psychological stress are summarized in Table 2. It concludes that 20.3% young adults strongly agreed, 58.9% are agreed, 17.2% are disagreed and 3.6% are strongly disagreed with the statement that during this coronavirus pandemic, they feel depressed and restless. It is also noted that 29.7% young adults strongly agreed, 57.2% are agreed, 11.6% are disagreed and 1.5% are strongly disagreed with the statement that if the pandemic continues, their condition will be worsen day by day. If we look at the statement, whether their life during pandemic seems to be very difficult and meaningless or not, then it will be observed that 21.5% young adult are strongly agreed, 53.3% are agreed, 21.4% are disagreed and 3.8% are strongly disagreed. Again, if we notice then we will find that 34.8% young adults are strongly agreed, 55.1% are agreed, 8.6% are disagreed and 1.5% are strongly disagreed with the statement that trapping in the same place for a long time due to the pandemic, the rhythm of work has slowed down and there is no proper interest in any work. Regarding confidence level, 18% are strongly agreed, 42.8% are agreed, 33.8% are disagreed and 5.8% are strongly disagreed with the statement that during the pandemic, confidence in everything have decreased and they feel very unconfident. The most perilous issue is that many of them don't smile even if there happens anything ridiculous in front of them. In this circumstance, nearly 8.8% young adults are strongly agreed, 33.1% are agreed, 48.5% are disagreed and 9.6% are strongly disagreed with the statement that it is not decent to them to laugh even if there is an incident of laughter in the pandemic.

In the similar way, 20.6% young adults are strongly agreed, 37.9% are agreed, 35.7% are disagreed and 5.8% are strongly disagreed with the statement that they sleep too much in this pandemic. Accordingly, 20.1% young adult are strongly agreed, 47% are agreed, 27.8% are disagreed and 5.1% are strongly disagreed with the statement that their attitude had become irritable during pandemic. When we look at their participation in social work then we can draw a noble attention. It indicates that 20% young adults are strongly agreed, 59.2% are agreed, 17.6% are disagreed and nearly 3.2% are strongly disagreed with the statement that they can't participate in social work like before.

Table 2. Frequency Distribution of the respondents according to psychological stress (N=1035)

	Depression Measure	
	Frequency (N)	**Percentage (%)**
During the coronavirus pandemic, I feel depressed and restless.		
Strongly Agreed	210	20.3
Agreed	610	58.9
Disagreed	178	17.2
Strongly Disagreed	37	3.6
If the pandemic continues like this, my condition will worsen day by day in the future.		
Strongly Agreed	307	29.7
Agreed	592	57.2
Disagreed	120	11.6
Strongly Disagreed	16	1.5
Life during the pandemic seems to be very difficult and meaningless now.		
Strongly Agreed	223	21.5
Agreed	552	53.3
Disagreed	221	21.4
Strongly Disagreed	39	3.8
Trapping in the same place for a long time due to the pandemic, the rhythm of work has slowed down and there is no proper interest in any work.		
Strongly Agreed	360	34.8
Agreed	570	55.1
Disagreed	89	8.6
Strongly Disagreed	16	1.5
During the pandemic my confidence in everything has decreased and I feel very unconfident.		
Strongly Agreed	186	18.0
Agreed	443	42.8
Disagreed	346	33.4

Strongly Disagreed	60	5.8
It is not good to laugh even if there is an incident of laughter in the pandemic.		
Strongly Agreed	91	8.8
Agreed	343	33.1
Disagreed	502	48.5
Strongly Disagreed	99	9.6
I sleep a lot now.		
Strongly Agreed	213	20.6
Agreed	392	37.9
Disagreed	370	35.7
Strongly Disagreed	60	5.8
My attitude has become irritable.		
Strongly Agreed	208	20.1
Agreed	486	47.0
Disagreed	288	27.8
Strongly Disagreed	53	5.1
I can't participate in social work like before.		
Strongly Agreed	207	20.0
Agreed	613	59.2
Disagreed	182	17.6
Strongly Disagreed	33	3.2
I can't do education or professional work like before.		
Strongly Agreed	338	32.7
Agreed	575	55.6
Disagreed	102	9.9
Strongly Disagreed	20	1.9

And lastly, the most significant and noteworthy fact about their education and profession life experience which states that 32.7% young adults are strongly agreed, 55.6% are agreed, 9.9% are disagreed and nearly 1.9% are strongly disagreed with the statement that they can’t perform education or professional work like before.

3.3 Psychological Stress Score (PSS)

PSS for each respondent were calculated from 10 related statement. The total PSS has been measured summing Likert-type scale from 10 statement. However, before going to fit a multiple regression model using the dependent variable PSS on independent variables, PSS should follow normality assumption as required. Kolmogorov-Smirnov test has been performed to check the normality of PSS. For more clearance the Q-Q plot of PSS has also been shown in Fig. 1.

Fig. 1. Normal Q-Q plot of PSS

3.4 Multiple linear regression model

The multiple linear regression model in terms of our perspective will be:

$$Y_i = \beta_0 + \beta_1 X_1 + \beta_2 X_2 + \beta_3 X_3 + \beta_4 X_4 + \beta_5 X_5 + \beta_6 X_6 + \beta_7 X_7 + \beta_8 X_8 + \beta_9 X_9 + \beta_{10} X_{10} + e_i$$

Parameter estimation and interpretation are given below:

Table 3. Parameter Estimation of multiple linear regression model

Dependent Variable: Stress Score

Parameter	Coefficients	p-value
Intercept	16.93	<0.001
Residence (Urban)	0.27	0.424
Residence (Rural)®	1	-
Location (Southern Bengal)	-0.16	0.699
Location (Central Bengal)	-0.17	0.689
Location (Eastern Bengal)	-0.85	0.367
Location (Northern Bengal)®	1	-
Sex (Female)	-1.31	<0.001
Sex (Male)®	1	-
Qualification of Education (Below Higher Secondary)	0.94	0.015
Qualification of Education (Higher Secondary and Above)®	1	-
Profession (Non-student)	0.62	0.379
Profession (Student)®	1	-
Marital Status (Others)	0.28	0.684
Marital Status (Married)®	1	-
Family Type (Joint Family)	-0.33	0.492
Family Type (Nuclear Family)®	1	-
Age	0.17	0.043
Number of Family Member	0.01	0.928
Monthly Family Income (in TK)	7.49E-6	0.261

® indicates the reference category and Adjusted R-square=83%

where, Y_i = Total stress score, X_1 = Residence, X_2 = Location, X_3 = Sex, X_4 = Qualification of Education, X_5 = Profession, X_6 = Marital status, X_7 = Family type, X_8 = Age, X_9 = Number of family member, X_{10} = Monthly family income (in TK), β_0 = intercept term, β_1 , …, β_{10} are the coefficients of independent variables respectively, and e_i = random error term in the model. From the above multiple linear regression model result (Table 3) we can conclude that if all other variables remain zero then a young adult has 16.93 score. This intercept term is significant in the model (p-value<0.001).

Urban young adults are 0.27 score more stressed than rural young adults. This coefficient is insignificant in the multiple linear regression model (p-value=0.424). Young adults from Southern Bengal are 0.16 score less stressed than young adults from northern Bengal with an insignificant effect (p-value=0.699). Young adults from central Bengal are 0.17 score less stressed than young adults from northern Bengal with an insignificant effect (p-value=0.689). Similarly, young adults from eastern Bengal are 0.85 score less stressed than young adults from northern Bengal with an insignificant effect in the model (p-value=0.367).

Female are 1.31 score less stressed than male young adults. The coefficient in this regard is significant in the model (p-value<0.001). In the context of young adults, it is often observed that females are closely linked to their parents or husbands, which may lead to the perception that they do not require financial independence. However, in contrast, males are commonly found to be the primary earners within their families, highlighting the significant role they play in providing for their loved ones. Young adults from below higher secondary education are 0.94 score more stressed than the young adults who belongs to higher secondary and above group with significant effect (p-value=0.015). Secondary students are often unaware of the lockdown restrictions and tend to resist them due to their lack of understanding and disregard for formalities. On the other hand, higher secondary and above students are more likely to handle the situation with less stress as they are more aware and knowledgeable about the pandemic. Those who are non-student young adults, they are 0.63 score more stressed than the young adults who are students with an insignificant effect (p-value=0.379).

Regarding marital status, young adults from others (like married, divorced and widow) category are 0.28 score more stressed than unmarried young adults with insignificant effect (p-value=0.684). Similarly, the young adults who belong to joint family are 0.33 score less stressed than the young adults who belong to nuclear family with an insignificant effect (p-value=0.492).

Apart from these, we have quantitative variables in the multiple linear regression model such as age (in Year), number of family member and monthly family income (in TK). We can conclude for the age variable that every one year increase in young adults, there will be 0.17 score increased in PSS and which is significant (p-value=0.043). The result suggests a positive correlation between age and responsibility, indicating that as one gets older, their level of responsibility tends to rise. Similarly, for number of family members, one unit increase in number of family member, there will be 0.01 score increased in output variable and which is insignificant (p-value=0.928). Last but not least, one unit increase in monthly family income (in TK), there will be <0.001 score increased in PSS which is also insignificant in the multiple linear regression model (p-value=0.26).

Conclusion

Young adults are the noteworthy and valuable future of Bangladesh. Due to COVID-19 Pandemic and pandemic related restrictions young adults have been forced to stay home which created psychological stress as well as physical illness. This study revealed that the young adults belong to urban area, nuclear family, unmarried, lower income family has more score to be stressed compared to the young adults belong to rural area, joint family status, married and higher family income status. There is a proverb that the higher the age is, the higher the psychological stress. Similarly, the non-student young adults are more stressed than students with an insignificant effect on the model. The below higher secondary educated young adults are more stressed compared to higher secondary and above group. Southern Bengal, central Bengal and eastern Bengal young adults are more stressed compared to northern Bengal young adults which indicates that urgently they are needed to be under proper meditation.

Ethical approval

The research protocol was reviewed and approved by the Research ethical committee (REC) of Institute of Biological Science (IBSc), University of Rajshahi, Rajshahi-6205, Bangladesh (Approval no. 37(21)/320/IAMEBBC/IBSc).

Limitations and Strength

This present study has been conducted through online platforms which depends on opinion based measures. In this circumstance, it may have been vulnerable to certain possible prejudices, like memory recall and social desirability. Moreover, this study was an online cross-sectional type and unable to regulate causality among variables beneath exploration. Despite these limitations, this study delivers novel knowledge regarding the psychological stress among young adult in Bangladesh due to COVID-19 Pandemic. The findings of this study might be helpful for policy makers to develop and conduct fruitful plan for recovering the current situation and combat pandemic related issues.

Author Contribution

Professor Dr. Dulal Chandra Roy and professor Dr. Papia Sultana perceived of the presented idea and supervised the findings of this work till the end. Mr. Ayub Ali discussed the theory and performed the computations section. Dr. Dulal Chandra Roy verified the analytical methods and encouraged Mr. Samiul Islam and Mr. Md. Maeen Molla to review literature and tabulation section. All authors discussed the results and contributed to the final manuscript.

Acknowledgments

We thank the anonymous 1035 participants for volunteering to participate in this study. We also thank the editor of the journal, and the reviewers for their consecutive criticism and comments on our manuscript.

References

Goldmann, Emily, and Sandro Galea (2014). *Mental health consequences of disasters*. Annual review of public health 35: 169-183.

Islam, Md Saiful, Most Zannatul Ferdous, and Marc N. Potenza (2020). *Panic and generalized anxiety during the COVID-19 pandemic among Bangladeshi people:*

An online pilot survey early in the outbreak. Journal of affective disorders 276: 30-37.

Islam, SM Didar-Ul, et al (2020). *Exploring COVID-19 stress and its factors in Bangladesh: a perception-based study.* Heliyon 6.7: e04399.

Khan, Abid Hasan, et al (2020). *The impact of COVID-19 pandemic on mental health & wellbeing among home-quarantined Bangladeshi students: a cross-sectional pilot study*. Journal of affective disorders 277: 121-128.

McFarlane, Alexander C., and Richard Williams (2012). *Mental health services required after disasters: Learning from the lasting effects of disasters.* Depression research and treatment 2012.

Morganstein, Joshua C., and Robert J. Ursano (2020). *Ecological disasters and mental health: causes, consequences, and interventions.* Frontiers in psychiatry 11: 1.

Naser, Abdallah Y., et al (2020). *Mental health status of the general population, healthcare professionals, and university students during 2019 coronavirus disease outbreak in Jordan: A cross-sectional study.* Brain and behavior 10.8: e01730.

Shammi M, Bodrud-Doza M, Islam AR, Rahman MM (2020). *COVID-19 pandemic, socioeconomic crisis and human stress in resource-limited settings: a case from Bangladesh*. Heliyon.; 22: e04063.

The Daily Star, 2020a. Coronavirus Outbreak: Govt. Orders Closure of Public, Private Offices from March 26 to April 4. Retrieved August 8, 2020, from: https://www.thedailystar.net/coronavirus-deadly-new-threat/news/govt-offices-closed-march-26-april-4-cabinet-secretary-1884730.

The Daily Star, 2020b. Coronavirus Outbreak: shutdown won't be extended after May 30, from:https://www.thedailystar.net/coronavirus-outbreak-shutdown-wont-be-extended-after-may-30-1905826.

Wang, Cuiyan, et al (2020). *Immediate psychological responses and associated factors during the initial stage of the 2019 coronavirus disease (COVID-19) epidemic among the general population in China.* International journal of environmental research and public health 17.5:1729.

World Economic Forum. In Bangladesh, COVID-19 threatens to cause a humanitarian crisis. Accessed May 5, 2020. https://www.weforum.org/agenda/2020/04/in-bangladesh-covid-19-could-cause-a-humanitarian-crisis/.

World Health Organization. Coronavirus disease 2019 (COVID-19) situation report—79. Accessed May 12, 2020. https://www.who.int/docs/defaultsource/coronaviruse /situationreports/20200408-sitrep-79-covid 19.pdf?sfvrsn=4796b143_6.

Xiong, Jiaqi, et al (2020). *Impact of COVID-19 pandemic on mental health in the general population: A systematic review*. Journal of affective disorders.

Effects on Natural Convection Heat Transfer in an Inclined Square Cavity with Uniformly and Non-Uniformly Heating Side Walls

Md. Aslam Hossain[1], Chinmayee Podder[2,*], Bijan Krishna Saha[2]

[1]*Department of Mathematics, Pabna University of Science and Technology, Pabna-6600*

[2]*Department of Mathematics, University of Barishal, Barishal-8254*

Abstract

This paper investigates the natural convection of two-dimensional incompressible, laminar, and steady flow in an inclined square cavity of uniformly and non-uniformly heated walls. The left vertical wall and the bottom wall of the cavity are heated uniformly and non-uniformly, whereas the right vertical wall is cooled by means of a constant temperature. The top wall is well insulated. The governing equations are changed to dimensionless form using non-dimensional variables and solved using a finite element-based computational tool named COMSOL Multiphysics. The parametric study of the Rayleigh number (Ra), the Prandtl number (Pr), the cavity length (L), and the angle of inclination of the cavity (φ) is investigated. The heat transfer rates at the heated walls are calculated in terms of the average Nusselt number. The investigation shows that non-uniform heating has a better heat transfer rate than uniform heating. When the cavity is inclined at a 60-degree angle, the heat transfer rate is high for the large value of the cavity length. The higher cavity length plays an important role in getting a higher-strength streamline. It is observed that the Rayleigh number has a greater impact on streamlines and isotherms compared to the Prandtl number.

Keywords: Uniform and non-uniform heating, Inclined Square Cavity, Rayleigh Number, Prandtl Number, Average Nusselt Number, COMSOL Multiphysics

**Corresponding author.*
E-mail address: chinmayeepodder1@gmail.com

Introduction

Convection is one of the modes of heat transfer which happens due to the movement of fluid mass. Convection could not occur without conduction and convection is possible only for liquid or gases. The study of natural convection and heat transfer in cavity is carried out in many industrial heating or cooling applications such as meteorology, geophysics, nuclear reactor systems, energy storage & conservation, fire control, and chemical, food & metallurgical industries, as well as in the more conventional fields of the fluid & thermal sciences (Roy and Basak, 2005). The research studies of (Patterson and Imberger, 1980), (Nicolette et al.,1985) (Hall et al.,1988), (Hyun and Lee,1989), (Fusegi et al.,1992), (Lage and Bejan,1991), (Lage and Bejan,1993) and (Xia and Murthy,2002) claim that several attempts have been made to gather a fundamental knowledge of natural convection flows & heat transfers characteristics in a cavity. In most studies, one vertical wall of the cavity is kept cool & another one is kept hot while the remaining top & bottom walls are well insulated. According to (Roy and Basak, 2005) investigation, in case of uniform heating, the maximum heat transfer rate is found at the right edge of the bottom wall & almost uniform at the rest part of the bottom wall as well as the hot vertical wall, and, in case of non-uniform heating, the heat transfer rate is minimum at the edges of the heated walls & it reaches to its highest point at the center of both the heated walls. In the investigation of (M. Leporini et al, 2018) it is shown that two vortices formed when the tilted angle is zero degree. (Karatas and Derbentli, 2017) examined natural convection of air in rectangular cavities with one active vertical wall. They came to know that the isotherms are concentrated near the active wall. The maximum heat transfer rate is found at near the bottom of the hot wall and near the top of the cold wall in the research of (Vimol Kishore et al., 2018), (Oztop et al.,

2012) claimed that for the enclosure with $Ra = 10^3$, the increase of inclination angles increases Nusselt number while for the enclosure with $Ra = 10^3$ and 10^5, the average Nusselt number decreases with the increase of inclination angle from 30 degree to 60 degree and then it increases with the increase of inclination angle from 60 degree to 90 degree. (Bouhalleb et al., 2015) have studied the natural convection in an inclined rectangular enclosure with sinusoidal temperature profile on one side wall. They discovered that maximum heat transfer occurs at 90-degree angle of inclination. E. (Natarajan et al., 2008) have examined that in case of uniform heating of the bottom wall, the heat transfer rate gradually decreases from the left of the bottom wall and increases to the right. In contrast, for the case of non-uniform heating at $Ra = 10^3$, the heat transfer rate increases from the left of the bottom wall and for $Ra = 10^5$ a sinusoidal type of heat transfer rate is obtained. In case of uniformly heated walls, the finite discontinuity in temperature distributions appears at the right edge of the bottom wall. The discontinuity can be avoided by choosing a non-uniform temperature distribution along the walls (i.e., non-uniformly heated walls) as discussed by (Minkowycz et al., 1988) where an investigation is made for a mixed convection flow on a vertical plate, which is non-uniformly heated or cooled. (Sheikhzadeh et al., 2011) have showed that for uniform heating, the minimum average nussselt number occurred for top-top case of the active portions of the side walls but the maximum average nusselt number occurred for the middle-bottom case for $Ra = 10^5$ and $Ra = 10^6$. It is shown by (Zhan et al., 2019) that the heat transfer effect of bottom heating is relatively best.

The aim of this paper is to analysis the effects of uniform & non-uniform heating walls, angle of the inclinations of the cavity, the cavity length, Prandtl number and Rayleigh number on natural convection in an inclined square cavity. This analysis includes temperature distributions and velocity distributions within the cavity and heat transfer rate at the heated walls in terms of average Nusselt number using COMSOL Multiphysics software which is based on finite element method. In both case of uniform and non-uniform heating, all walls are in no slip conditions. The reference pressure is chosen to be zero. The cavity is inclined at 30 degree and 60-degree angle with respect to x axis. A parametric study of Rayleigh number (Ra), $10^3 \leq Ra \leq 10^6$, Prandtl number (Pr), $0.2 \leq Pr \leq 10$, the cavity length (L), $0.25 \leq L \leq 0.50$ and the angle of inclinations of the cavity $(\varphi), 0 \leq \varphi \leq 60$ is performed. The results are presented by describing streamlines, isotherm contours and heat transfer rate in terms of average Nusselt number.

Governing Equations

In our study, the thermo-physical properties of the fluid are considered to be constant. The Boussinesq approximation is applied for the fluid properties to relate density changes to temperature changes, and to couple in this way the temperature field to the flow field as (Roy and Basak, 2005) have considered for their investigation. The governing equations for steady natural convection flow using conservation of mass, momentum and energy can be written as:

$$\frac{\partial u}{\partial x} + \frac{\partial v}{\partial y} = 0 \tag{1}$$

$$u\frac{\partial u}{\partial x} + v\frac{\partial u}{\partial y} = -\frac{1}{\rho}\frac{\partial p}{\partial x} + \nu\left(\frac{\partial^2 u}{\partial x^2} + \frac{\partial^2 u}{\partial y^2}\right) \tag{2}$$

$$u\frac{\partial v}{\partial x} + v\frac{\partial v}{\partial y} = -\frac{1}{\rho}\frac{\partial p}{\partial y} + \nu\left(\frac{\partial^2 v}{\partial x^2} + \frac{\partial^2 v}{\partial y^2}\right) + g\beta(T - T_c) \tag{3}$$

$$u\frac{\partial T}{\partial x} + v\frac{\partial T}{\partial y} = \alpha\left(\frac{\partial^2 T}{\partial x^2} + \frac{\partial^2 T}{\partial y^2}\right) \tag{4}$$

with boundary conditions

$u(x,0) = u(x,L) = u(0,y) = u(L,y) = 0$

$v(x,0) = v(x,L) = v(0,y) = v(L,y) = 0$

$T(x,0) = T_h$, or $T(x,0) = (T_h - T_c)sin\left(\frac{\pi x}{L}\right) + T_c$, $\frac{\partial T}{\partial y}(x,L) = 0$ (5)

$T(0,y) = T_h$, or $T(0,y) = (T_h - T_c)sin\left(\frac{\pi y}{L}\right) + T_c$, $T(L,y) = T_c$

Using the following change of variables, $X = \frac{x}{L}$, $Y = \frac{y}{L}$, $U = \frac{uL}{\alpha}$, $P = \frac{pL^2}{\rho\alpha^2}$ and $\theta = \frac{T-T_c}{T_h-T_c}$

where x and y are the distances measured along the horizontal and vertical directions, respectively; u and v are the velocity components in the x- and y-directions, respectively; T denotes the temperature; ν and $\alpha(=1)$ are kinematic viscosity and thermal diffusivity, respectively; p is the pressure and $\rho$is the density; T_h and T_c are the temperatures at hot and cold walls, respectively; L is the side of the square cavity.

The governing equations are reduced to the following non-dimensional form:

$$\frac{\partial U}{\partial X} + \frac{\partial V}{\partial Y} = 0 \quad (6)$$

$$U\frac{\partial U}{\partial X} + V\frac{\partial U}{\partial Y} = -\frac{\partial P}{\partial X} + Pr\left(\frac{\partial^2 U}{\partial X^2} + \frac{\partial^2 U}{\partial Y^2}\right) \quad (7)$$

$$U\frac{\partial V}{\partial X} + V\frac{\partial V}{\partial Y} = -\frac{\partial P}{\partial Y} + Pr\left(\frac{\partial^2 V}{\partial X^2} + \frac{\partial^2 V}{\partial Y^2}\right) + RaPr\theta \quad (8)$$

$$U\frac{\partial \theta}{\partial X} + V\frac{\partial \theta}{\partial Y} = \left(\frac{\partial^2 \theta}{\partial X^2} + \frac{\partial^2 \theta}{\partial Y^2}\right) \quad (9)$$

where, $\frac{g\alpha(T_h-T_c)L^3}{\nu k} = Ra$, $\frac{\nu}{\alpha} = Pr$ and $\alpha = \beta = k = 1$

with the boundary conditions

$U(X,0) = U(X,L) = U(0,Y) = U(L,Y) = 0$

$V(X,0) = V(X,L) = V(0,Y) = V(L,Y) = 0$

$\theta(X,0) = 1$, or $\theta(X,0) = \sin\left(\frac{\pi X}{L}\right)$, $\frac{\partial\theta}{\partial Y}(X,L) = 0$

$\theta(0,Y) = 1$, or $\theta(0,Y) = \sin\left(\frac{\pi Y}{L}\right)$, $\theta(L,Y) = 0$ (10)

Here X and Y are dimensionless coordinates varying along horizontal and vertical directions respectively, U and V are dimensionless velocity components in the X and Y directions respectively, θ is the dimensionless temperature, P is the dimensionless pressure, Ra and Pr are Rayleigh number and Prandtl number respectively. Now comparing equation (2) and (7) we get, $\rho = 1$ and $Pr = \mu$. Comparing (4) and (9) we get, $\alpha = 1$. Comparing boundary conditions (5) and (10) we get, $T_h = 1, T_c = 0$. The heat transfer rate in terms of average Nusselt number is defined by, $N_u = -\frac{\partial\theta}{\partial n}$, where n denoted the normal direction on a plane.

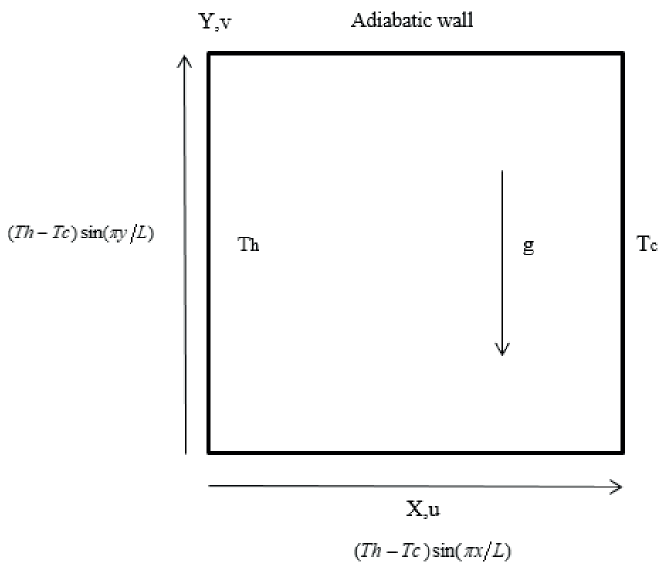

Fig 1: Schematic diagram of the cavity

Model Validation

The test case is the natural convection and the heat transfer in a differentially heated square cavity filled with air. Table 1 shows the average Nusselt number of the hot side wall for different Rayleigh numbers obtained by the present simulation. As it can be observed from this table, a very good agreements exist between the Nusselt numbers obtained by the present simulation and the results of other investigators for $10^5 \leq Ra \leq 10^6$.

Table 1: Comparisons of average Nusselt Number with the same results of other investigators

Rayleigh Number	Present work	(Barakos and Mitsoulis,1994)	(Markatos and Pericleous,1984)	(Davis, 1983)
10^5	4.518	4.510	4.430	4.519
10^6	8.806	8.806	8.754	8.799

Mesh Generation

To investigate the effects of natural convection on 2D incompressible, laminar and steady flows in an inclined square cavity of uniformly and non-uniformly heated walls, governing equations are discretized using the finite element method and graphical representation are found by COMSOL Multiphysics software. The free triangular element of extremely fine size is chosen for mesh generation. The Figure 2 shows the mesh generation of the current study. The number of elements of the mesh is 33154 whereas the number of degrees of freedom is approximately 67412.

The maximum element size is 0.0025, the minimum element size is 5×10-6 and maximum element growth rate is 1.1.

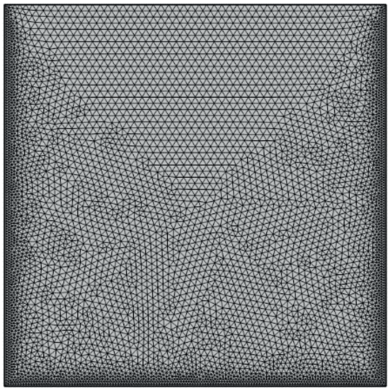

Fig 2: Mesh Generation

Results & Discussion

A study of natural convection on 2D incompressible, laminar and steady flow in an inclined square cavity of uniformly and non-uniformly heated walls is investigated for Rayleigh numbers, Prandtl numbers, angles of inclination and length of the cavity.

Effects of Cavity Length on Streamlines and Isotherms

The figure (3) shows the streamlines (on the left) and the isotherm contours (on the right) inside the cavity for $Ra = 10^6$, $Pr = 10$, $L = 0.25, 0.50$ and $\varphi = 30$ in case of both uniform & non-uniform heating. A clockwise rotation is developed inside the cavity. The strength of the velocity is highly noticed near the cold wall. Increasing the length of the cavity from 0.25 to 0.50, the velocity magnitude rises significantly in both case of uniform and non-uniform heating but the size of vortex at the middle of the cavity increases if the uniform heating turns into non-uniform heating. Also, the velocity magnitude of uniform heating is always greater than that of non-uniform heating. The streamlines are almost similar in both case of uniform and non-uniform heating except the creations of stagnant fluid attached to the lower corner of the left vertical heated wall under along for the values of $Ra = 10^6$, $Pr = 10$, $L = 0.50$ and $\varphi = 30$ in case of non-uniform heating.

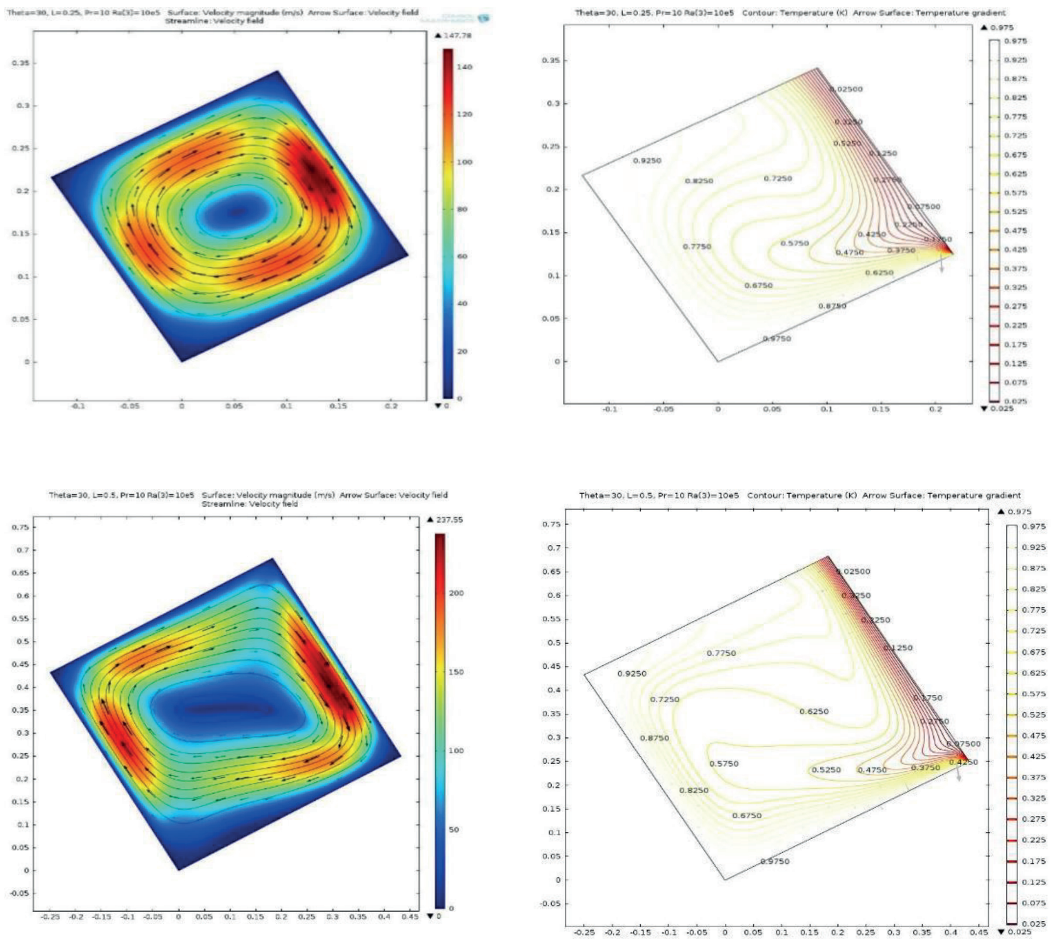

[a] Uniform heating

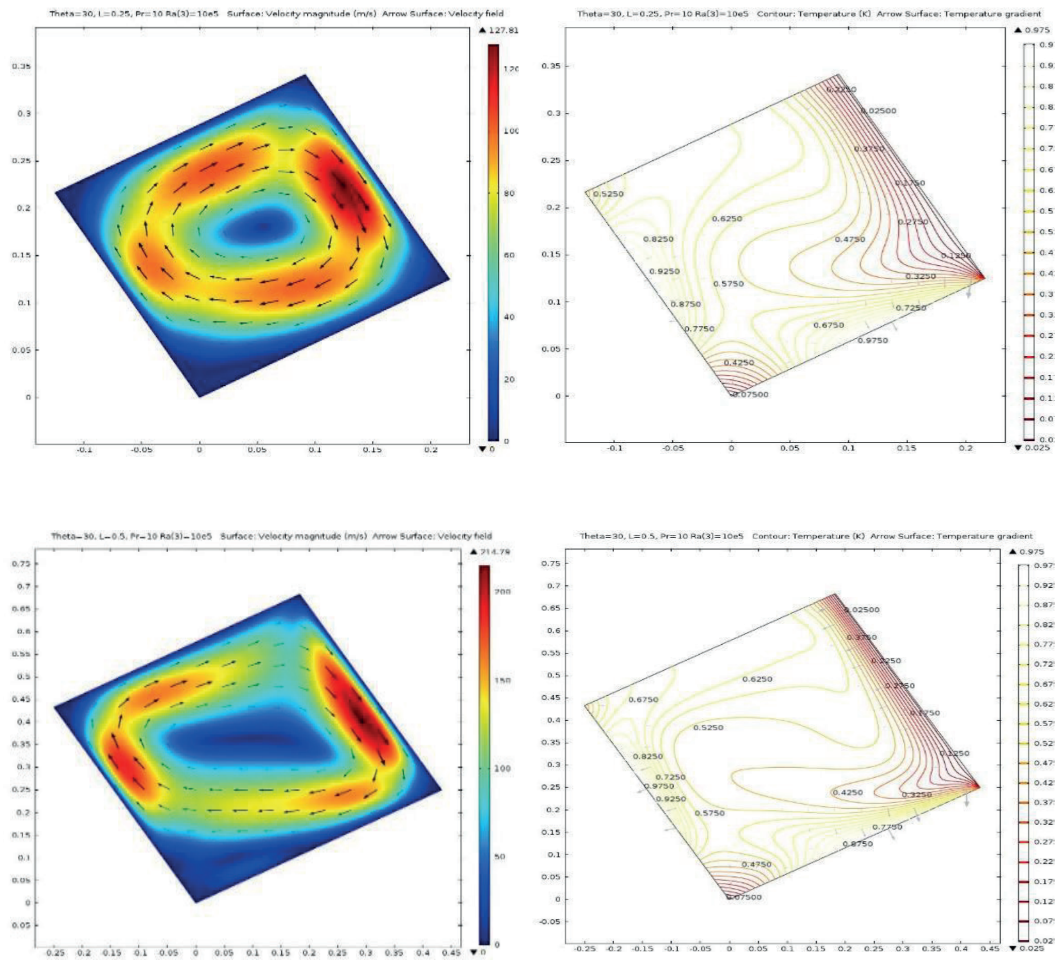

[b] Non-Uniform heating

Fig 3: Streamlines (on the left) and isotherm contours (on the right) in case of [a]uniform heating and [b]non-uniform heating for the values of $Ra = 10^5, Pr = 10, L = 0.25{,}0.5$ and $\varphi = 30$.

The concentrated streamlines and isotherms in the boundary layer along the heated walls indicate higher velocities & more convection heat transfer in these areas. The direction of heat transfers is from the cold vertical wall to heated walls.

Effects of Rayleigh Number on Streamlines and Isotherms

The figure (4) shows the streamlines (on the left) and the isotherm contours (on the right) inside the cavity for $L = 0.5$, $Pr = 10$, $Ra = 10^3, 10^6$ and $\varphi = 30$ in case of both uniform & non-uniform heating. From the figure 4, it can be seen that the strength of the velocity is highly noticed near the cold wall though the velocity field dominate most of the areas of the cavity. With the increment of Rayleigh number from 10^3 to 10^6, the velocity magnitude changes surprisingly in both case of uniform and non-uniform heating. In case of uniform heating, the velocity magnitude for $Ra = 10^6$ is approximately 347 times of that for $Ra = 10^3$ and in case of non-uniform heating the velocity magnitude for $Ra = 10^6$ is approximately 407 times of that for $Ra = 10^3$. Here, we can also see that the velocity magnitude of uniform heating is always greater than that of non-uniform heating. The streamlines are almost similar in both case of uniform and non-uniform heating except the creations of stagnant fluid attached to the lower corner of the left vertical heated wall for the values of $Ra = 10^6$, $Pr = 10$, $L = 0.50$ and $\varphi = 30$ in case of non-uniform heating.

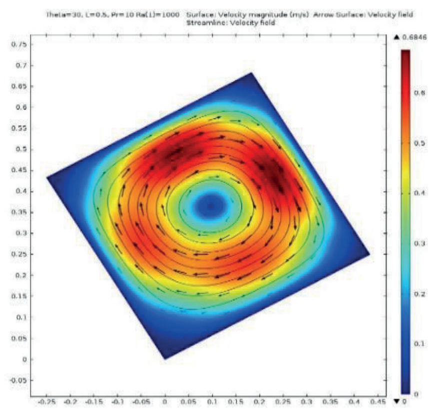

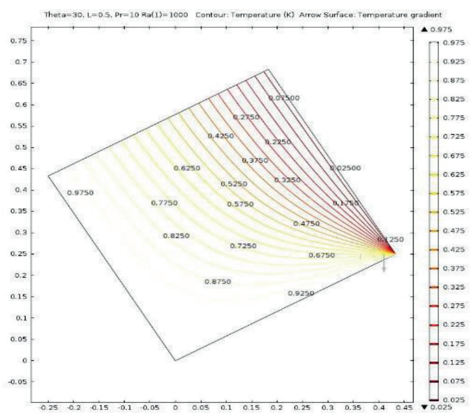

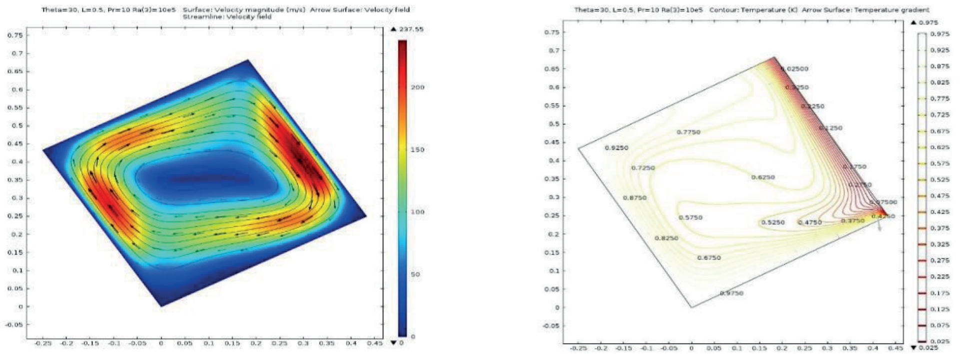

[a] Uniform heating

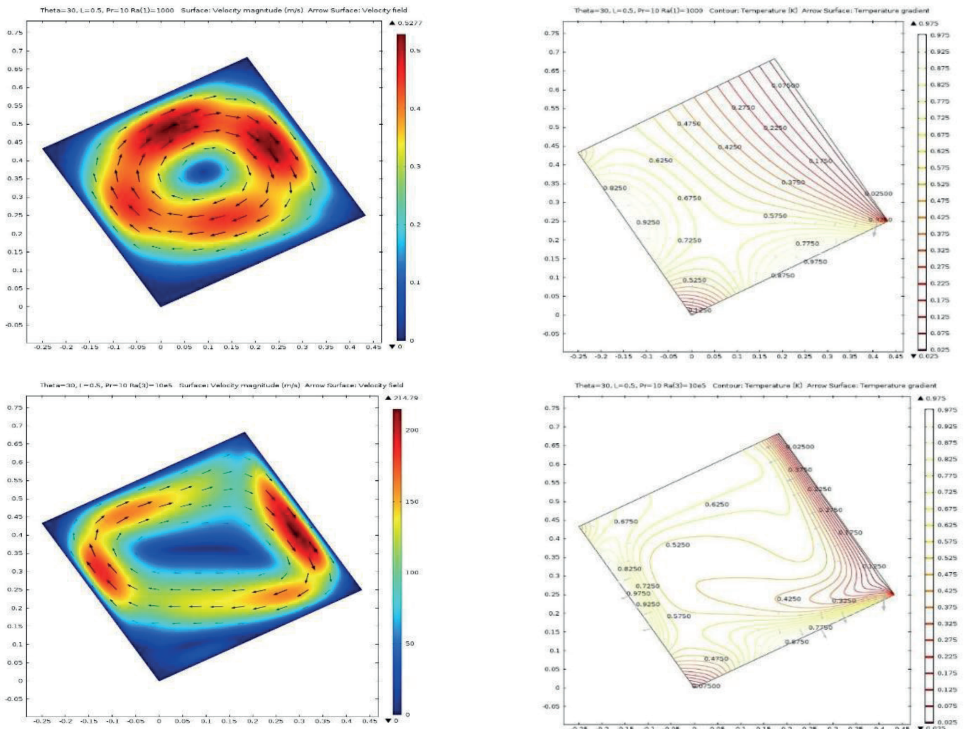

[b] Non-Uniform heating

Fig 4: Streamlines (on the left) and isotherm contours (on the right) in case of [a]uniform heating and [b]non-uniform heating for the values of $L = 0.5, Pr = 10, \varphi = 30$ and $Ra = 10^3, 10^6$

As expected, a more compact streamlines and isotherms are noticed for $Ra = 10^6$ near the cold wall. It is noticed that the isotherm patterns change in case of both uniform and non-uniform heating with the enhancement of Rayleigh number from 10^3 to 10^6. The patterns of isotherms changes when the type of heating changes.

Effects of Prandtl Number on Streamlines and Isotherms

The figure (5) shows the streamlines (on the left) and the isotherm contours (on the right) inside the cavity for $L = 0.5$, $Ra = 10^6, Pr = 0.2{,}10$ and $\varphi = 60$ in case of both uniform & non-uniform heating. From the figure 5, it can be seen that the strength of the velocity is highly noticed near all wall when $Pr = 0.2$ but comparatively a less strength of velocity is developed near the left vertical wall when $Pr = 10$ though the velocity field dominate most of the areas of the cavity for all values of Prandtl number. With the increment of Prandtl number from 0.2 to 10, the velocity magnitude changes slightly in both case of uniform and non-uniform heating. In case of uniform heating, the velocity magnitude for $Pr = 10$ is approximately 1.18 times of that for $Pr = 0.2$ and in case of non-uniform heating the velocity magnitude for $Pr = 10$ is approximately 1.19 times of that for $Pr = 0.2$. The streamlines are almost similar in both case of uniform and non-uniform heating for the value of $Pr = 0.2$. An extra vortex is developed near the top wall in case of uniform heating for the values of $L = 0.5$, $Ra = 10^6, Pr = 10$ and $\varphi = 60$ whereas in case of non-uniform heating one vortex is formed near the lower corner of right vertical wall for the values of $L = 0.5$, $Ra = 10^6, Pr = 0.2$ and $\varphi = 60$ and one comparatively much bigger vortex is found near the bottom wall for the values of $L = 0.5$, $Ra = 10^6, Pr = 10$ and $\varphi = 60$.

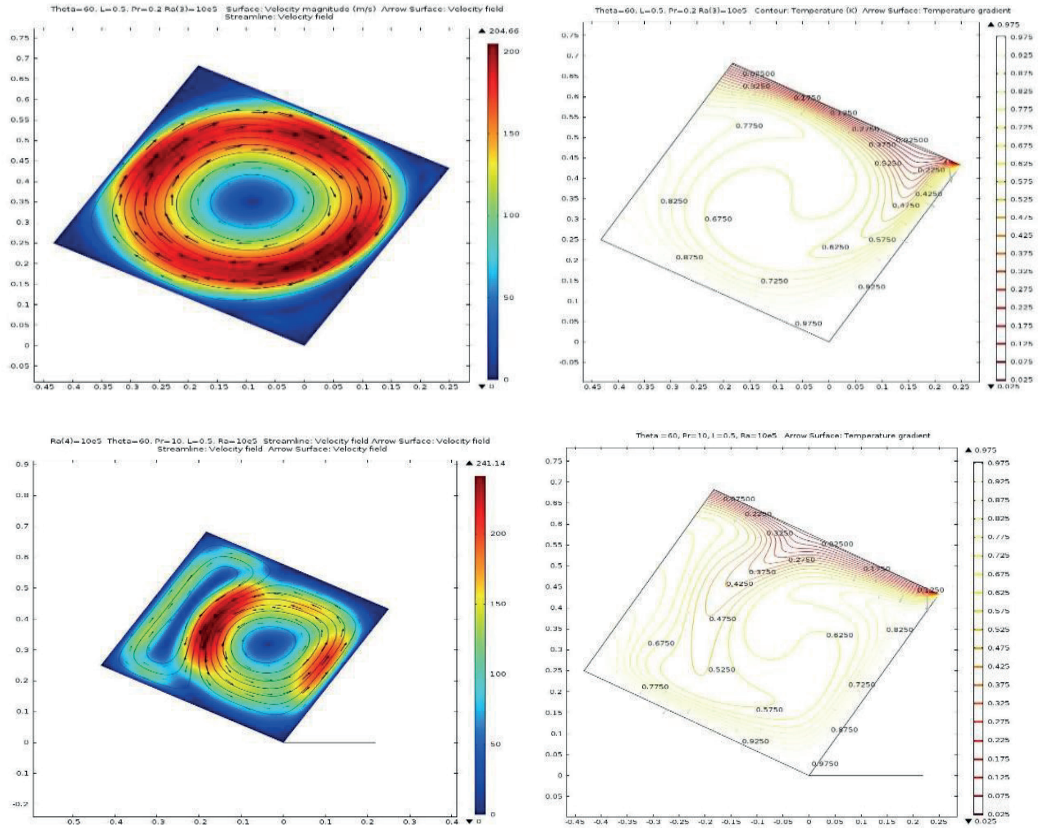

[a] Uniform heating

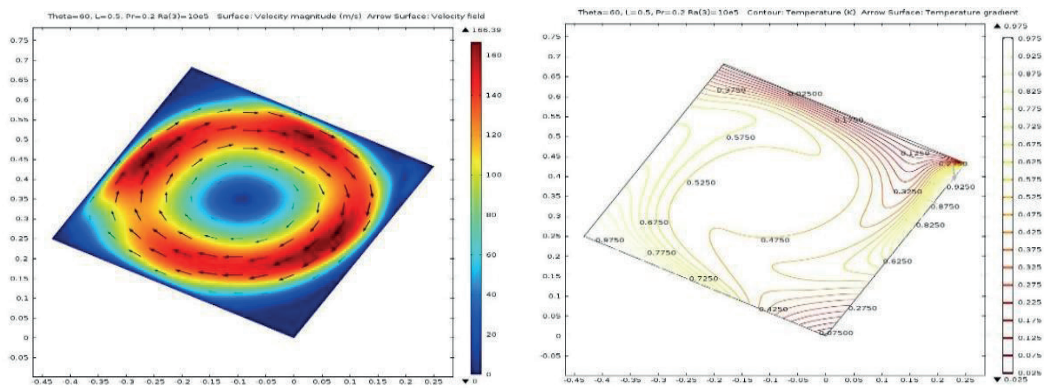

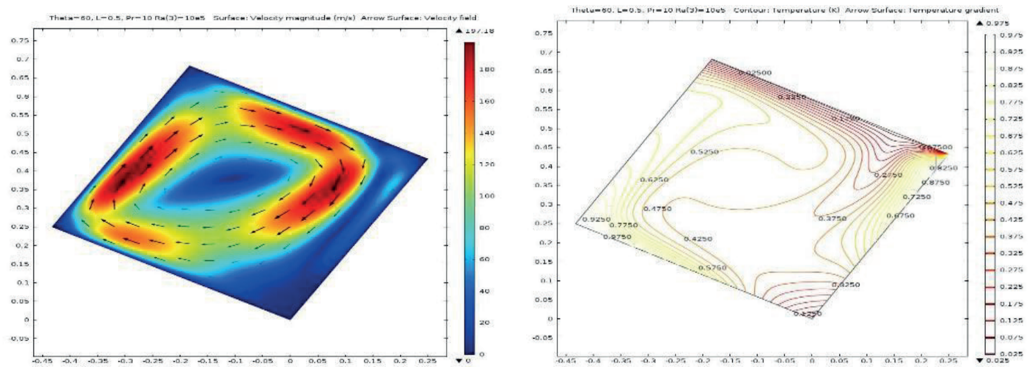

[b] Non-Uniform heating

Fig 5: Streamlines (on the left) and isotherm contours (on the right) in case of [a]uniform heating and [b]non-uniform heating for the values of $L = 0.5, Ra = 10^6, \varphi = 60$ and $Pr = 0.2, 10$

A more compact streamlines noticed for $Pr = 0.2$ near the cold wall. It is noticed that the isotherm patterns change slightly in case of both uniform and non-uniform heating with the enhancement of Prandtl number from 0.2 to 10. That is, Prandtl number has less effect on isotherm than that on streamline.

Effects of the angle of inclination on Streamlines and Isotherms

The figure (6) shows the streamlines (on the left) and the isotherm contours (on the right) inside the cavity for $L = 0.5$, $Ra = 10^6, \varphi = 0,30,60$ and $Pr = 10$ in case of both uniform & non-uniform heating. The strength of the velocity is highly noticed near the two vertical wall when $L = 0.5$, $Ra = 10^6, \varphi = 0,30$ and $Pr = 10$ in case of both uniform and non-uniform heating but for $L = 0.5$, $Ra = 10^6, \varphi = 60$ and $Pr = 10$ for both cases the strength of velocity is developed near the left vertical wall though the velocity field dominate most of the areas of the cavity for all values of angle of the inclination. With the increment of the angle of the inclination, the velocity magnitude changes slightly in both case of uniform and non-uniform heating. In case of uniform heating, the velocity magnitude for $\varphi = 60$ is approximately 1.09 times of that for $\varphi = 0$ and in case of non-uniform heating the velocity magnitude for $\varphi = 60$ is approximately equal of that for $\varphi = 0$. Here, we can also see that the velocity magnitude of uniform heating is always greater than that of non-uniform heating. An extra vortex is developed near the top wall in case of uniform heating for the values of $L = 0.5$, $Ra = 10^6, Pr = 10$ and $\varphi = 60$ whereas in case of non-uniform heating one vortex is formed near the lower corner of left vertical wall for the values of $L = 0.5$, $Ra = 10^6, Pr = 10$ and $\varphi = 30$ and one comparatively much prominent vortex is found near the bottom wall for the values of $L = 0.5$, $Ra = 10^6, Pr = 10$ and $\varphi = 60$. A more compact streamlines noticed for $\varphi = 0$ near the cold wall. It is noticed that the isotherm patterns change slightly in case of both uniform and non-uniform heating with the enhancement of angle of inclination. That is, angle of inclination has less effect on isotherm than that on streamline.

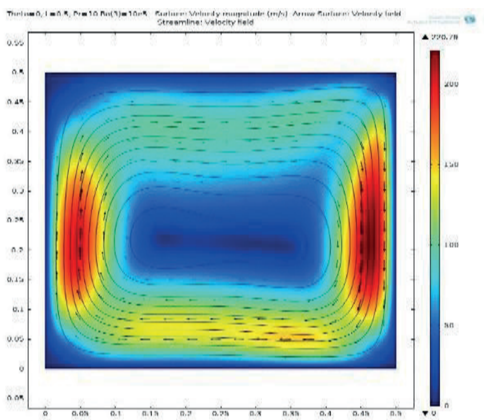

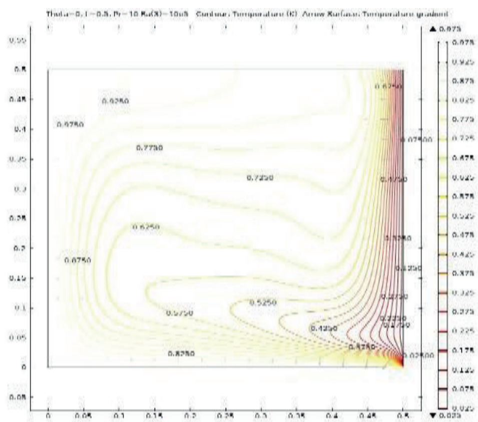

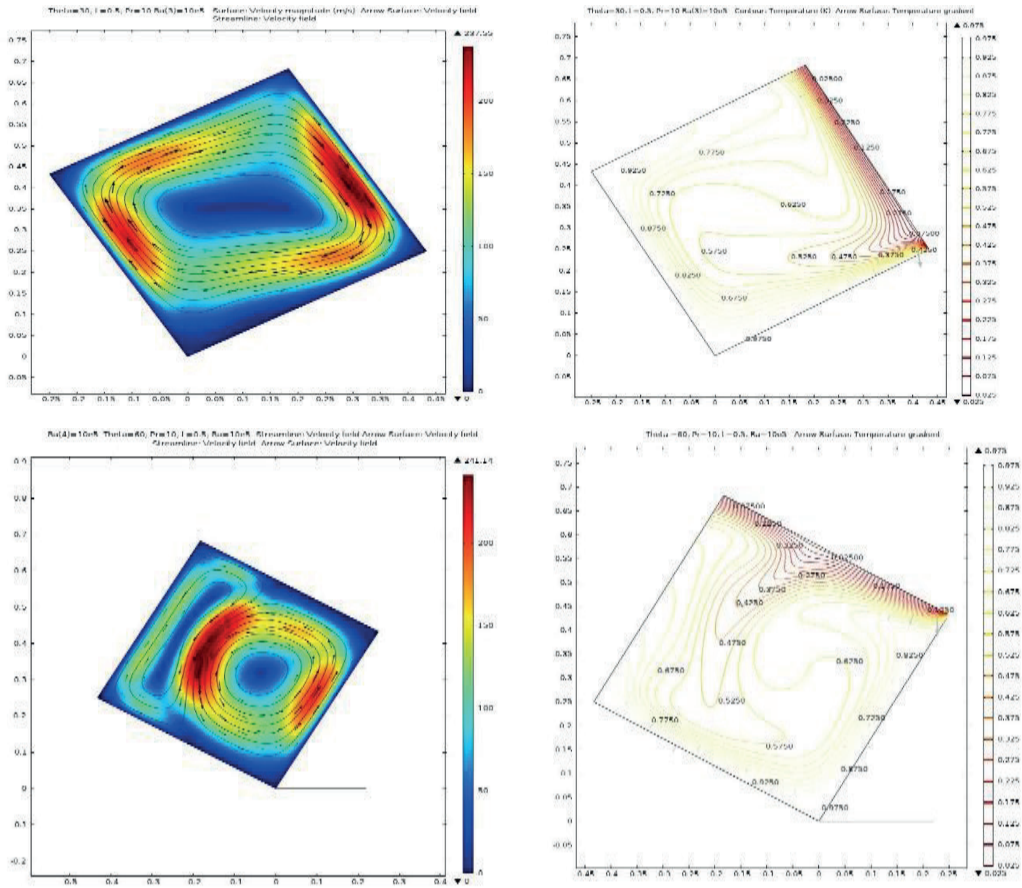

[a] Uniform heating with $\varphi = 0$ degree, $\varphi = 30$ degree and $\varphi = 60$ degree

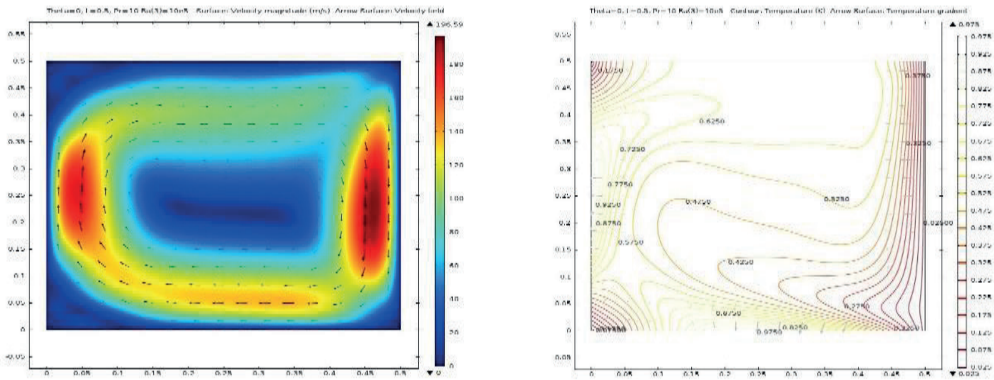

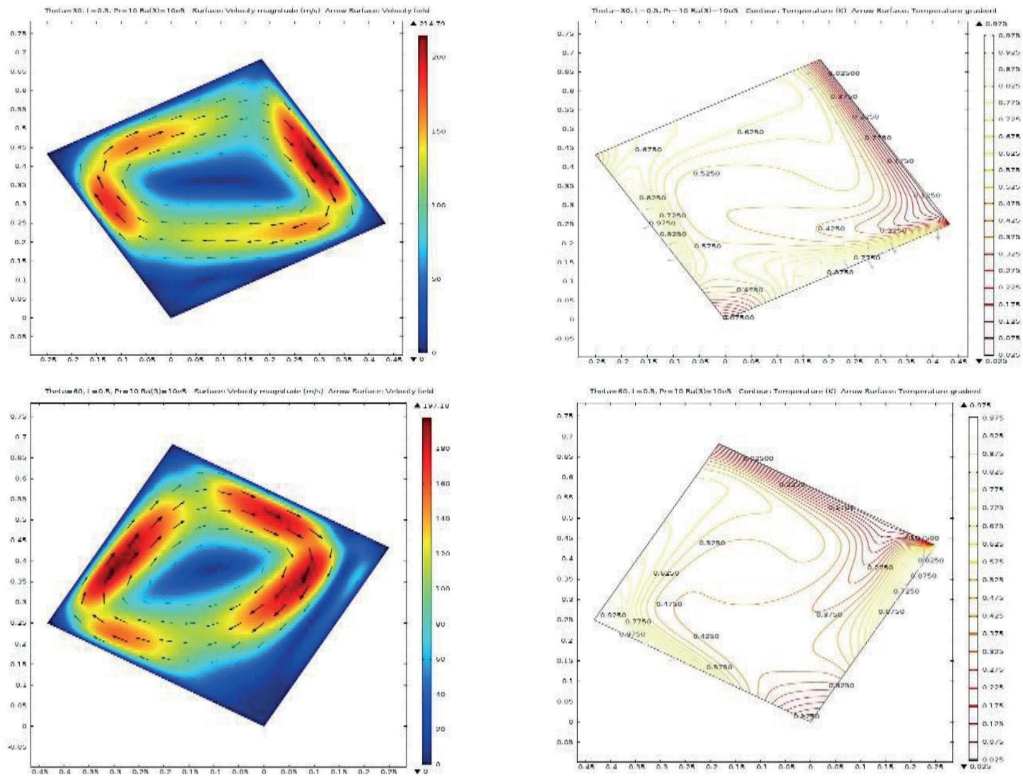

[b] Non- Uniform heating with $\varphi = 0$ degree, $\varphi = 30$ degree and $\varphi = 60$ degree

Fig 6: Streamlines (on the left) and isotherm contours (on the right) in case of [a]uniform heating and [b]non-uniform heating for the values of $L = 0.5, Pr = 10, Ra = 10^6$ and $\varphi = 0, 30, 60$

Effects on average Nusselt Number in case of angle of inclination:

From the figure 7[a], it is clear that in case of uniform heating, average Nusselt number at left vertical heated wall increases with increment of the angle of inclination of the cavity for all Rayleigh numbers. On the other hand, in case of non-uniform heating, average Nusselt number at left side heated wall decreases with the enhancement of the angle of inclination of the cavity for all Rayleigh numbers. The figure 7[b] reveals that, in case of uniform heating, the average Nusselt number at the bottom heated wall decreases with the increase of angle of inclination at $Ra = 10^3$. But at $Ra = 10^6$, average Nusselt number at bottom wall decreases when the angle of inclination increases from 0 to 30 degree for the values of $L = 0.25$ and $Pr = 0.2, 10$ while Nusselt number at that wall increases with the increasing of the angle of inclination from 30 to 60 degree for the values of $L = 0.25, Pr = 10$ and $L = 0.5, Pr = 0.2$. In rest of the cases, average Nusselt number at the bottom wall in uniform heating decreases with the increment of the angle of the inclination. Again, in case of non-uniform heating, the average Nusselt number at bottom heated wall first increases when φ increases from 0 to 30 degree but it decreases when φ increases from 30 to 60 degree for the cavity length of 0.25 meter. For the cavity length of 0.5 meter, in case of non-uniform heating, the average Nusselt number decreases when φ increases from 0 to 30 degree but it increases when φ increases from 30 to 60 degree.

[a]

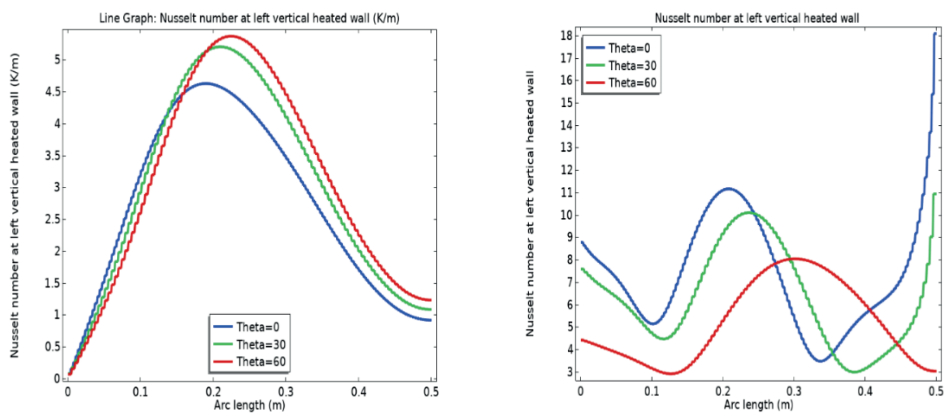

[b]

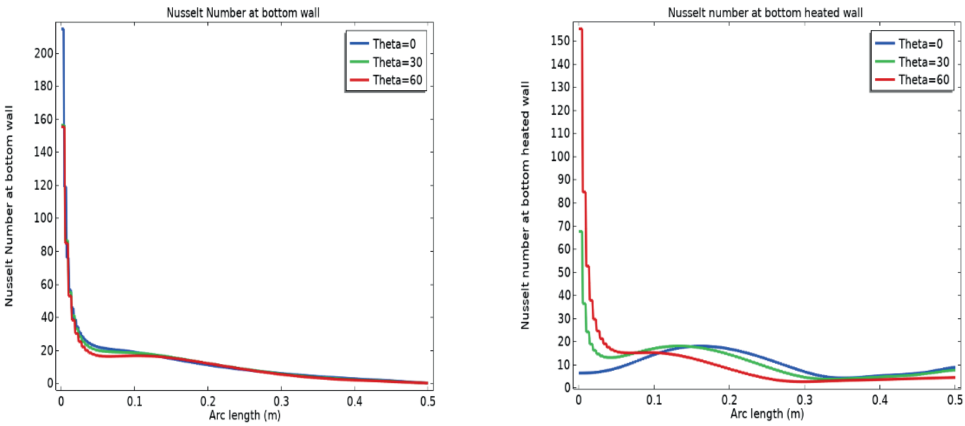

Fig 7: Variations of average Nusselt number with the variations of angle of inclination in case of uniform heating (on the left) and non-uniform heating (on the right) for $L = 0.50, Pr = 0.2, Ra = 10^6$ at [a] left vertical heated wall and [b] bottom heated wall

[a]

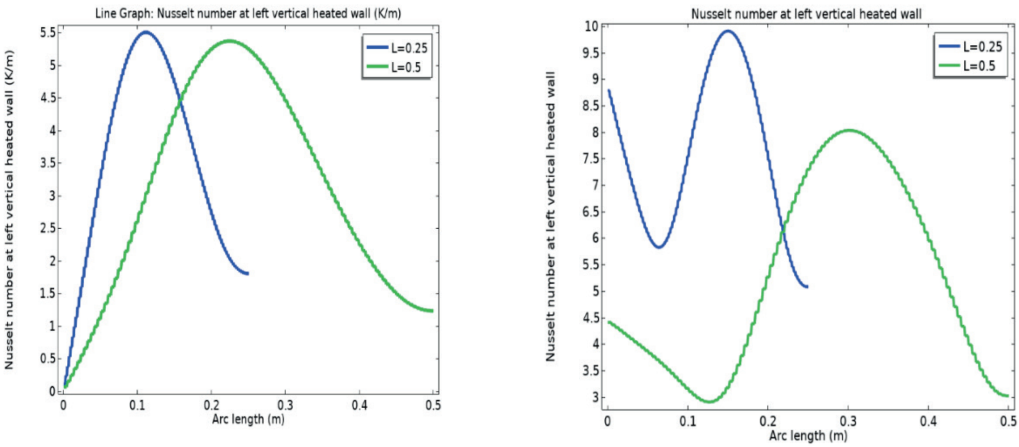

[b]

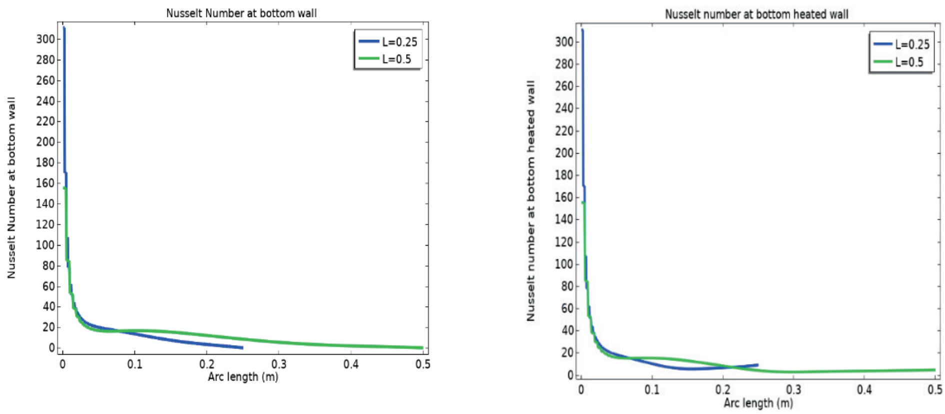

Fig 8: Variations of average Nusselt number with the variations of cavity length in case of uniform heating (on the left) and non-uniform heating (on the right) for $\varphi = 60, Pr = 0.2, Ra = 10^6$ at [a] left vertical heated wall and [b] bottom heated wall

Effects on average Nusselt Number in case of Cavity Length:

The figure 8[a] reveals that in case of uniform heating, the average Nusselt number at left vertical heated wall decreases with the increase of the cavity length at $Ra = 10^3$ but for Rayleigh number 10^6, when the cavity length increases, the heat transfer rate decreases and increases for $Pr = 0.2$ and $Pr = 10$ respectively. In case of non-uniform heating, the average Nusselt number at left vertical heated wall decreases with the enhancement of cavity length. On the other hand, the figure 8[b] demonstrates that, in case of uniform heating the average Nusselt number at bottom wall decreases along with the increment of cavity length. Irregular behavior of average Nusselt number at bottom wall is noticed in case of non-uniform heating. Th heat transfer rate decreases when the cavity length increases for the values of $\varphi = 0, Pr = 10, Ra = 10^3$; $\varphi = 60, Pr = 10, Ra = 10^3$; $\varphi = 0, Pr = 10, Ra = 10^6$.

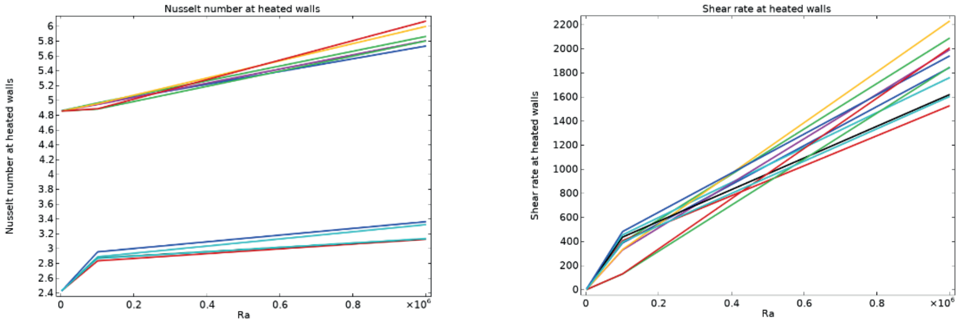

Fig 9(a): Variations of Nusselt number and Shear rate with the variations of Rayleigh number in case of uniform heating for various values of L, Pr and φ.

But it is clear that, when the cavity is inclined at 30-degree angle, the average Nusselt number decreases with the increment of cavity length for all values of Rayleigh numbers and Prandtl numbers.

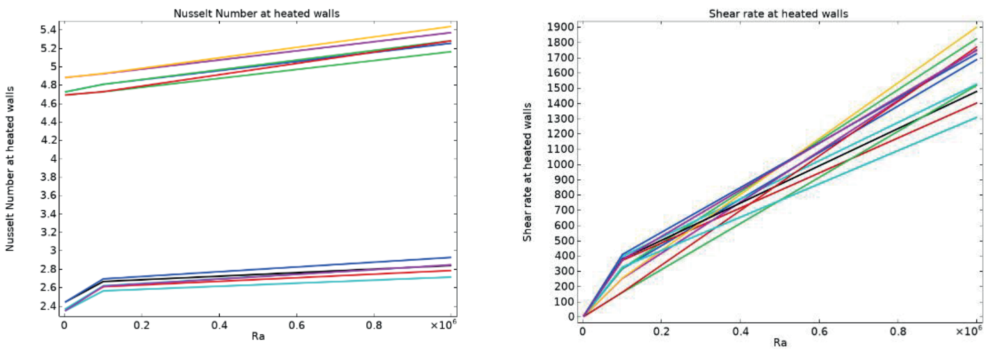

Fig 9(b): Variations of Nusselt number and Shear rate with the variations of Rayleigh number in case of non-uniform heating for various values of L, Pr and φ.

Again, at $Ra = 10^3$, the heat transfer rate at the bottom wall in non-uniform heating case increases when the cavity length increases for the values of $\varphi = 0, Pr = 0.2$; $\varphi = 60, Pr = 10$ and at $Ra = 10^6$, it increases along with the increment of cavity length when the cavity is inclined at 60 degree angle for all values of Prandtl number and also increases for the values of $\varphi = 0, Pr = 0.2$.

Effects Rayleigh Number on average Nusselt Number:

The figure (9) displays the heat transfer rate at the heated walls in terms of average Nusselt number and shear rate. From the figure, it is obvious that the heat transfer rate in terms of average Nusselt number at heated walls increases with the increment of Rayleigh number. Viscosity increases with the decreases of shear rate. That is viscosity maintains inverse relation with shear rate. As expected, it is observed from the figure that shear rate increases with the enhancement of Rayleigh number.

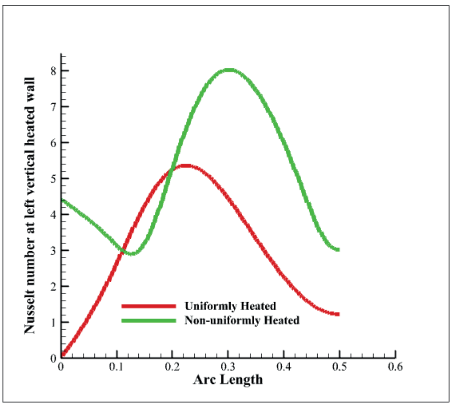

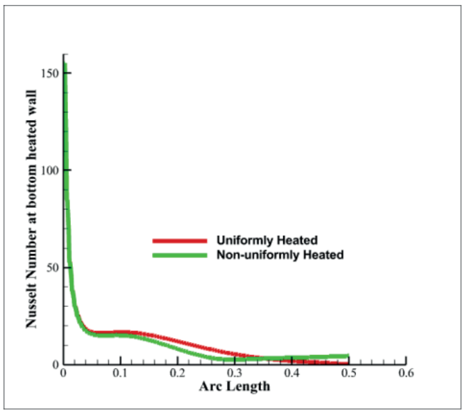

Fig 10: Variation of Nusselt number with the variation of type of heating at the left vertical heated wall (on the left) and bottom heated wall (on the right)

Effects on average Nusselt Number in case of Uniform and Non-uniform heating:

The figure (10) displays the comparison of uniform heating and non-uniform heating to analyze the heat transfer rate in terms of average Nusselt number at the heated walls. It is noticed that, heat transfer rate at the both heated walls are high for the non-uniform heating case. That is, non-uniform heating has a greater impact on average Nusselt number than uniform heating. In case of uniform heating, the maximum heat transfer at left side heated wall occurs for the values of $\varphi = 30$ degree, $L = 0.5, Pr = 10$ and $Ra = 10^6$ whereas the minimum heat transfer at that wall occurs for the values of $\varphi = 0$ degree, $L = 0.5, Pr = 0.2$ and $Ra = 10^3$. The highest and the lowest heat transfer at left vertical heated wall in case of non-uniform heating are found for the values of $\varphi = 0$ degree, $L = 0.25, Pr = 10, Ra = 10^6$ and $\varphi = 60$ degree, $L = 0.5, Pr = 0.2, 10$ and $Ra = 10^3$ respectively. The maximum and minimum heat transfer rate at bottom wall in case of uniform heating are noticed for the values of $\varphi = 0, L = 0.25, Pr = 10, Ra = 10^6$ and $\varphi = 60, L = 0.5, Pr = 0.2, Ra = 10^3$ whereas the maximum and minimum heat transfer rate at the bottom wall in case of non-uniform heating are noticed for the values of $\varphi = 30, L = 0.25, Pr = 10, Ra = 10^6$ and $\varphi = 30, L = 0.5, Pr = 0.2, 10$ and $Ra = 10^3$ respectively.

Conclusion

Here, the effects of uniform heating and non-uniform heating, Rayleigh number, Prandtl number, cavity length and the angle of inclination of the cavity is well investigated. The findings on the analysis can be summarized as follow:

- In case of uniform and non-uniform heating, the changing of the angle of inclination of the cavity doesn't have too much significant effect on streamlines at $Ra = 10^5$ but have a comparatively better effect at $Ra = 10^6$
- In both cases, the surface average velocity & the flow rate increase as the value of Rayleigh number, Prandtl number, cavity length and angle of inclination of the cavity increase.
- For non-uniform heating, the isotherm's patterns are almost similar in spite of the increase in the cavity length and the angle of inclination.
- In case of uniform heating, the average nusselt number and shear rate at the heated wall increase the angle of inclination, φ increases from 0 to 30 degree but they decrease when φ increases from 30 to 60 degree. And, in case of non-uniform heating the average nusselt number at the left vertical heated wall and bottom heated wall decreases as φ, the angle of inclination, increases from 0 to 60 degree while the average shear rate at the both heated wall increases as Ra and the cavity length increase in later case.
- In case of uniform heating, the maximum average nusselt number is found for $L = 0.25, Pr = 10$, $\varphi = 30$ and $Ra = 10^6$ and the minimum average nusselt number is found for $L = 0.50, Pr = 0.2, \theta = 0$ and $Ra = 10^5$
- In non-uniform heating case, the maximum average nusselt number at the left vertical heated wall is found for $L = 0.50, Pr = 10$, $\varphi = 30$ and $Ra = 10^6$ and the minimum average nusselt number at the left vertical heated wall is found for $L = 0.25, Pr = 0.2$, $\varphi = 60$ and $Ra = 10^5$. Again, the maximum average nusselt number at the bottom heated wall is found for $L =$

$0.25, Pr = 0.2,\ \varphi = 0$ and $Ra = 10^6$ and the minimum average nusselt number at the bottom heated wall is found for $L = 0.25, Pr = 10,$ $\varphi = 60$ and $Ra = 10^5$.

In future, the authors are interested to investigate the mixed convection in the presence of magnetic field and mass transfer for the same problem.

References

C. Xia, J. Y. Murthy. 2002. Buoyancy-driven flow transitions in deep cavities Heated from below, ASME Trans. Journal of Heat Transfer 124: 650-659.

E. Natarajan, Tanmay Basak, S. Roy. 2008. Natural convection flows in a trapezoi-dale nclosure with uniform and non-uniform heating of bottom wall, International Journal of Heat and Mass Transfer 51: 747-756.

G. A. Sheikhzadeh et al. 2011. Natural convection of Cu-water in a cavity with partially active side wall, European Journals of Mechanics B/Fluids 30: 166-176.

G. Barakos, E. Mitsoulis. 1994. Natural convection flow in a square cavity revisit-ed: laminar and turbulent models with wall functions, International Journal of Numerical Methods Fluids 18: 695-719

G. Dr Vahl Davis. 1983. Natural convection of air in a square cavity, a benchmark numerical solution, International Journal of Numerical Methods Fluids 3:249-264.

Hakan F. Oztop, Moghtada Mobedi, Eiyad Abu-Nada, Ioan Pop. 2012. A heatline analysis of natural convection in a square inclined enclosure filled with a CuO nanofluid under non-uniform wall heating condition, International Journal of Heat and Mass Transfer 55: 5076-5086

Hakan Karatas, Taner Derbentli. 2017. Natural convection in rectangular cavities with one active vertical wall, International Journal of Heat and Mass Transfer 105: 305-315

J. D. Hall, A. Bejan, J.B. Chaddock. 1988. Transient natural convection in a rectangular enclosure with one heated side wall, International Journal of Heat and Fluid Flow 9: 396-404.

J. L. lage, A. Bejan. 1991. The Ra-Pr domain of laminar natural convection in an enclosure heated from the sider, Numerical Heat Transfer Part A 19: 21-41.

J. L. Lage, A. Bejan. 1993. The resonance of natural convection in an enclosure heated periodically from the side, International Journal of Heat and Mass Transfer 36: 2027-2038.

J. M. Hyun, J.W. Lee. 1989. Numerical solutions of transient natural convection in a square cavity with different side wall temperature, International Journal of heat and Fluid Flow 10: 146-151.

J. Patterson, J. Imberger. 1980. Unsteady natural convection in a rectangular cavity, Journal of Fluid Mechanics. 100: 65-86.

Mefteh Bouhalleb, Hassan Abbassi. 2015. Natural convection in an inclined rectangular rectangular enclosure filled by CuO-H_2O nanofluid with sinusoidal temperature distribution, International Journal of Hydrogen Energy.40:13676-13684.

M. Leporini, F. Corvaro, B. Marchetti, F. Polonara, M. Benucci. 2018. Experimental and numerical investigation of natural convection in tilted square cavity filled with air, Experimental Thermal and Fluid Science, 99: 572-583.

N.C. Markatos, K.A. Pericleous. 1984. Laminar and turbulent natural convection in an enclosed cavity, International Journal of Heat and Mass Transfer 27: 772-775

N. Zhan et al. 2019. Experimental study on natural convective heat transfer in a closed cavity, Thermal Science and Engineering 9: 132-141

S. Roy, T. Basak. 2005. Finite element analysis of natural convection flows in a square cavity with non-uniformly heated wall(s), International Journal of Engineering Science 43: 668-680.

T. Fusegi, J. M. Hyun, K. Kuwahara. 1992. Natural convection in a differentially heated square cavity with internal heat generation, Numerical Heat Transfer Part A 21:215-229.

V. F. Nicolette, K.T. Yang, J.R. Lloyd. 1985. Transient cooling by natural convection in a two-dimensional square enclosure, International Journal of Heat and Mass Transfer 28: 1721-1732

Vimal Kishor, Suneet Singh, Atul Srivastava. 2018. Investigation of convective heat transfer phenomena in differentially-heated vertical closed cavity: Whole field experiments and numerical simulations, Experimental Thermal and Fluid Science 99: 71-84

W. J. Minkowycz, E.M. Sparrow, G. E. Schneider, R. H Fletcher. 1988. Handbook of Numerical Heat Transfer, Wiley, New York.

BICYCLIC LACTAM TEMPLATE: A USEFUL TOOL FOR THE SYNTHESIS OF FUNCTIONALISED PYRROLIDONES

Halima Bagum[1], * and Mark G. Moloney[2]

[1] *Department of Chemistry, University of Barishal, Barishal-8254, Bangladesh*

[2] *Department of Chemistry, University of Oxford, 12 Mansfield Road, Oxford, United Kingdom*

Abstract

Development of an efficient methodology to synthesise pyrrolidones has gained significant importance as pyrrolidones are known as compounds having potent biological activities. This review will explore the preparative methods of this class of compounds from bicyclic lactams. The route will permit easy access to pyrrolidones.

Keywords: Lactam, Pyrrolidone, Pyroglutamate, Oxazolomycin, Natural Products.

Introduction

Pyrrolidones 1, 2 are heterocyclic organic compounds consisting of a 5-membered lactam (Fig. 1). Their derivatives have been reported as having various medicinal property. (Jouyban et al., 2010; Miguel et al., 2009) Bicyclic lactam 3 can be used to prepare various derivatives of pyrrolidone. This review will explain the use of this moiety as a key tool to synthesise library of pyrrolidone derivatives.

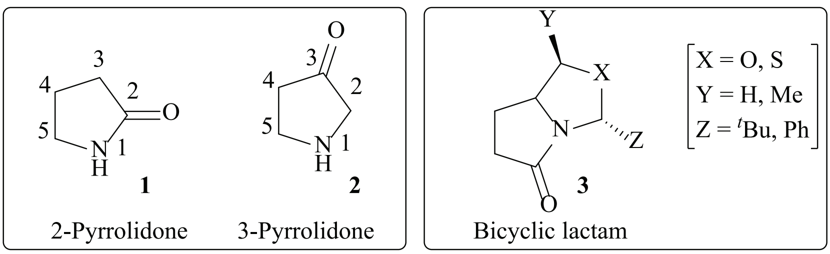

Fig. 1: Pyrrolidones and Bicyclic lactam

Functionalised Pyrrolidones Derived from Bicyclic Lactam Template

3-Substituted Pyroglutaminols and Pyroglutamates

**Corresponding author.*
E-mail address:halimaju35@gmail.com

The Moloney group(Jeong et al., 2011) has been interested in the development of methodology for the efficient synthesis of functionalised pyrrolidinones, since this class of compounds has potent biological activity and application in the synthesis of bio-active compounds.

Bailey and co-workers(Bailey et al., 2000) reported the synthesis of functionalised pyroglutamates following methodology developed by Dyer.(Dyer et al., 1998) They used a bicyclic lactam template 4 with C-7 ethoxycarbonyl activating group, which allowed effective conjugate addition, providing protection of amide and hydroxy functional groups in a single benzylidene protecting group (Scheme 1). Conjugate addition of triethyl methanetricarboxylate to acylated lactam 4, prepared by literature procedure,(Bailey et al., 1997) under phase transfer conditions(Skarzewski, 1990) (Bu4NHSO4, K2CO3, anhydrous toluene at 60°C) gave the adduct 5a as a single diastereomer (6S,7S).

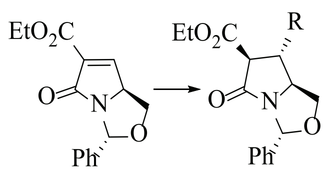

4 **5**

Product	**Conditions**	**Diastereomeric ratio**	**Yield (%)**
5a: R = $C(CO_2Et)_3$	A	1	60
5b: R = $CH(CN)CO_2Me$	B	1:1	54
5c: R = $CH(C(O)Me)CO_2Et$	C	1:1:4.5:4.5	72
5d: R = $CH_2CO_2{}^tBu$	D	1:5.5:43.5	77
5e: R = CH_2CO_2Et	E	Not determined	27
5f: R = $CH(Me)CO_2Me$	F	1:5:9:35	56
5g: R = $CH(Ph)CO_2Me$	G	1:17:17:74	53

Conditions: A = Bu_4NHSO_4, K_2CO_3; B = $NaNH_2$, DMPU, THF; C = $Ba(OH)_2$, EtOH; D = Zn, ultrasound, THF, DMPU, 30-35°C; E = Zn, ultrasound, dioxane, 35°C; F = Zn, ultrasound, THF, -5°C; G = Zn, ultrasound, THF, -10°C.

Scheme 1: Conjugate additions to acylated lactam 4(Bailey et al., 1997)

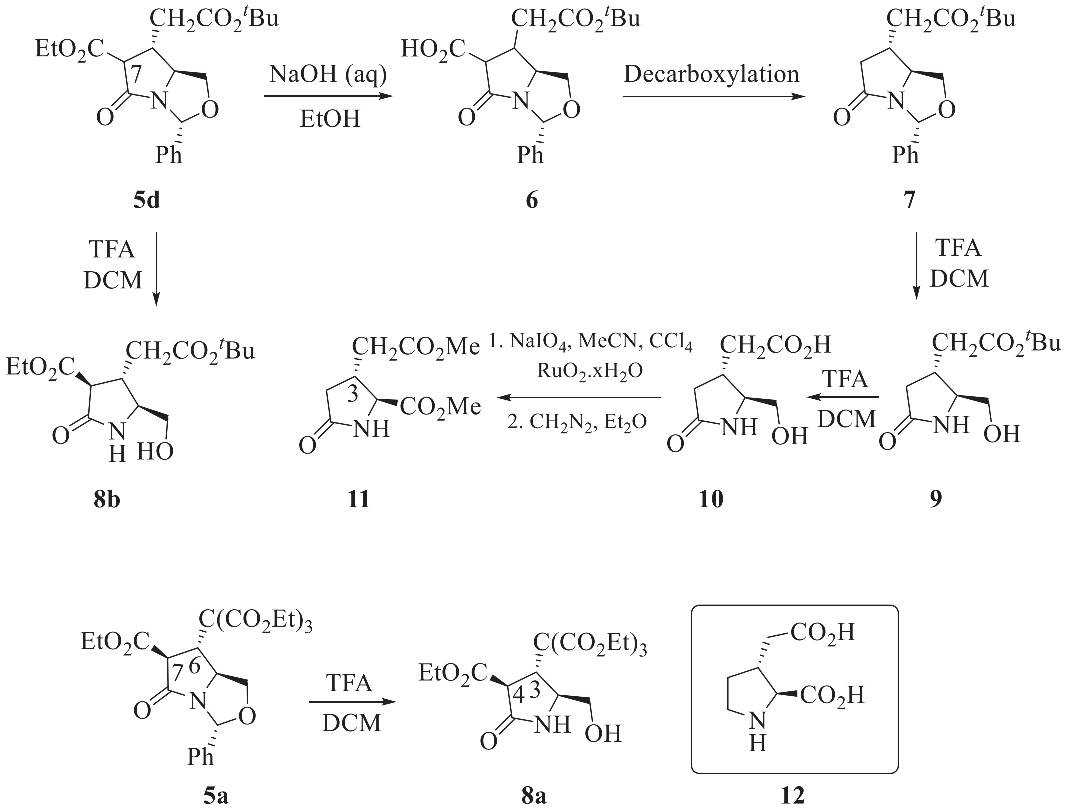

Scheme 2: Synthesis of 3-substituted pyroglutaminols and pyroglutamates **8a**, **8b** and **11** by Moloney group(Bailey et al., 2000)

However, the reactions of methyl cyanoacetate and ethyl acetoacetate with lactam **4** gave an inseparable mixture of diastereoisomers **5b** and **5c**. Improved yields were observed by changing the conditions to Reformatsky conditions,(Leonard et al., 1998) and compounds **5d-g** were generated under these conditions. Carboxylic acid **6** was obtained by selective hydrolysis of the ethyl ester over the *tert*-butyl ester of **5d**, and subsequent decarboxylation(Krapcho, 1982) yielded compound **7** (Scheme 2). Finally, functionalised pyrrolidinones **8** were achieved by *N,O*-acetal deprotection.

Treatment of lactam **5a** with TFA resulted in pyroglutaminol **8a**. The same conditions at even shorter reaction time gave pyrrolidinone **8b**. Treatment of **7** with TFA in DCM afforded pyroglutaminol **9**, which was reported as an intermediate(Ikeda et al., 1995) in the synthesis of (-)-(*2S,3R*)-2-carboxypyrrolidine-3-acetic acid (CPAA) **12**, an NMDA receptor agonist.(Tsai et al., 1988) Further treatment with TFA removed *tert*-butyl ester to yield **10**, which upon oxidation afforded 3-substituted pyroglutamate **11**.

3,4-Disubstituted Pyroglutaminols and Pyroglutamates

In continuation of the works described above, Dyer and co-workers(Dyer et al., 2000) investigated the ring functionalisation at C7 of esters **5a** and **5d**, in order to access conformationally constrained 4-aryl-5-oxo and 4-arylmethyl-5-oxo analogues of kainic acid **13** (Scheme 3).(Dyer et al., 1998) Attempted ring functionalisation by arylation with phenyllead triacetate was found futile for adduct **5a**, whereas **5d** was used successfully to access desired kainoid analogues **22**. Compound **5d** was treated with aryllead reagents, which afforded products **14** and **15** as inseparable mixture of diastereomers.

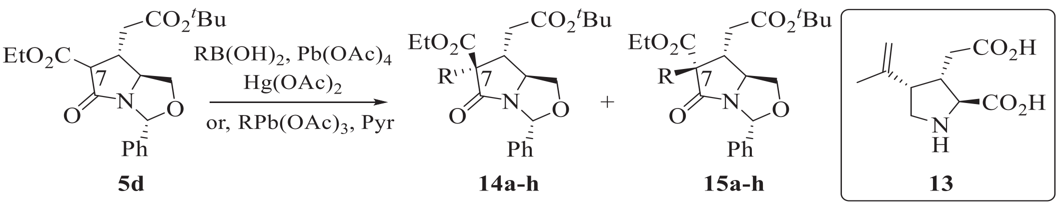

Product	Diasteriomeric ratio (14:15)	Yield (14, 15) (%)
a: R = Ph	2.4:1	61, 25
b: R = *o*-$MeOC_6H_4$	1.7:1	45, 27
c: R = *m*-$MeOC_6H_4$	4:1	67, 17
d: R = *p*-$MeOC_6H_4$	2.3:1	42, 18
e: R = *p*-$CF_3C_6H_4$	2.3:1	50, 22
f: R = *p*-BrC_6H_4	2.3:1	52, 22
g: R = *p*-$MeOC_6H_4$	2.3:1	26, 12
h: R = $PhCH_2$	1:12	34, 41

Scheme 3: Arylation and alkylations of lactam **5d**.

Deprotection of lactams **14a**,**g**,**h** and **15a**,**g**,**h** was performed with TFA in DCM, which gave diastereomerically pure alcohols **16** and **17** (Scheme 4).To remove the ethoxycarbonyl substituent at C7 position, hydrolysis and decarboxylation was performed on **16a**,**h**, resulting in the diastereomers **18** and **19** with higher proportion of **18** having the desired kainic acid configuration.

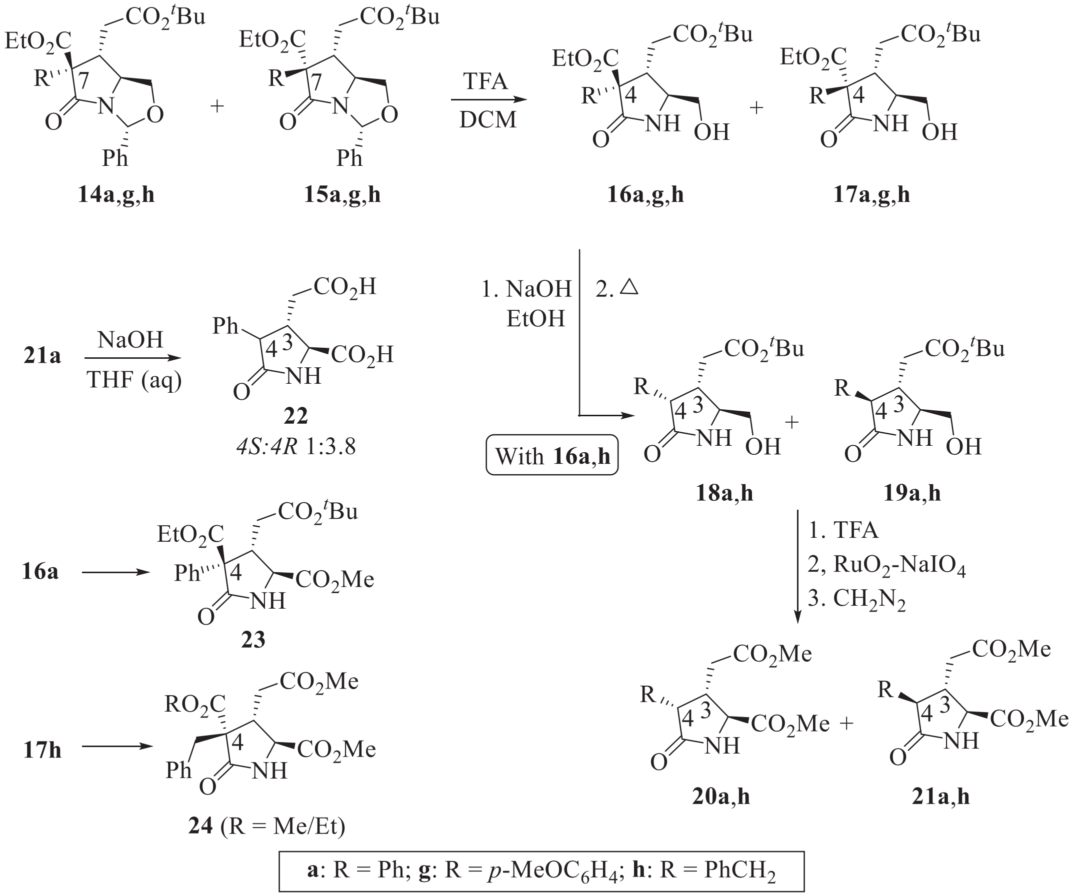

Scheme 4: Synthesis of 3,4-substituted pyroglutaminols and pyroglutamates by Moloney group(Dyer et al., 2000)

Treatment of alcohols **18** and **19** with TFA removed the *tert*-butyl group and subsequent oxidation with ruthenium(IV) oxide/sodium periodate and methylation with diazomethane gave the expected diastereomers **20** and **21**. Hydrolysis of dimethyl ester **21a** with NaOH in aqueous THF afforded kainoid analogues **22** as a mixture of *4S* and *4R* isomers with *4R* as major isomer. Pyrrolidinone **16a** was converted to **23** via oxidation and esterification, while **17a** failed under the same conditions. Conversion of **17h** by hydrolysis, decarboxylation and oxidation, as described for the conversion of **16** to **20**/**21**, gave an almost equal mixture of methyl ester and ethyl ester (at C4) **24** (Scheme 4).

Recently, the Moloney group has been interested in modification at C7 of bicyclic tetramate type **28**, leading to 3-acyl tetramic acid moiety **25**, found in natural products with antibacterial activities.(Gänzle, 2004; Tuske et al., 2005; Vinale et al., 2009) Josa-Cullere *et al*.(Josa-Culleré et al., 2017) reported the use of Weinreb amides in the chemoselective formation and reaction of densely functionalised bicyclic tetramic acids **28** with Grignards(Scheme 5). Treatment of oxazolidine/thiazolidine(Andrews et al., 1998)**26** with methoxy(methyl)carbamic chloride gave tricarbonyl compound **27**, which was then cyclised to Weinreb amide **28** using DBU/THF.

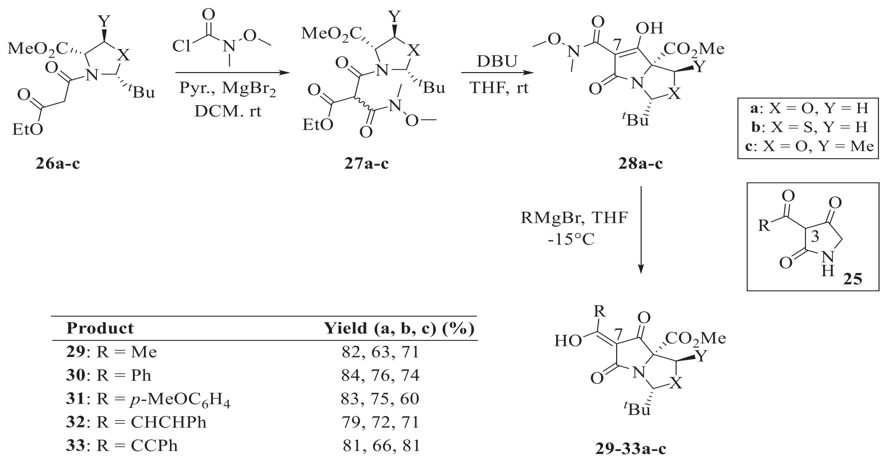

Product	Yield (a, b, c) (%)
29: R = Me	82, 63, 71
30: R = Ph	84, 76, 74
31: R = p-MeOC$_6$H$_4$	83, 75, 60
32: R = CHCHPh	79, 72, 71
33: R = CCPh	81, 66, 81

Scheme 5: Preparation and reaction of Weinreb amides(Josa-Culleré et al., 2017)

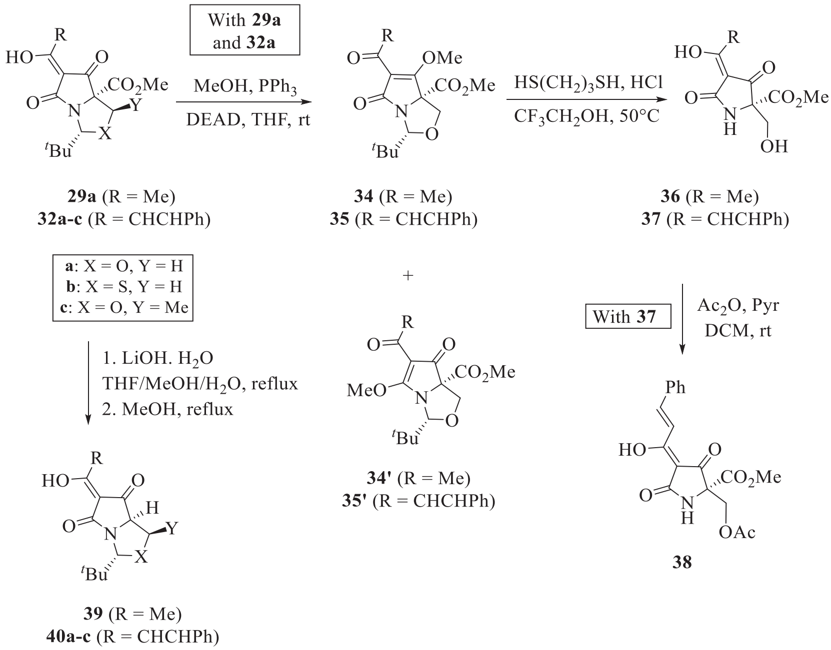

Scheme 6: *N,O*-Acetal deprotection and hydrolysis of **29a** and **32a-c** (*Eur. J. Org. Chem*, 2017, 7055-7059)

Attempted *N,O*-acetal deprotection was not successful for all of the synthesised compounds **29-33** with a variety of deprotection reagents.(Josa-Culleré et al., 2017) These deprotected compounds were instead accessed by methylating **29a** and **32a** using Mitsunobu reaction conditions,(Bajwa & Anderson, 1990) which gave a mixture of enolates **34/35** and **34'/35'**, followed by treatment with propane-1,3-diol and 2,2,2-trifluroethanol at 50°C, resulting in the formation of deprotected alcohol **36** from **34** (Scheme 6). A similar conversion for **35** was found to be difficult at the purification stage of **37**, hence crude **37** was treated with an acylating reagent to isolate protected alcohol **38**. Decarboxylated products **39** and **40a-c** were prepared diastereoselectively via hydrolysis with excess LiOH and reflux in MeCN.

Characteristic Examples of Natural Products Having Lactam Moiety

Oxazolomycin

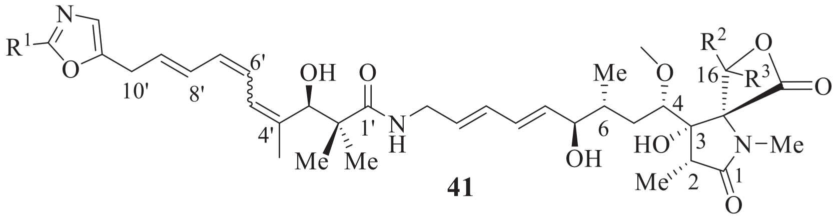

41

Oxazolomycin A	**a**: R^1 = H, R^2 = H, R^3 = H; 4'Z,6'Z,8'E
Oxazolomycin B	**b**: R^1 = H, R^2 = H, R^3 = H; 4'E,6'E,8'E
Oxazolomycin C	**c**: R^1 = H, R^2 = H, R^3 = H; 4'Z,6'E,8'E
16-Methyloxazolomycin	**d**: R^1 = H, R^2 = H, R^3 = Me; 4'Z,6'Z,8'E
Curromycin A	**e**: R^1 = Me, R^2 = H, R^3 = CH_2OMe; 4'Z,6'Z,8'E
Curromycin B	**f**: R^1 = Me, R^2 = H, R^3 = Me; 4'Z,6'Z,8'E
KSM-2690 B	**g**: R^1 = H, R^2 = Me, R^3 = H; 4'Z,6'Z,8'E
KSM-2690 C	**h**: R^1 = H, R^2 = Me, R^3 = H; 4'Z,6'E,8'E

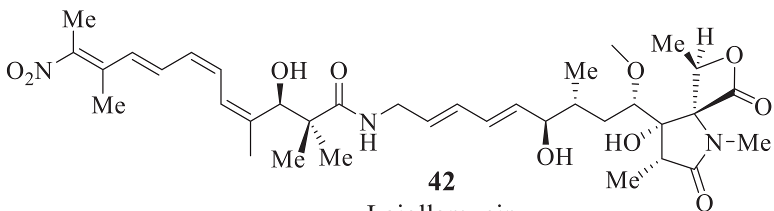

42
Lajollamycin

Fig. 2: Structure of oxazolomycin class of natural products (*Org. Biomol. Chem.*, 2012, **10**, 3472-3485).

The oxazolomycin class of natural products (Fig. 2), oxazolomycin A-C **41a-c**, 16-methyloxazolomycin **41d**, curromycin A-B **41e-f**, KSM2690 **41g-h** and lajollamycin **66**, are well-known for their structural features and wide range of biological activity.(Moloney et al., 2004) For example, lajollamycin **42** shows antibacterial activity against drug-sensitive and drug-resistant micro-organisms (Table 1) and inhibits the growth of murine melanoma cell line B16-F10, with an EC_{50} of 9.6 μM.(Manam et al., 2005)

Table 1: Minimum inhibitory concentration (MIC) values for lajollamycin **42** against bacterial strains (*Journal of Natural Products*, 2005, **68**, 240-243)

SL	Microorganism	MIC (μg/mL)
1	*Staphylococcus aureus* - methicillin sensitive	4
2	*Staphylococcus aureus* – methicillin resistant	5
3	*Streptococcus pneumoniae* – penicillin sensitive	2
4	*Streptococcus pneumoniae* – penicillin resistant	1.5
5	*Enterococcus faecalis* – vancomycin sensitive	14
6	*Enterococcus faecium* – vancomycin resistant	20
7	*Escherichia coli - imp*	12

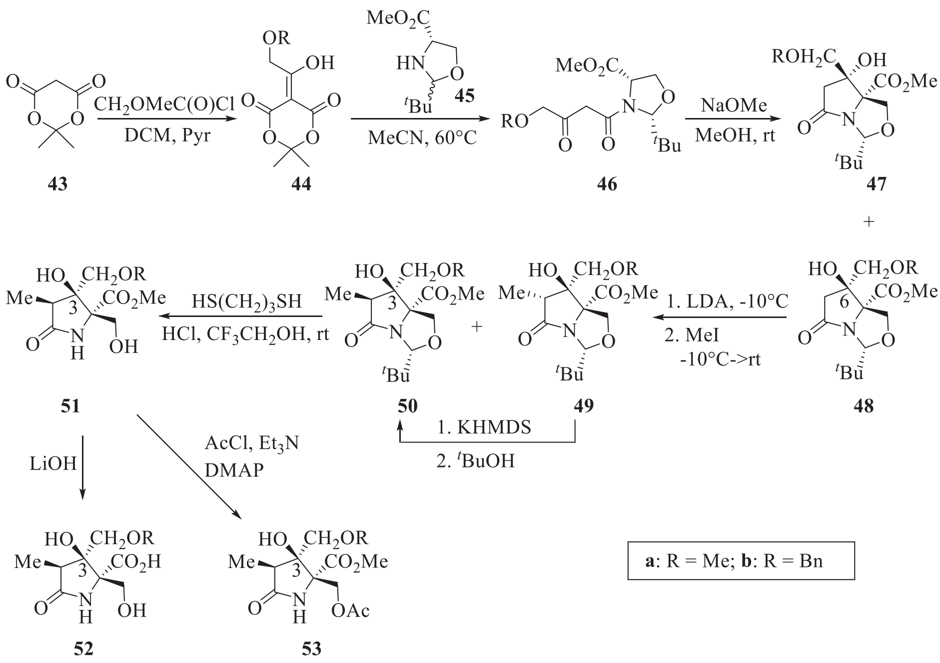

Scheme 7: Synthesis of mimics of the complex spirolactam-lactone system of the oxazolomycins via 6-substituted bicyclic pyroglutamates **48**.(Angelov et al., 2012)

Angelov *et al.*(Angelov et al., 2012)reported the synthesis of functionalised pyroglutamates, which are simpler mimics of the more complex spirolactam-lactone system of the oxazolomycins (Scheme 7). Acylation of Meldrum's acid **43** using methoxyacetyl chloride generated **44**, which was treated with oxazolidine **45** at 60 °C to give amide **46**. Intramolecular Aldol reaction of ketoamides **46** was achieved in presence of sodium methoxide and methanol, and the product was obtained as mixture of diastereomers **47** and **48** (major) among which the major one had correct relative stereochemistry for oxazolomycin.(Angelov et al., 2012)*C*-Alkylation on **48** was carried out using LDA and excess MeI, giving the products **49** (major) and **50** (minor). Fortunately, treatment of **49** with KHMDS followed by ^{t}BuOH yielded **50**, having the correct relative stereochemistry for oxazolomycins. Deprotection of **50** was carried out following Corey's procedure(Corey & Reichard, 1992) to yield pyroglutaminols **51**. Ester hydrolysis of **51** gave corresponding acids **52**, with the correct relative configuration for the right-hand fragment of oxazolomycins. Similarly, successful acetylation was carried out on **51** yielding pyroglutamates of the type **53**. Of the compounds with correct relative configuration for the right-hand fragment of oxazolomycins, **51b** and **53b** were found to be active against *S. aureus*, and **50b**, **51a**, **51b**, **52a**, **53b** were active against *E. coli*.

Pramanicin

Paramanicin **54**, containing a highly functionalised pyroglutaminol moiety and functionalised fatty acid chain, was shown to exhibit antibacterial activity(Schwartz et al., 1994) against *Bacillus subtilis* with minimum inhibitory concentration (MIC) of 4μM.

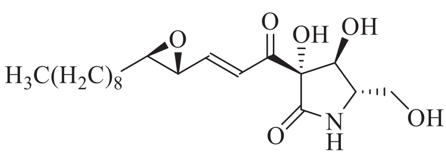

54

Fig. 3: Structure of pramanicin (*Org. Biomol. Chem.*, 2017, **15**, 1889-1912)

Microtiter dish broth dilution assays were used in determining antifungal activity. The results are shown in Table 2.

Table 2: Antimicrobial activity of Paramanicin **54** (*Tetrahedron*, 1994, **50**(6), 1675-1686)

SL NO	Organism	MIC of Pramanicin, μM
1	*Candida albicans*	20.0
2	*Candida parapsilosis*	4.0
3	*Candida tropicalis*	20.0
4	*Candida krusei*	>100.0
5	*Cryptococcus neoformans*	20.0
6	*Cryptococcus neoformans*	0.062
7	*Aspergillus fumigatus*	100.0

Lincosamides

Lincosamides(Spížek et al., 2004) are naturally occurring compounds, with a chemically distinct pyrrolidine core structure (Fig. 4) and having wide range of biological activities. The first member of this family discovered was lincomycin **55**,(Hoeksema et al., 1964) which was first introduced clinically in 1963. Lincomycin was shown to be clinically effective in a number of bacterial infections including *Staphylococcus osteitis*, infective dermatoses, and respiratory infections.(HOLLOWAY et al., 1963) Excellent results were found in the treatment of penicillin-resistant infections, including penicillinase-producing *Staphylococcus pyogenes* in children.(Bentley & Pollock, 1968) Later, the original lincosamide antibiotic was superseded by a semi-synthetic drug clindamycin **56**, a derivative of lincomycin, because of its wide activity and better absorption behaviour after oral adminstration.(Birkenmeyer & Kagan, 1970)

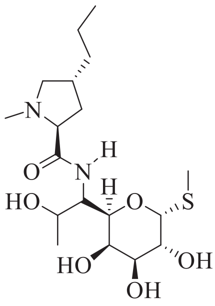

55
Lincomycin

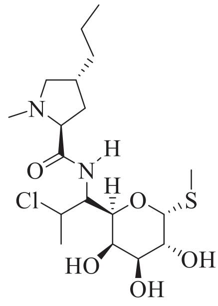

56
Clindamycin

Fig. 4: Structure of Lincosamides (*J. Mol. Model*, 2012, **18**, 2727-2740)

The spectrum of activity for lincosamides includes staphylococci, penicillinase-producing strains, haemolytic streptococci, pneumococci, and *C. diptheriae* and the minimum inhibitory concentration for most strains of these compounds is usually less than 2 μg/mL.(Bentley & Pollock, 1968)

Lucentamycins

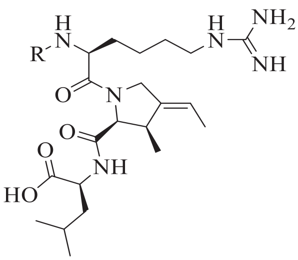

57

Lucentamycin A, R = 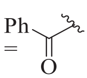

Lucentamycin C, R = 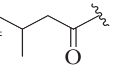

Lucentamycin D, R = 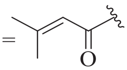

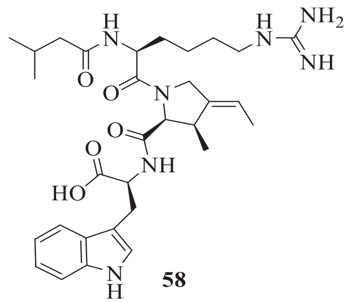

58

Lucentamycin B

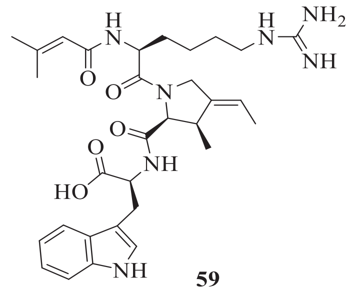

59

Lucentamycin E

Fig. 5: Structure of Lucentamycins (*J. Nat. Prod.,* 2012, **75**, 1648-1651)

The lucentamycins(Cha et al., 2012; Cho et al., 2007; Ranatunga et al., 2012) are a family of tripeptides produced by *Nocardiopsis lucentensis* (strain CNR-712) from the fermentation broth of a marine-derived actinomycete.(Cho et al., 2007) They are structurally novel with 3-methyl-4-ethylideneproline unit (Fig. 5) and show significant *in vitro* cytotoxicity against HCT-116 human colon carcinoma.(Cho et al., 2007)

Conclusions

This review extensively describes the efficient synthetic strategy for the conversion of bicyclic lactam to 3-substituted and 3,4-disubstituted pyrrolidones. Though some compounds was found as mixture of diastereoisomers, **5a** was found as a single diastereomer. Ester **5d** was used successfully to furnish desired kainoid analogues **22**. An intermediate **9** in the synthesis of CPAA, an NMDA receptor agonist, was prepared efficiently. Conversion of **16a,h** to **18** and **19** permitted a compound having kainic acid configuration. Moloney group successfully modified bicyclic tetramate **28** leading to 3-acyl tetramic acid core, found in natural products with antibacterial activities. Fortuitously, correct relative stereochemistry for oxazolomycins was found by treatment of **49** with KHMDS followed by ^{t}BuOH. Fruitful acylation was carried out on **51** yielding **53**.

Among the synthesized compounds with correct relative configuration for the right-hand fragment of oxazolomycins, **51b** and **53b** were found to be active against *S. aureus*, and **50b**, **51a**, **51b**, **52a**, **53b** were active against *E. coli*.

Acknowledgements

I wish to express my sincere gratitude to Professor M. G. Moloney for giving me the opportunity to carry out this work in his research group.

References

Andrews, M. D., Brewster, A. G., Crapnell, K. M., Ibbett, A. J., Jones, T., Moloney, M. G., Prout, K., & Watkin, D. 1998. Regioselective Dieckmann cyclisations leading to enantiopure highly functionalised tetramic acid derivatives. *Journal of the Chemical Society, Perkin Transactions 1*, **2**, 223–236.

Angelov, P., Chau, Y. K. S., Fryer, P. J., Moloney, M. G., Thompson, A. L., & Trippier, P. C. 2012. Biomimetic synthesis, antibacterial activity and structure–activity properties of the pyroglutamate core of oxazolomycin. *Organic & Biomolecular Chemistry*, **10(17)**, 3472.

Bailey, J. H., Cherry, D. T., Crapnell, K. M., Moloney, M. G., Shim, S. B., Bamford, M. J., & Lamont, R. B. 1997. Functionalised Pyrrolidinones Derived from (S)-Pyroglutamic Acid by Cycloaddition Reactions. *Tetrahedron*, **53(34)**, 11731–11744.

Bailey, J. H., Cherry, D. T., Dyer, J., Moloney, M. G., Bamford, M. J., Keeling, S., & Lamont, R. B. 2000. Pyrrolidinones derived from (S)-pyroglutamic acid. Part 1. Conformationally constrained glutamate. *Journal of the Chemical Society, Perkin Transactions 1*, **66(16)**, 2783–2792.

Bajwa, J. S., & Anderson, R. C. 1990. Regiospecific O-alkylation of δ-tetronic acids under mitsunobu-reaction conditions. *Tetrahedron Letters*, **31(48)**, 6973–6976.

Bentley, J. F. R., & Pollock, D. 1968. Lincomycin in the treatment of penicillin-resistant staphylococcal infections in children. *Archives of Disease in Childhood*, **43(227)**, 58–61.

Birkenmeyer, R. D., & Kagan, F. 1970. Lincomycin. XI. Synthesis and structure of clindamycin, a potent antibacterial agent. *Journal of Medicinal Chemistry*, **13(4)**, 616–619.

Cha, J. W., Park, J.-S., Sim, T., Nam, S.-J., Kwon, H. C., Del Valle, J. R., & Fenical, W. 2012. Structure Assignment of Lucentamycin E and Revision of the Olefin Geometries of the Marine-Derived Lucentamycins. *Journal of Natural Products*, **75(9)**, 1648–1651.

Cho, J. Y., Williams, P. G., Kwon, H. C., Jensen, P. R., & Fenical, W. 2007. Lucentamycins A−D, Cytotoxic Peptides from the Marine-Derived Actinomycete Nocardiopsis lucentensis. *Journal of Natural Products*, **70(8)**, 1321–1328.

Corey, E. J., & Reichard, G. A. 1992. Total synthesis of lactacystin. *Journal of the American Chemical Society*, **114(26)**, 10677–10678.

Dyer, J., King, A., Keeling, S., & Moloney, M. G. 2000. Pyrrolidinones derived from (S)-pyroglutamic acid. Part 2. Conformationally constrained kainoid analogues. *Journal of the Chemical Society, Perkin Transactions 1*, **16,** 2793–2804.

Dyer, J., Moloney, M. G., & Keeling, S. 1998. Direct versatile route to conformationally constrained glutamate analogues. *Chemical Communications*, **0(4)**, 461–462.

Gänzle, M. G. 2004. Reutericyclin: biological activity, mode of action, and potential applications. *Applied Microbiology and Biotechnology*, **64(3)**, 326–332.

Hoeksema, H., Bannister, B., Birkenmeyer, R. D., Kagan, F., Magerlein, B. J., MacKellar, F. A., Schroeder, W., Slomp, G., & Herr, R. R. 1964. Chemical Studies on Lincomycin. I. The Structure of Lincomycin. *Journal of the American Chemical Society*, **86(19)**, 4223–4224.

Holloway, W. J., Kahlbaugh, R. A., & Scott, E. G. 1963. Lincomycin: A Clinical Study. *Antimicrobial Agents and Chemotherapy*, **161**, 200–203.

Ikeda, M., Sato, T., Matsubayashi, K., Yamamoto, K., Ishikawa, H., & Ishibashi, H. 1995. Synthesis of a Simple Kainic Acid Analogue by Means of Carbamoylmethyl Radical Cyclization. *Heterocycles*, **40(1)**, 261.

Jeong, Y.C., Anwar, M., Nguyen, T. M., Tan, B. S. W., Chai, C. L. L., & Moloney, M. G. 2011. Control of chemoselectivity in Dieckmann ring closures leading to tetramic acids. *Organic & Biomolecular Chemistry*, **9(19)**, 6663.

Josa-Culleré, L., Towers, C., Thompson, A. L., & Moloney, M. G. 2017. Chemoselective Formation and Reaction of Densely Functionalised Bicyclic Tetramic Acids and Their Biological Activity. *European Journal of Organic Chemistry*, **2017(47)**, 7055–7059.

Jouyban, A., Fakhree, M. A. A., & Shayanfar, A. 2010. Review of pharmaceutical applications of N-methyl-2-pyrrolidone. *Journal of Pharmacy and Pharmaceutical Sciences*, **13(4)**, 524–535.

Krapcho, A. P. 1982. Synthetic Applications of Dealkoxycarbonylations of Malonate Esters, β-Keto Esters, α-Cyano Esters and Related Compounds in Dipolar Aprotic Media - Part I. *Synthesis*, 805–822.

Leonard, J., Díez-Barra, E., & Merino, S. 1998. Control of Asymmetry Through Conjugate Addition Reactions. *European Journal of Organic Chemistry*, **1998(10)**, 2051–2061.

Manam, R. R., Teisan, S., White, D. J., Nicholson, B., Grodberg, J., Neuteboom, S. T. C., Lam, K. S., Mosca, D. A., Lloyd, G. K., & Potts, B. C. M.(2005. Lajollamycin, a Nitro-tetraene Spiro-β-lactone-γ-lactam Antibiotic from the Marine Actinomycete Streptomyces n odosus. *Journal of Natural Products*, **68(2)**, 240–243.

Miguel, B. S., Ghayor, C., Ehrbar, M., Jung, R. E., Zwahlen, R. A., Hortschansky, P., Schmoekel, H. G., & Weber, F. E. 2009. N-methyl pyrrolidone as a potent bone morphogenetic protein enhancer for bone tissue regeneration. *Tissue Engineering - Part A*, **15(10)**, 2955–2963.

Moloney, M., Trippier, P., Yaqoob, M., & Wang, Z. 2004. The Oxazolomycins: A Structurally Novel Class of Bioactive Compounds. *Current Drug Discovery Technologies*, **1(3)**, 181–199.

Ranatunga, S., Tang, C. H. A., Hu, C. C. A., & Del Valle, J. R. 2012. Total synthesis and structural revision of lucentamycin A. *Journal of Organic Chemistry*, **77(21)**, 9859–9864.

Schwartz, R. E., Helms, G. L., Bolessa, E. A., Wilson, K. E., Giacobbe, R. A., Tkacz, J. S., Bills, G. F., Liesch, J. M., Zink, D. L., Currotto, J. E., Pramanik, B., & Onishi, J. C. 1994. Pramanicin, a novel antimicrobial agant from a fungal fermentation. *Tetrahedron.*, **50(6)**, 1675–1686.

Skarzewski, J. 1990. The Michael Reaction of Methanetricarboxylic Esters. A Simple Method for Two-Carbon Chain Elongation. *Synthesis*, 1125–1127.

Spížek, J., Novotná, J., & Řezanka, T. 2004. Lincosamides: Chemical Structure, Biosynthesis, Mechanism of Action, Resistance, and Applications. In *Advances in Applied Microbiology*. **56**, 121–154).

Tsai, C., Schneider, J. A., & Lehmann, J. 1988. Trans-2-carboxy-3-pyrrolidineacetic acid (CPAA), a novel agonist at NMDA-type receptors. *Neuroscience Letters*, **92.**

Tuske, S., Sarafianos, S. G., Wang, X., Hudson, B., Sineva, E., Mukhopadhyay, J., Birktoft, J. J., Leroy, O., Ismail, S., Clark, A. D., Dharia, C., Napoli, A., Laptenko, O., Lee, J., Borukhov, S., Ebright, R. H., & Arnold, E. 2005. Inhibition of Bacterial RNA Polymerase by Streptolydigin: Stabilization of a Straight-Bridge-Helix Active-Center Conformation. *Cell*, **122(4)**, 541–552.

Vinale, F., Flematti, G., Sivasithamparam, K., Lorito, M., Marra, R., Skelton, B. W., & Ghisalberti, E. L. 2009. Harzianic Acid, an Antifungal and Plant Growth Promoting Metabolite from Trichoderma harzianum. *Journal of Natural Products*, **72(11)**, 2032–2035.

Barishal University Journal of Science and Engineering, Vol. 8: 129-140 (2023) ISSN: 2411-247X

FIRST DERIVATIVE OF AUTOMORPHIC FUNCTION OF TRIANGLE GROUP

Md. Shafiul Alam[1*], Bijan Krishna Saha[1], and Chinmayee Podder[1]
[1]*Department of Mathematics, University of Barishal, Barishal-8254, Bangladesh*

Abstract

For a triangle group G, the G-automorphic function is the inverse of Schwarz triangle function. In this paper, we compute the first derivative of the G-automorphic function for the triangle group G in terms of the Gaussian hypergeometric function.

2020 Mathematics Subject Classification: 11F03; 33C05.

Keywords: Automorphic function, Triangle group, Hypergeometric function.

1. Introduction

If $\alpha, \beta, \gamma \in \mathbb{C}$ for $\gamma \neq 0,-1,-2,\ldots$ and $j \in \mathbb{N} \cup \{0\}$, then the function ${}_2F_1(\alpha,\beta;\,\gamma;\xi)$ defined by

$$ {}_2F_1(\alpha,\beta;\,\gamma;\xi) = \sum_{j=0}^{\infty} \frac{(\alpha,j)(\beta,j)}{(\gamma,j)\, j!} \xi^j, \quad |\xi| < 1, $$

where
$$ (\alpha,j) = \begin{cases} 1 & \text{if } j = 0 \\ \alpha(\alpha+1)\cdots(\alpha+j-1) & \text{if } j \geq 1. \end{cases} $$

is known as the Gaussian hypergeometric function. By the Euler's integral representation formula, one can extend ${}_2F_1(\alpha,\beta;\,\gamma;\xi)$ analytically to $\mathbb{C} \setminus [1,+\infty)$ (cf. Chapter II of (Bateman, 1953) and Chapter XIV of (Whittaker and Watson, 1927)).

*Corresponding author.
E-mail address:msalam@bu.ac.bd

For the group $\mathrm{SL}_2(\mathbb{R})$ given by

$$\mathrm{SL}_2(\mathbb{R}) = \left\{\begin{pmatrix} a & b \\ c & d \end{pmatrix} : a, b, c, d \in \mathbb{R},\ ad - bc = 1\right\},$$

the group $\mathrm{PSL}_2(\mathbb{R})$ is defined as

$$\mathrm{PSL}_2(\mathbb{R}) = \mathrm{SL}_2(\mathbb{R})/\{I_2, -I_2\},$$

where I_2 is the 2×2 identity matrix (see Chapter VII of (Serre, 1973)). Let $\mathcal{H}$ denote the complex upper half-plane $\mathcal{H} = \{w \in \mathbb{C} : \operatorname{Im} w > 0\}$. The action of $\mathrm{PSL}_2(\mathbb{R})$ on $\mathcal{H}$ is given by

$$w \mapsto \begin{pmatrix} a & b \\ c & d \end{pmatrix} w = \frac{aw + b}{cw + d}$$

for $\begin{pmatrix} a & b \\ c & d \end{pmatrix} \in \mathrm{PSL}_2(\mathbb{R})$ and $w \in \mathcal{H}$.

Let $A = \begin{pmatrix} a & b \\ c & d \end{pmatrix} \in \mathrm{PSL}_2(\mathbb{R})$. The element A is called parabolic if $a + b = \pm 2$, elliptic if $(a + b) \in \mathbb{R}$ and $|a + b| < 2$, hyperbolic if $(a + b) \in \mathbb{R}$ and $|a + b| > 2$, loxo-dromic if $(a + b) \in \mathbb{C}$ (see Theorem 15, Section 10 of (Ford, 1929)). Let $G \subset \mathrm{PSL}_2(\mathbb{R})$ be a triangle group with signature $(0; n_1,\ n_2, n_3)$ acting on $\mathcal{H}$. Consider a parabolic element $A_1 \in G$ and an elliptic element $A_2 \in G$. If $A_1(x) = x$, where $x \in\ \mathbb{R} \cup \{\infty\}$, then the point x is called a cusp of the group G. If $A_1(w) = w$, where $w \in \mathcal{H}$, then we call the point w an elliptic point of G. Since the action of G on $\mathcal{H}$ is properly discontinuous, we obtain the quotient Riemann surface $G\backslash\mathcal{H}$ (see (Beardon, 1983) and (Katok, 1992)). In (Alam, 2021) and (Alam and Sugawa, 2022), a special type of triangle group known as the Hecke group is investigated to study modular equations.

For a hyperbolic triangle $[w_1, w_2, w_3]$ with angles $\frac{\pi}{n_1}, \frac{\pi}{n_2}, \frac{\pi}{n_3}$, let f denote the Schwarz triangle function. The G-automorphic function $\xi : \mathcal{H} \to G\backslash\mathcal{H}^*$, where $\mathcal{H}^*$ is the union of $\mathcal{H}$ and the set of cusps of G, is the inverse of f and

$$\xi\left(\frac{aw + b}{cw + d}\right) = \xi(w)$$

for $w \in \mathcal{H}$ and $\begin{pmatrix} a & b \\ c & d \end{pmatrix} \in G$. The function $\xi(w)$ can be normalized in such a way that the orders of the ramifications are n_1, n_2, n_3 over $0, 1, \infty$, respectively (see (Cohen et al., 1994). Suppose that n_1, n_2 and n_3 are the orders of the elliptic points w_1, w_2 and w_3, respectively, such that

$$\xi(w_1) = 0, \quad \xi(w_2) = 1, \quad \xi(w_3) = \infty.$$

Then, $\xi(w)$ satisfies the following hypergeometric differential equation

$$\xi(1-\xi)\frac{d^2 g}{d\xi^2} + \{\gamma - (\alpha+\beta+1)\xi\}\frac{dg}{d\xi} - \alpha\beta g = 0. \tag{1.1}$$

Let $g_1(\xi)$ and $g_2(\xi)$ be linearly independent solutions of (1.1), then

$$f(\xi) = \frac{g_2(\xi)}{g_1(\xi)}$$

is the Schwarz triangle function. The Schwarzian derivative, denoted by $\{f, \xi\}$, of $f(\xi)$ is given by

$$\{f, \xi\} = \left(\frac{f''(\xi)}{f'(\xi)}\right)' - \frac{1}{2}\left(\frac{f''(\xi)}{f'(\xi)}\right)^2.$$

The function $f(z)$ satisfies the Schwarzian equation given by

$$\{f, \xi\} = \frac{1-p_1^2}{2\xi^2} + \frac{1-p_2^2}{2(1-\xi)^2} + \frac{1-p_1^2-p_2^2+p_3^2}{2\xi(1-\xi)}, \tag{1.2}$$

where p_1, p_2, p_3 are known as accessory parameters and

$$p_1 = \frac{1}{n_1}, \qquad p_2 = \frac{1}{n_2}, \qquad p_3 = \frac{1}{n_3}$$

(cf. Chap. V, Sect. 7 of (Nehari, 1952)). These facts are presented in the following theorem.

Theorem A (Theorem 6.2 of (Bayer and Travesa, 2007)). *For* $\gamma \neq 1$, *let*

$$\alpha' = \alpha - \gamma + 1, \qquad \beta' = \beta - \gamma + 1, \qquad \gamma' = 2 - \gamma,$$

then the functions

$$g_1(\xi) = {}_2F_1(\alpha, \beta;\, \gamma; \xi) \quad and \quad g_2(\xi) = \xi^{1-\gamma}\, {}_2F_1(\alpha', \beta';\, \gamma'; \xi)$$

are linearly independent solutions of (1.1). *Let*

$$w = f(\xi) = \frac{g_2(\xi)}{g_1(\xi)},$$

then $\mathcal{H} = \{\xi \in \mathbb{C} : Im\, \xi > 0\}$ *is mapped by* $f(\xi)$ *conformally to the hyperbolic (non-Euclidean) triangle* $[w_1, w_2, w_3]$ *in the* w*-plane, where*

$$w_1 = f(0) = 0,$$

$$w_2 = f(1) = \frac{\Gamma(2-\gamma)\Gamma(\gamma-\alpha)\Gamma(\gamma-\beta)}{\Gamma(\gamma)\Gamma(1-\alpha)\Gamma(1-\beta)},$$

$$w_3 = f(1) = \frac{\Gamma(\alpha)\Gamma(\gamma-\beta)\Gamma(2-\beta)}{\Gamma(\gamma)\Gamma(\alpha-\gamma+1)\Gamma(1-\beta)}.$$

The interior angles at the vertices w_1, w_2 *and* w_3 *are, respectively,* $(1-\gamma)\pi$, $(\gamma-\alpha-\beta)\pi$ *and* $(\beta-\alpha)\pi$.

For $w_1, w_2 \in \mathcal{H}$, let us denote the hyperbolic (non-Euclidean) distance between w_1 and w_2 by $d_h(w_1, w_2)$. Since at the vertices w_1, w_2 and w_3 of the hyperbolic triangle $[w_1, w_2, w_3]$, the angles are $\frac{\pi}{n_1}$, $\frac{\pi}{n_2}$ and $\frac{\pi}{n_3}$, respectively, we have

$$\tanh^2 \frac{d_h(w_1, w_2)}{2} = \frac{\cos\left\{\frac{1}{2}\left(\frac{1}{n_1} + \frac{1}{n_2} + \frac{1}{n_3}\right)\pi\right\} \cos\left\{\frac{1}{2}\left(\frac{1}{n_1} + \frac{1}{n_2} - \frac{1}{n_3}\right)\pi\right\}}{\cos\left\{\frac{1}{2}\left(\frac{1}{n_2} + \frac{1}{n_3} - \frac{1}{n_1}\right)\pi\right\} \cos\left\{\frac{1}{2}\left(\frac{1}{n_3} + \frac{1}{n_1} - \frac{1}{n_2}\right)\pi\right\}} \tag{1.3}$$

(see Equation (75.1) of (Carathéodory, 1954), where $a_i = d_h(w_1, w_2)$, $\alpha_i = \frac{\pi}{n_3}$, $\alpha_j = \frac{\pi}{n_1}$, $\alpha_k = \frac{\pi}{n_2}$). Also, by Equation (85.3) of (Carathéodory, 1954), we have

$$\tanh^2 \frac{d_h(w_1, w_2)}{2} = |\frac{w_2 - w_1}{w_2 - \bar{w}_1}|. \tag{1.4}$$

In the following section, we present the main results and their proofs.

2. Main Results and Proofs

Theorem 2.1. *Suppose that* G *is a triangle group with signature* $(0;\ n_1, n_2, n_3)$. *Let*

$$\xi : \mathcal{H} \to G \backslash \mathcal{H}^*$$

be the G*-automorphic function and let* w_1, w_2, $w_3 \in \mathcal{H}$ *be the elliptic points of orders* n_1, n_2 *and* n_3, *respectively, such that*

$$\xi(w_1) = 0, \quad \xi(w_2) = 1, \quad \xi(w_3) = \infty.$$

Then,

$$\frac{d\xi}{dw} = C\, \xi^{(1-\frac{1}{n_1})}(1-\xi)^{(1-\frac{1}{n_2})} \left({}_2F_1(\alpha, \beta;\ \gamma; \xi) \ - K \xi^{\frac{1}{n_1}}\ {}_2F_1(\alpha', \beta';\ \gamma'; \xi)\right)^2, \tag{2.1}$$

where $C \in \mathbb{C} \setminus \{0\}$, α, $\beta \neq \mathbb{Z}$, $\alpha' = \alpha - \gamma + 1$, $\beta' = \beta - \gamma + 1$, $\gamma' = 2 - \gamma$ *and*

$$K = \left(\frac{\Gamma(1-\alpha)\Gamma(1-\beta)\Gamma(\alpha')\Gamma(\beta')}{\Gamma(\alpha)\Gamma(\beta)\,\Gamma(1-\alpha')\Gamma(1-\beta')}\right)^{\frac{1}{2}} \frac{\Gamma(\gamma)}{\Gamma(\gamma')}.$$

We need the following lemma in the proof of Theorem 2.1.

Lemma 2.2. *Let w_1, $w_2 \in \mathcal{H}$ be the elliptic points of orders n_1 and n_2, respectively. Then the hyperbolic (non-Euclidean) distance, $d_h(w_1, w_2)$, between w_1 and w_2 is given by*

$$\tanh^2 \frac{d_h(w_1, w_2)}{2} = \frac{\sin \pi\alpha \sin \pi\beta}{\sin \pi\alpha' \sin \pi\beta'}.$$

Proof. We have

$$(2.2) \qquad \frac{1}{n_1} = 1 - \gamma, \qquad \frac{1}{n_2} = \gamma - \alpha - \beta, \qquad \frac{1}{n_3} = \beta - \alpha$$

and

$$(2.3) \qquad \alpha' = \alpha - \gamma + 1, \qquad \beta' = \beta - \gamma + 1, \qquad \gamma' = 2 - \gamma.$$

From (2.2) and(2.3), it follows that

$$(2.4) \quad \alpha = \frac{1}{2}\left(1 - \frac{1}{n_1} - \frac{1}{n_2} - \frac{1}{n_3}\right), \ \beta = \frac{1}{2}\left(1 - \frac{1}{n_1} - \frac{1}{n_2} + \frac{1}{n_3}\right), \ \gamma = 1 - \frac{1}{n_1}$$

and

$$(2.5) \quad \alpha' = \frac{1}{2}\left(1 + \frac{1}{n_1} - \frac{1}{n_2} - \frac{1}{n_3}\right), \ \beta' = \frac{1}{2}\left(1 + \frac{1}{n_1} - \frac{1}{n_2} + \frac{1}{n_3}\right), \ \gamma' = 1 + \frac{1}{n_1}.$$

Thus,

$$\frac{1}{n_1} + \frac{1}{n_2} + \frac{1}{n_3} = 1 - 2\alpha,$$

$$\frac{1}{n_1} + \frac{1}{n_2} - \frac{1}{n_3} = 1 - 2\beta,$$

$$-\frac{1}{n_1} + \frac{1}{n_2} + \frac{1}{n_3} = 1 - 2\alpha',$$

$$-\frac{1}{n_1} + \frac{1}{n_2} - \frac{1}{n_3} = 1 - 2\beta'.$$

From (1.3), we have

$$\tanh^2 \frac{d_h(w_1, w_2)}{2} = \frac{\cos\left\{\frac{1}{2}(1-2\alpha)\pi\right\}\cos\left\{\frac{1}{2}(1-2\beta)\pi\right\}}{\cos\left\{\frac{1}{2}(1-2\alpha')\pi\right\}\cos\left\{-\frac{1}{2}(1-2\beta')\pi\right\}}$$

$$= \frac{\sin\pi\alpha\sin\pi\beta}{\sin\pi\alpha'\sin\pi\beta'}. \qquad \square$$

Recall that the linearly independent solutions of (1.1) are

$$g_1(\xi) = {}_2F_1(\alpha, \beta;\, \gamma; \xi)$$

and

$$g_2(\xi) = \xi^{1-\gamma}\, {}_2F_1(\alpha', \beta';\, \gamma'; \xi)$$

for $0 < \gamma < 1$. The quotient

$$w = f(\xi) = \frac{g_2(\xi)}{g_1(\xi)}$$

maps conformally $\mathcal{H}$ to the interior of $[w_1, w_2, w_3]$. Let $\partial[w_1, w_2, w_3]$ and $\partial\mathcal{H}$ denote the boundary of the triangle $[w_1, w_2, w_3]$ and the boundary of $\mathcal{H}$, respectively. Then $f(\xi)$ forms a homeomorphism between $\partial\mathcal{H} = \mathbb{R} \cup \{\infty\}$ and $\partial[w_1, w_2, w_3]$. The orders of w_1, w_2 and w_3 are n_1, n_2 and n_3, respectively, where n_1, n_2, n_3 are integers greater than 2 or infinity. Since

$$\frac{1}{n_1} + \frac{1}{n_2} + \frac{1}{n_3} < 1,$$

the inverse $\xi(w)$ of the Schwarz triangle function $f(\xi)$ is single-valued (see p. 416 in (Sansone and Gerretsen, 1969)). Also,

$$\xi(w_1) = 0, \quad \xi(w_2) = 1 \text{ and } \quad \xi(w_3) = \infty.$$

Consider the elliptic point $w_1 \in \mathcal{H}$ of order n_1 and let $A \in G$ be the generator of the stabilizer subgroup for w_1, then

(2.6)
$$\frac{Aw - w_1}{Aw - \overline{w}_1} = e^{\frac{2\pi i}{n_1}} \frac{w - w_1}{w - \overline{w}_1}$$

(see (9) of Section 48 in (Ford, 1929)). Also, for $\begin{pmatrix} a & b \\ c & d \end{pmatrix} \in G$ and $w = \frac{g_2}{g_1}$, we have

(2.7)
$$w \mapsto \begin{pmatrix} a & b \\ c & d \end{pmatrix} w = \frac{aw + b}{cw + d} = \frac{ag_2 + bg_1}{cg_2 + g_1}.$$

The two sides (hyperbolic lines) of $[w_1, w_2, w_3]$ through w_1 are mapped to straight lines through the origin by the Möbius transformation

$$w \to \frac{w - w_1}{w - \overline{w}_1}.$$

Proof of Theorem 2.1. The points on $G\backslash\mathcal{H}$ are the G-orbits of w near the elliptic point w_1 such that

$$\frac{w - w_1}{w - \overline{w}_1} = K \frac{w_2}{w_1}$$

(2.8)
$$\frac{w - w_1}{w - \overline{w}_1} = K \frac{\xi^{1-\gamma}\ {}_2F_1(\alpha', \beta';\ \gamma'; \xi)}{{}_2F_1(\alpha, \beta;\ \gamma; \xi)}$$

for a nonzero constant K (see (48) of (Elkies, 1998)). By assumptions, $\xi(w_2) = 1$ and

$$\gamma' - \alpha' - \beta' = \gamma - \alpha - \beta,$$

$$\gamma' - \beta' = 1 - \beta,$$

$$\gamma' - \alpha' = 1 - \alpha.$$

Thus,
$${}_2F_1\big(\alpha, \beta;\ \gamma; \xi(w_2)\big) = \frac{\Gamma(\gamma)\Gamma(\gamma-\alpha-\beta)}{\Gamma(\gamma-\alpha)\Gamma(\gamma-\beta)}$$

(see Section 14.11 of (Bateman, 1953)) and

$$ {}_2F_1\big(\alpha', \beta';\ \gamma'; \xi(w_2)\big) = \frac{\Gamma(\gamma')\Gamma(\gamma' - \alpha' - \beta')}{\Gamma(\gamma' - \alpha')\Gamma(\gamma' - \beta')} $$

$$ = \frac{\Gamma(\gamma')\Gamma(\gamma - \alpha - \beta)}{\Gamma(1 - \alpha)\Gamma(1 - \beta)}. $$

Therefore, when $w \to w_2$, from (2.8) we have

$$ \frac{w_2 - w_1}{w_2 - \overline{w}_1} = K \frac{\Gamma(\gamma')\Gamma(\gamma - \alpha)\Gamma(\gamma - \beta)}{\Gamma(\gamma)\Gamma(1 - \alpha)\Gamma(1 - \beta)} $$

or,

$$ K = \frac{w_2 - w_1}{w_2 - \overline{w}_1} \frac{\Gamma(\gamma)\Gamma(1 - \alpha)\Gamma(1 - \beta)}{\Gamma(\gamma')\Gamma(1 - \alpha')\Gamma(1 - \beta')}. \tag{2.9} $$

Since $\sin \pi\alpha = \frac{\pi}{\Gamma(\alpha)\Gamma(1-\alpha)}$ for $\alpha \neq \mathbb{Z}$, by Lemma 2.2 we have

$$ \tanh^2 \frac{d_h(w_1, w_2)}{2} = \frac{\sin \pi\alpha \sin \pi\beta}{\sin \pi\alpha' \sin \pi\beta'} $$

or,

$$ \tanh^2 \frac{d_h(w_1, w_2)}{2} = \frac{\Gamma(\alpha')\Gamma(1 - \alpha')\Gamma(\beta')\Gamma(1 - \beta')}{\Gamma(\alpha)\Gamma(1 - \alpha)\Gamma(\beta)\Gamma(1 - \beta)} \tag{2.10} $$

From (1.4), it follows that

$$ \tanh^2 \frac{d_h(w_1, w_2)}{2} = \left(\frac{w_2 - w_1}{w_2 - \overline{w}_1}\right)^2. \tag{2.11} $$

Thus, from (2.9), (2.10) and (2.11), we have

$$ K = \left(\frac{\Gamma(1 - \alpha)\Gamma(1 - \beta)\Gamma(\alpha')\Gamma(\beta')}{\Gamma(\alpha)\Gamma(\beta)\,\Gamma(1 - \alpha')\Gamma(1 - \beta')}\right)^{\frac{1}{2}} \frac{\Gamma(\gamma)}{\Gamma(\gamma')}. $$

Now, (2.8) implies

$$w = \frac{w_1 g_1 - K\bar{w}_1 g_2}{g_1 - K g_2}. \tag{2.12}$$

Therefore,

$$\frac{dw}{d\xi} = K(w_1 - \bar{w}_1)\frac{g_1 \frac{dg_2}{d\xi} - \frac{dg_1}{d\xi} g_2}{(g_1 - K g_2)^2}. \tag{2.13}$$

Let W denote the Wronskian of g_1 and g_2 given by

$$W = g_1 \frac{dg_2}{d\xi} - \frac{dg_1}{d\xi} g_2.$$

Then,

$$\frac{dw}{d\xi} = K(w_1 - \bar{w}_1)\frac{W}{(g_1 - K g_2)^2}. \tag{2.14}$$

From (1.1), we have

$$\frac{d^2 g}{d\xi^2} + P(\xi)\frac{dg}{d\xi} + Q(\xi)g = 0, \tag{2.15}$$

where

$$P(\xi) = \frac{\gamma-(\alpha+\beta+1)\xi}{\xi(1-\xi)} \quad \text{and}$$

$$Q(\xi) = \frac{\alpha\beta}{\xi(1-\xi)}.$$

Since the linearly independent solutions of (2.15) are $g_1(\xi)$ and $g_2(\xi)$, we have by Abel's theorem (see Theorem 3.3.2 of (Boyce et al., 2021))

$$W(\xi) = W(\xi_0)\exp\left(-\int_{\xi_0}^{\xi} P(\xi)d\xi\right), \tag{2.16}$$

where $W(\xi_0) \neq 0$. For some constant $C_0 \in \mathbb{C} \setminus \{0\}$, it follows from (2.16) that

$$W(\xi) = C_0 \xi^{-\gamma}(1-\xi)^{\gamma-\alpha-\beta-1}. \tag{2.17}$$

Therefore, from (2.14) and (2.17) we have

$$\frac{dw}{d\xi} = C_0 K(w_1 - \overline{w}_1) \frac{\xi^{-\gamma}(1-\xi)^{\gamma-\alpha-\beta-1}}{(g_1 - K g_2)^2} \tag{2.18}$$

which implies

$$\frac{d\xi(w)}{dw} = C\, \xi^{\left(1-\frac{1}{n_1}\right)}(1-\xi)^{\left(1-\frac{1}{n_2}\right)} \left({}_2F_1(\alpha,\beta;\, \gamma;\xi) - K\xi^{\frac{1}{n_1}}\, {}_2F_1(\alpha',\beta';\, \gamma';\xi) \right)^2,$$

where

$$C = \frac{1}{C_0 K(w_1 - \overline{w}_1)}. \tag{2.19}$$ □

Corollary 2.2.1. The constants C and K in Theorem 2.1 are inversely proportional to each other.

Proof. From (2.19), it follows that $C \propto \frac{1}{K}$. □

Acknowledgments

The first author was supported by the University Grants Commission (UGC) of Bangladesh. The authors are grateful to the anonymous referees for their valuable suggestions and comments.

References

Alam, Md. S., 2021. On Ramanujan's modular equations and Hecke groups. *Preprint*, *arXiv:2105.13152*.

Alam, Md. S. and Sugawa, T., 2022. Geometric deduction of the solutions to modular equations. *The Ramanujan Journal, 59(2)*, pp. 459–477.

Bateman, H., 1953. *Higher Transcendental Functions* (Vol. I). New York: McGraw-Hill.

Bayer, P. and Travesa, A., 2007. Uniformizing functions for certain Shimura curves, in the case D = 6. *Acta Arithmetica, 126*, pp. 315–339.

Beardon, A. F., 1983. *The Geometry of Discrete Groups*. Graduate Texts in Mathematics 91, New York: Springer-Verlag.

Boyce, W. E., DiPrima, R. C. and Meade, D. B., 2021. *Elementary differential equations and boundary value problems*. John Wiley & Sons.

Carathéodory, C., 1954. *Theory of Functions of a Complex Variable*. New York: Chelsea.

Cohen, P. B., Itzykson, C. and Wolfart, J., 1994. Fuchsian triangle groups and Grothendieck dessins. Variations on a theme of Belyi. *Communications in Mathematical Physics, 163(3)*, pp. 605–627.

Elkies, N.D., 1998, June. Shimura curve computations. In *International Algorithmic Number Theory Symposium*. Berlin, Heidelberg: Springer Berlin Heidelberg, pp. 1–47.

Ford, L. R., 1929. *Automorphic Functions*. New York: McGraw–Hill.

Katok, S., 1992. *Fuchsian Groups*. Chicago and London: The University of Chicago Press.

Nehari, Z., 1952. *Conformal Mapping*. New York: McGraw-Hill.

Sansone, G. and Gerretsen, J., 1969. *Lectures on the Theory of Functions of a Complex Variable: II. Geometric Theory*. Groningen: Wolters-Noordhoff.

Serre, J.-P., 1973. *A Course in Arithmetic*. Graduate Texts in Mathematics 7, New York: Springer-Verlag.

Whittaker, E. T. and Watson, G. N., 1927. *A Course of Modern Analysis* (4^{th} Edition). Cambridge: Cambridge University Press.

Barishal University Journal of Science and Engineering
ISSN:2411-247X
University of Barishal, Barishal-8254, Bangladesh

INSTRUCTIONS TO THE CONTRIBUTORS

Preparation of manuscripts

The following guidelines should be followed strictly in submitting the manuscript of the journal. All manuscripts must be written in English and typed on a good quality (A4) bond paper with double space and sufficient margins (left and top 3.80 cm. right and bottom 2.55 cm) and be submitted in duplicate to the Associate Editor at the University address stated below. The Editorial Board will arrange review of the article. Decision of the Editorial Board on any article is final.

The manuscript of a full paper or review papers within fifteen typed pages including tables, figures, graphs, etc. while that of a short communication should not exceed six pages.

The manuscript should contain the following subtitles in sequence; Title, Abstract, Keywords, Introduction, Materials and Methods, Results and Discussion, Acknowledgements, if any, and References. These sub-titles however may not be applicable in case of short communication or review paper.

Title: Title of the paper should be brief and specific. The author should prepare the manuscript in such a way that there should be a title page with only the title of the paper, the names and address of the authors, and running head on it. The second page should carry the title of the paper with Abstract to be followed by Introduction, etc. without author's name.

Abstract: It should not exceed 200 words. It should include only the gist of the paper, i.e. just the results. Abstract is not the summary and in any case, it should not contain the subject of the mat rials and methods and /or any descriptive part of the paper.

Keywords: Should not exceed 6 words.

Introduction: It should be concise and include relevant literature and define clearly the objective of the study.

Materials and Methods: Special / standard methods should be cited only as references and should not be described except for the modification which should be stated. No sub-heads should be used.

Results and Discussion: The section should include precise statement of results obtained, figures, tables, and discussion.

Table, Graphs and Figures: The paper should contain minimum number of tables, graphs, and figures. However, these should be typed separately. Table title should be on the top of the table and written as Table 1. Caption for the figures graphs and graphs should be on the bottom of the figure and be written as Fig 1. The same data should not be used in both the tables and figures or graphs. The figures and graphs should be properly labeled with bold, solid lines so that these can stand reduction up to half or less of the original. The photographs should be submitted on glossy paper. Legend of the graphs and figures should be typed and given separately at the end of text.

The references and specific names are extremely important. The authors must be sure about the corrections of citations and spellings.

Citation style: In the text, references should be cited within brackets quoting author's surname and the year of the publication in the appropriate place. Two or more references when put within the same bracket should be separated by a comma. For example, (Khan, 2005), (Parvin and Zakia, 2009) and (Rahman, 2010), salinity is widely (Khan et al., 2002); (Parvez and Rahim, 2004; and Rafi, 2005), results are partially agree well with the findings of (Harun, 2010 and Akter, 2011). Units of measurements to be used as SI units.

References: References should be arranged alphabetically according to author's surname at the end of the paper. Names of journals and books should be in italics giving edition, year of publication and name of the publishers.

Examples:

Islam. M. S., M. R. Islam and M. M. Rahman. 2015. Incompatibility relationship in wild housefly Musca domestica L. collected from different parts of Bangladesh. Journal of Asiatic Society of Bangladesh (Science). 29: 23-30.

Islam. A. K. M and K. Moniruzzaman. 2015. Euglenophyta of Bangladesh. L. Genus Trachelomonas Her. Inc. Revue ges Hydrobioligy. 66: 109-125.

Khan, M. S. 2013. Angiosperms. In: Two Centuries of plant Sciences in Bangladesh and Adjacent Regions (ed. A. K. M Nurul Islam). pp. 175-194. Asiatic Society of Bangladesh. Dhaka.

Bhuiyan. A. L. 2010. Fishes of Dhaka. Asiatic Society of Bangladesh, Dhaka. 148pp.

The author (s) must submit one printed copy of the revised paper and soft copy in the CD as MS Word format.

Final galley proof will be sent author (s) and is expected to be returned within five days as notice. No major alternations in the text are desirable at this stage.

Papers should be submitted in duplicate to:

Dr. Bijan Krishna Saha, Associate Editor, Barishal University Journal of Science and Engineering, Faculty of Science and Engineering, & Associate Professor, Department of Mathematics, University of Barishal, Barishal-8254, Bangladesh.

Off-Prints

Author(s) of each paper is/are entitled to get off-prints upon request.

Declaration

While submitting a paper the authors are to sign a declaration to the effect that (i) the work reported has been carried out by them and they jointly prepared the manuscript; (ii) they take public responsibility for the contents of the paper; (iii) the paper has not been published before in any referred scientific journal or has not been submitted to such journal for publication; and (iv) the accord consent to the Barishal University Journal to publish the paper.